Majid Anvari

Simulation of dynamic fracture in aluminum structures

PhD- thesis

Department of Engineering Design and materials
Faculty of Engineering Science and technology
Norwegian University of Science and Technology

To my eldest brother
Hamid Anvari
and in the memory of my late uncle
Mahmoud Rejaie Sani

Table of Contents

Acknowledgments

Doing a PhD thesis is not a straightforward work in the way that you know where you start and where you finish (although it might look like that in the beginning). It is a process during which you learn a lot and you experience a lot. This experience involves many people who have inspired the work, whether explicitly or implicitly, and their influences are precious.

First of all, I want to express my gratitude to my supervisor Professor Christian Thaulow. He was always encouraging and creative in showing me the way ahead. Most of all, I want to thank him for believing in me as someone who is enable to do this job and supporting my ideas and approaches.

It was also a fortune to discuss the work and share some of the problems with Professor Zhiliang Zhang, Professor Bjørn Skallerud and Professor Odd S. Hopperstad all from NTNU. Performing dynamic tests using split-Hopkinson tension bar was not possible without the assistance and guidance of Professor Arild H. Clausen from Department of Structural Engineering at NTNU.

I received plenty of help from the employees working at Department of Machine Design and Material Technology at NTNU. My special thanks go to other PhD candidates then, Dr. Jun Liu and Dr. Torsten Mann. The experimental part of the thesis was performed by the efforts and cooperation of Jun. The present book owes Torsten who helped me with Latex ranging from installing the related software on my computer till helping me with some details in editing the texts and equations.

During my studies, I had the chance to be in contact with Fracture Mechanics group of SINTEF. Among them I would like to particularly thank Dr. Jack Ødegard, Mr. Bård Nyhus, Dr. Erling Østby, Mr. Hans I. Lange, Dr. Mario Polanco, Dr. Bård W. Tveiten and Mrs. Vigdis Olden for their supports and friendship.

Using cohesive zone modeling as the main approach in the thesis was inspired by the presentation that Professor Wolfgang Brocks held at NTNU in 2002 on this subject. Later I spent around six months, between January and June 2004, at the WMS department of GKSS research center in Geesthacht Germany where I received a lot of support from Professor Brocks. During my stay at GKSS, I received invaluable help from Dr. Ingo Scheider. Ingo was always available and incredibly helpful and friendly. Meeting Dr. Dirk Steglitch and becoming friend with him was one of the best things that could happen to me during my stay at GKSS. I not only learned scientific issues from him, but also many aspects of life which I will always be grateful for. I should also thank Dr. Patricia Négre for good discussions and providing me with some data from her ongoing thesis.

Having other friends during my stay in Trondheim was also a fortune. Among them I should particularly name Dr. Alireza Ashrafian and Mr. Daniel Hefley.

During the last two years, I have been working at Det Norske Veritas in Bergen where I am happy to have many good colleagues. Delivering the final version of the thesis was only possible by the understandings and supports of Mr. Kurt Eide.

My whole education owes my parents who have always shown infinite support and sacrifice. I am very indebted to my beautiful wife, Azadeh, for her great company during

these years. Ending, and even starting, this journey without her accompanies and trust was not possible. Azadeh did also most of the drawings in the present thesis and high quality of the graphics owes her efforts. I am also thankful to my lovely son, Borna, for showing me the face of love again.

Finally, I would like to acknowledge Hydro Aluminium and the Research Council of Norway for their support through the NorLight project.

Abstract

The present thesis treats the simulation of crack initiation and growth by the use of cohesive zone models under dynamic loading conditions . The first chapter reviews the aspects of fracture mechanics that are related to the subject. The rest of the thesis consists of two self-contained articles and one conference paper. Finite element models containing rate dependent cohesive elements have been introduced in the papers. The rate dependency of cohesive elements is obtained through calculations on single elements obeying rate dependent Gurson type equations. The papers represent three main aspects: model establishment, validation, and application.

In the first article, the aim is to establish a model which has the ability to account for crack growth simulations under dynamic loading conditions. A rate-dependent Gurson type model has been used to define rate and triaxiality dependency of cohesive elements. The rate- and triaxiality-dependent cohesive elements are used in a finite element model to simulate crack propagation in a middle-cracked tension M(T) specimen made of aluminum alloy. The calculations show the importance of strain rate and stress triaxiality on the rate of the crack growth and the change of the load.

The second paper examines the validation of the rate sensitive cohesive elements and the proposed procedure by comparing the results of the simulations and experiments on aluminum round bars under dynamic loading conditions. Smooth and notched round bars are tested and simulated and the load-diameter reduction curves are compared.

The third paper applies the model to a bi-material (laser welded) compact tension C(T) specimen under dynamic loading conditions. The specimen made of aluminum alloy contains an initial crack on the interface of fusion zone and base metal. The crack growth is simulated by rate dependent cohesive elements which are oriented in different directions so that mixed mode crack propagation is feasible.

The articles show the importance of considering rate dependency in the calculation of both the energy dissipated by plastic deformation and the energy of separation. They also show that the approach used is convenient for the simulation of dynamic ductile crack initiation and growth. The procedure considered can also be used for other areas of fracture simulation where the energy of separation is a function of variables that exist at the crack tip area.

Introduction

Fracture mechanics is a field of solid mechanics that deals with the behavior of cracked bodies subjected to mechanical and environmental loads. The problem is usually treated using the framework of continuum mechanics, thus field quantities like stresses and strains are used to describe the loading of a part or a structure by solving a boundary value problem. In this regard, approaches are needed to be developed which can not only provide solutions to assess mechanical integrity of structures in simple situations like small scale yielding under pure mode I isothermal loading, but also more complex situations, i.e. large-scale yielding, mixed-mode crack growth and non-isothermal loading.

Since many of structural failures are the results of crack growth, fracture mechanics has a wide application in different fields of industry, e.g. marine technology, offshore industry, aerospace, automotive industry, power plants and pipelines. The increasing application of aluminum alloys in industry, especially in car body and aircraft construction, has promoted the need for better understanding of the mechanical behavior of aluminum cracked structures under various loading conditions, e.g. cyclic and dynamic loadings. Since in many cases, crack growth in aluminum alloys is the result of the formation and growth of cavities, ductile fracture has been considered in the present study. In the case of dynamic loading conditions, in a macroscopic scale, when the inertia of large pieces of material is so high that the balance of energy in the structure requires the consideration of kinetic energy, dynamic fracture mechanics is regarded. In this case, in addition to inertia, rate dependency of the material, stress waves and adiabatic heating effects are necessary to be considered. The formulation of a constitutive law accounting for the relevant effects is thus a key issue.

The present study aims to develop a framework for finite element simulation of ductile crack initiation and growth in aluminum structures under dynamic loading conditions. Both simulation and experimental works have been performed.

Fracture mechanics can generally be performed on a variety of length scales ranging from the macroscopic to the atomic scales. In the approaches which are applied in macroscopic scales, known as global approaches, it is assumed that the fracture resistance can be measured in terms of a single parameter, i.e. K_{Ic}, J_{Ic} or $CTOD$. In more recent global approaches, a second parameter (T and Q stresses) have been introduced. Although this area of fracture mechanics has a wide application, it has many limitations related to the amount of plasticity, constraint and geometry. The limitations related to constraint means that the criteria defined are not material properties and may change from one geometry to another or depend on the mode of loading.

Besides the analyses performed in a specific scale, there are approaches where results from one scale can be transferred into another scale. The transition of stress or displacement from micro- to macro-scale is performed via a so called meso zone which can be analyzed e.g. by the use of local approaches. The background for local approaches is that the global failure of the material is triggered by the local behavior in the area where stress concentration exists, i.e. crack tip. Since local behavior is considered in this approach, transferability from one structure (or sample) to another is possible as long as the micro-

mechanism of failure remains unchanged. This advantage of local approaches has been the main motivation of using them in the present study.

To perform a local approach, it is necessary to fulfill two conditions: to establish a micromechanically based model, and to provide reliable knowledge of the crack tip stress-strain field. To establish a micromechanically based model for ductile rupture, fully coupled damage models have been proposed which introduce the effect of growing cavities on the constitutive equations of porous materials. A well-known model of this kind is Gurson model which has been further developed to capture void coalescence known as Gurson-Tvergaard-Needleman (GTN) model. In a so-called Gurson type model, the presence of a void results in a reduction of the stresses to be transformed in a material volume and therefore the plastic flow potential is not only a function of stress and strain, but also a function of porosity (the ratio of the total volume of the cavities to the volume of the body). Another local approach known as cohesive zone modeling is a phenomenological model in which a crack initiates and grows by the separation of the two crack surfaces in the process zone. In the finite element representation of the cohesive zone models, the cohesive elements are inserted as interfaces between the continuum non-damage elements. One of the advantages of using cohesive elements in modeling fracture is to split the total dissipated energy into the energy dissipated by plastic deformation and the energy of separation. In this way, it is possible to evaluate the damage and deformation processes separately, but coupled. Besides, as long as cohesive elements adequately resolve the fracture process zone of the material, no mesh dependency is expected in using cohesive zone models.

Since cohesive zone models are phenomenological, Gurson type models have been employed in this study as michromechanism based models in order to obtain the properties of the cohesive elements. By the use of a single rate-dependent Gurson type element, the effect of stress triaxiality and strain rate on the properties of the representative cohesive elements have been examined. The cohesive elements are introduced as interfaces on the boundaries of continuum elements in finite element models. The values of strain rates and stress triaxiality are calculated in the surrounding continuum elements and they are transferred to the adjacent cohesive elements. The properties of each cohesive element are updated based on these transferred variables. All the simulations are performed in ABAQUS finite element code and based on the FORTRAN subroutine developed in the code. Transient dynamic analyses have been used to take into account the inertia and stress waves globally.

In order to achieve the desired framework for simulating dynamic ductile fracture, the work has been divided into three main parts: model establishment, validation and application. In the first part, it has been shown that the recommended approach has the ability to explain the local effects of strain rate, stress triaxiality and inertia in a proper manner. The second part uses experimental results to show the abilities and limitations of the approach to obtain the global mechanical response of the aluminum samples tested under dynamic loading conditions. It shows that the approach has partly succeeded to obtain reasonable results compared to the tests. It also discusses the limitations regarding the use of Gurson type elements to obtain cohesive element properties. The third part uses the described approach in the simulation of crack extension in an aluminum welded

structure driven by dynamic loading. It shows the abilities and limitations of the approach in simulating mixed-mode crack growth in a mismatch welded connection.

In general, the thesis shows that the recommended approach has reasonable capabilities, both qualitatively and quantitatively, to model crack initiation and growth in aluminum structures influenced by dynamic loading. Moreover, limitations and deficits of the proposed approach have been discussed in details. The three parts of the thesis have been presented in the form of three papers as explained on the following.

Paper I. Model establishment

In the first paper entitled *Simulation of dynamic ductile crack growth using strain-rate and triaxiality-dependent cohesive elements* [9], a finite element model is established in which cohesive elements are both strain-rate and stress triaxiality dependent. The crack growth is considered to be ductile. To account for the effect of stress triaxiality and strain rate on the cohesive properties, a unit cell obeying the constitutive equations of a rate-dependent Gurson type model has been used. The aim is to investigate the influence of these variables on the energy absorption of a fracture specimen, center cracked M(T) specimen, and on the rate of the crack growth for slow and fast loading speeds. The specimen is made of aluminum alloy 6xxx series and only mode I is simulated. The unit cell is loaded under a variety of stress biaxialities and loading speeds (strain rates). The resulting stress-elongation curves have then been used as input to define traction separation laws (TSL) for the cohesive elements. In this way, it is possible to define cohesive properties as functions of both strain rate and stress triaxiality simultaneously. The calculations show that the variation of the maximum stress in the cell vs. the loading speed (initial applied strain rate) has similar behavior to the rate sensitivity of the bulk material. In other words, the cohesive strength has the same rate of change as the bulk material as a function of strain rate. In the simulations performed, the values of strain rate and stress triaxiality are calculated in the continuum elements and are then transferred to the adjacent cohesive elements to update the cohesive properties.

The simulations show that ignoring the influence of strain rate results in overestimation of the energy absorbed by the specimen, whereas considering it for only bulk material results in highly underestimation of the absorbed energy. They also show that although strain rate sensitivity postpones the crack growth initiation, it favors the crack to grow faster compared to rate independent material. It is also worth noting that for the case under study, ignoring triaxiality variation results in a contrast with ductile fracture assumption due to the high speed of crack growth prediction. The analyses also show that the value of triaxiality increases initially and it drops very quickly when the crack starts to grow, whereas in quasi static cases the value of triaxiality does not decrease. The decrease of the stress triaxiality in dynamic loading is due to the inertia effect. In general, the paper shows that strain rate sensitivity and triaxiality have significant effects on the energy absorption. It also shows that the introduced procedure has the ability to quantify the local effects of stress triaxiality, strain rate and inertia in a proper way.

Paper II. Model verification

In the second paper entitled *Dynamic fracture in aluminum round bars: Experiments and simulations* [7], it has been attempted to validate the procedure used in paper I with experiments. The mechanical properties of the bulk material, aluminum alloy 6060-T6 have been defined through quasi-static and dynamic tests on smooth round bars. Similar procedure as in Paper I has been employed to obtain the effect of strain rate and stress triaxiality on cohesive properties. Dynamic tests have been performed by split-Hopkinson tension bar and a high speed digital camera to measure load and diameter reduction for a variety of notch radii and applied strain rates.

The notched round bars have been modeled by axisymmetric continuum and cohesive elements. The simulations show that the most precise results on load vs. time are obtained when both cohesive and continuum elements are rate sensitive with the same rate dependency as found in the smooth bar experiments. They also show that for the cases studied, the effect of mesh size and adiabatic heating on the load and on the diameter reduction is insignificant. These influences are considerable only at the very last part of deformation. Since the range of the stress triaxiality is relatively low for the cases studied, the authors have not succeeded to use triaxiality dependent cohesive elements similar to paper I. It has been shown that Bridgman's equation is an acceptable assumption to calculate average stress triaxiality for obtaining the cohesive properties. It is also discussed that the cohesive energy calculated by the recommended method needs to be modified for high notch radius due to the very low stress triaxiality values. The models can simulate diameter reduction during deformation in a proper manner; however, they cannot calculate final diameter reduction precisely. This is due to high local strains, the use of axisymmetric elements and adiabatic heating. Finally it is shown that the model has the ability to simulate the crack initiation from the notch root for very sharp notches.

Paper III. Model application

The third paper entitled *Simulation of crack extension in aluminum weldment using rate-dependent cohesive elements* [10] reports the application of the model in an aluminum welded compact tension C(T) specimen. The weldment is the source of strength mismatch in the simulated specimen. In this investigation, mixed mode is possible and the crack has the possibility to change its path during the deformation. Triaxiality dependency of cohesive elements has not been considered in this paper, but cohesive properties that have resulted good agreement with quasi-static experiments have been employed. Rate dependency of the cohesive elements has been defined based on the experience of the two previous papers. Since multilayer cohesive elements are applied in different orientations in the model, the subroutine in use needs to have the possibility to automatically recognize and transfer variables between continuum elements and their adjacent cohesive elements. This request has been implemented in the developed subroutine. To simplify the model, strengths of the different areas in the joint have been idealized to lead to a bi-material

mismatch (undermatch) case.

The simulations show that with decreasing the amount of strength mismatch (increasing the strength of the soft zone), the maximum load increases, but there is only a minor influence on the crack growth rate, the crack growth resistance curve and the direction of crack growth. Mismatch introduces a significant effect on these results compared to the model with homogeneous material. The calculations to evaluate the effect of the speed of loading show that although the rate of crack growth increases with the increase in loading rate, the crack growth resistance curves remain unchanged. The influence of element orientation is investigated by introducing another model with a different angle for the cohesive elements. The results show that in the latter model, the crack changes its direction immediately to mode I after extension into the softer material. The results demonstrate that the finite element models in which cohesive elements are imposed at the boundaries of undamaged continuum elements suffer from the dependency of the orientation of the cohesive elements. If the orientations of these elements are defined properly, the model has the ability to perform mixed mode crack growth under dynamic loading while the cohesive zone is rate dependent. The paper also shows that although the maximum load and the crack speed change, the introduced resistance curve is almost insensitive to the considered global changes.

Other articles

In addition to the mentioned articles, three other papers [8,11,12] have been prepared and presented in scientific conferences. These articles are not printed in this dissertation.

Shortcomings of the present work

Using Gurson model to obtain cohesive properties has limited the applied cohesive models to the simulation of ductile crack growth. In addition, Gurson model does not have the possibility to model void growth when tangential load is high. Therefore, it is not possible to obtain cohesive properties in the tangential directions based on Gurson type elements.

In paper II [7], it has been discussed how the recommended approach has limitations for low values of stress triaxialities. It should be noted that it does not mean any limitations for using Gurson model or cohesive models when the stress triaxiality is relatively low. It means that if a single Gurson model is used to obtain cohesive energy, as proposed in the present work, modifications are necessary to be performed on the obtained cohesive energy when the value of applied stress triaxiality is relatively low.

In all the analyses, only 2D elements (plane strain, axisymmetric, plane stress) elements have been used. Using 3D elements extends the application of the present procedure and can improve the accuracy of the results. The finite element model used with the cohesive elements has also the limitation of having the crack move on the boundaries of continuum elements. This limitation has made the crack growth dependency on the

element orientation.

In using split-Hopkinson tension bar, the digital camera was not synchronized with the test rig measurements. This drawback can slightly affect the experimental curves obtained for diameter reduction vs. time.

Recommendations for future works

Cohesive elements which are compatible with shell elements have recently been introduced by other authors, see e.g. [114]. Using rate dependent cohesive elements as proposed here, but in models with shell elements will be of more interest for automotive and aerospace industry.

Adiabatic heating can play an important role in crack propagation, especially for fast running cracks. If cohesive elements which are temperature dependent in addition to rate dependent are used, they will improve the results of simulations in comparison with tests. In general, the developed subroutine proposed here has the ability to consider different local effects simultaneously. If these effects are considered correctly, they can be used in different loading and geometric cases without the need to consider major changes in cohesive properties. It should also be reminded that the experimental rate dependency obtained is for the strain rates up to 1000 1/s and the related curve has been extrapolated for higher values of strain rates. Obtaining rate dependency of the material for higher strain rates can also improve the simulation results.

A bi-material model is assumed for the welded joints which is a major simplification for welded joints. If the aim is to compare the simulation results with real welded joints tested, this simplification will be considerable. To improve the model, it is recommended to use rate dependent cohesive elements with tri-material. Recently, cohesive elements have been used under dynamic loading conditions for functional graded materials (FGM). Similar approaches, but for rate dependent cohesive elements, can be used for welded joints in which graded inhomogeneity of material is considered. It should be reminded that considering FGM in this case might be complicated and needs high amount of information on material properties at the weld area.

Dynamic Fracture and Cohesive Zone Modeling

Abstract

The increasing application of aluminum alloys in automotive and aerospace industries and the importance of estimating the effect of growing cracks on the energy absorption of the structures under dynamic loading, e.g. crashworthiness, is an important issue nowadays. Since in many cases, the failure mechanism in such structures is ductile, it will be very useful for design purposes to provide a reliable numerical model which can simulate ductile crack initiation and growth under dynamic loading conditions. One of the important applications of the model is for the aluminum welded structures which is a multi material case.

This chapter reviews the physical aspects that are necessary to be explained in order to solve ductile dynamic crack growth problems. The emphasis will be on using local approaches and in particular cohesive elements for simulating crack growth under dynamic loading conditions. Section 1 addresses macroscopic linear elastic fracture mechanics (LEFM) and elastic plastic fracture mechanics (EPFM) in quasi-static cases and their limitations. Section 2 discusses the effect of dynamic loading on structures and the related important phenomena. In section 3, local approaches and specifically cohesive zone modeling are discussed. Section 4 pays attention to the application of Gurson type models and cohesive zone modeling in simulation of fast running cracks. Section 5 has a brief review on the application and fracture simulation of aluminum weldment. In section 6, split-Hopkinson tension bar as the test rig used in the thesis is reviewed briefly.

1 Macroscopic fracture mechanics

Macroscopic fracture mechanics represents formulations in order to obtain the stress and strain distribution in structures containing crack(s). It also represents criteria to predict the capacity of structures to resist the growth of the existing cracks. This field of mechanical science is generally divided into "linear elastic fracture mechanics" (LEFM) and "elastic plastic fracture mechanics" (EPFM).

1.1 Linear elastic fracture mechanics (LEFM)

Stress values around a crack tip are always higher than the surrounding material because of geometric discontinuity. If this stress is lower than the yield stress of the material or the nonlinear material deformation is limited to a very small region around the crack tip, linear elastic formulations can be used. In this case, the theory of elasticity can be employed to calculate the stress field at the crack tip area.

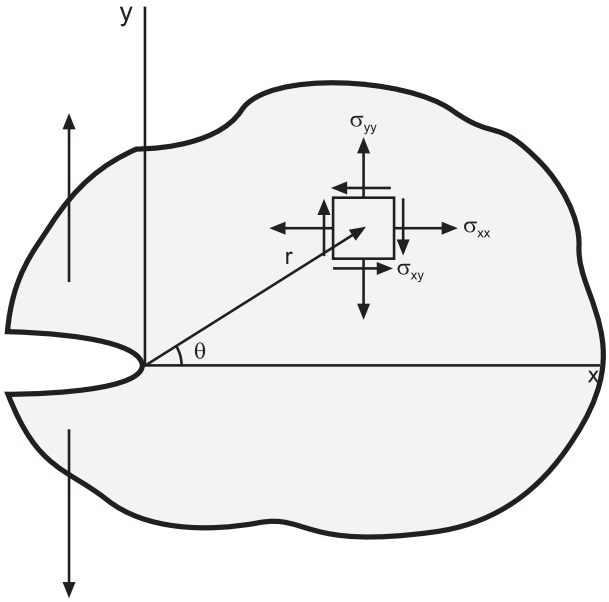

Figure 1: Stresses and coordinates at the tip of an arbitrary crack

The stresses for a material element shown in Fig. 1, for $r \to 0$, is expressed as:

$$\sigma_{ij} = \frac{K}{\sqrt{2\pi r}} f_{ij}(\theta) \tag{1}$$

As Eq. 1 is derived for an arbitrary crack in an arbitrary body with an arbitrary loading, it must be able to describe the stress distribution for each and every crack in each and every elastic body. Therefore, K will appear in every crack problem. K is known as the stress intensity factor and is shown by K_I, K_{II} and K_{III} depending on the direction of the stresses at the crack tip. In a general form, K can be expressed as:

$$K = \beta(\frac{a}{L}, mode\ of\ loading)\sigma\sqrt{\pi a} \tag{2}$$

where β is an elastic geometry factor, σ is the applied stress, a is the crack length and L is a length dimension describing the geometry of the cracked body. Equation 2 shows that K is not only dependent on the mode of loading, but also the crack and the part dimensions. Because of the simplicity with theory of elasticity, formulations have been developed to obtain β as functions of different geometries and loading modes.

Fracture will occur when the stresses at the crack tip exceed a value which the material can bear. This means that the fracture can occur when K becomes too high for the material. The allowable maximum value of K for each material can be obtained by test and is known as the fracture toughness of the material shown as K_c.

If yielding happens at the crack tip area, the size of the plastic zone at the crack plane

will be:

$$r_p = \frac{K^2}{\alpha\pi\sigma_y^2} \tag{3}$$

where σ_y is the yield strength of the material and α is a parameter depending on the stress state at the crack tip (α=2 for plane stress and α=6 for plane strain). The size of plastic zone can be used as a measure for validity of LEFM approaches.

Based on Eq. 1, the stress becomes zero far from the crack tip which is incorrect since this value is equal to the applied stress. The reason is that Eq. 1 does not provide the complete solution which is a series of terms. In fact, the stress value normal to the crack surfaces on the symmetry line for mode I loading is:

$$\sigma_{yy} = \frac{K_I}{\sqrt{2\pi x}} + Cx^0 + Dx^{\frac{1}{2}} + Ex^1 + ... \tag{4}$$

It should be noted that Eq. 3 was derived using only the first term of the stress distribution in Eq. 4. If the plastic area is so large that the other terms of the stress series come into play, stress values will not be only a function of K and using the same K values does not guarantee equal stress distributions. In this case, fracture is not likely to happen at the same value of K known as K_c. Since r_p depends on both K and σ_y, it is concluded that K_c is better applicable for materials of low toughness and high yield strength. It is worth noting that to obtain K_c from tests (usually on C(T) specimens), the obtained load-displacement curves must be linear or close to linear to ensure small plastic deformation at the crack tip. In the cases where plastic area at the crack tip is large (high toughness, low yield strength), EPFM is used.

1.2 Elastic-plastic fracture mechanics (EPFM)

If the material surrounding the crack tip experiences local plastic stresses and the size of the plastic zone is not ignorable, EPFM is used. Two important parameters that can characterize the crack tip conditions are J contour integral and "crack tip opening displacement" (CTOD) of which only the former one is described briefly as follows.

Rice [105] introduced J integral in 1968. The J integral is defined as:

$$J = \int_\Gamma \left(wdy - T_i \frac{\partial u_i}{\partial x} ds \right) \tag{5}$$

where w is the strain energy density, T_i are components of the traction vector, u_i are the displacement vector components, and ds is a length increment along the contour Γ around the crack tip. Rice also proved, based on a theorem of Eshelby [42], that for hyperelastic materials, this integral is path independent. The parameter is actually equivalent to energy release rate, the rate at which energy is absorbed by growth of a crack, but in a nonlinear elastic body. This condition does not put any restriction on the use of J only as long as there is no unloading. In the other words, the resulting equations are valid for load control cases, so that the fracture analysis is meaningful only up to the maximum load.

Regarding J integral being path independent (based on the deformation theory of plasticity) and by considering power law for plastic stress-strain of material, Hutchinson [56] and Rice and Rosengren [106] showed how J integral can describe the stress and strain distribution at the region around the crack tip :

$$\sigma_{ij} = \sigma_0 \left(\frac{EJ}{\alpha \sigma_0^2 I_n r} \right)^{\frac{1}{n+1}} \tilde{\sigma}_{ij}\left(n, \theta\right) \tag{6}$$

and

$$\epsilon_{ij} = \frac{\alpha \sigma_0}{E} \left(\frac{EJ}{\alpha \sigma_0^2 I_n r} \right)^{\frac{n}{n+1}} \tilde{\epsilon}_{ij}\left(n, \theta\right) \tag{7}$$

where I_n is an integration constant as a function of n, the strain hardening exponent of the material. α is a dimensionless parameter used in the power law equations and $\tilde{\sigma}$ and $\tilde{\epsilon}$ are dimensionless functions of n and θ. Equations 6 and 7 are known as HRR singularity since they show stress and strain singularities (infinite stresses and strains at the crack tip). It is worth noting that the analysis that results in HRR singularity does not consider the effect of blunted crack on the stress field.

Similar to LEFM, it is possible to define a J value from test where the crack growth is initiated. This J is known as the critical J or material toughness which ensures similar stress and strain distribution at the crack tip area when fracture happens in a structure at hand.

Using J integral as a single parameter to characterize crack tip conditions fails in the presence of excessive plasticity. In such cases, fracture toughness is not a material property anymore and depends on the specimen size and geometry and loading mode. This argument was a motivation for developing two parameter fracture theories, one of which is the $J-Q$ methodology developed by O'Dowd and Shih [95, 96]. In this methodology, Q is defined as:

$$Q = \frac{\sigma_{\theta\theta} - \left(\sigma_{\theta\theta}\right)_{HRR}}{\sigma_0} \; at \; \theta = 0 \; and \; \frac{r\sigma_0}{J} = 2 \tag{8}$$

where $\sigma_{\theta\theta}$ is the stress value calculated from finite element analysis containing sufficient fine mesh to resolve the field at length $r = \frac{2J}{\sigma_0}$ and $\left(\sigma_{\theta\theta}\right)_{HRR}$ is the stress obtained from HRR singularity formulation. Q in this case represents the constraint at the crack tip. Based on the two parameters approach, a laboratory specimen must match the constraint of the structure at hand, therefore the two geometries should have the same Q at failure in order to have the same critical J.

2 Dynamic loading and fracture mechanics

Dynamic fracture mechanics is regarded in two general cases [91]: (i) Stationary crack subjected to impact loading, *impact fracture mechanics* and (ii) Fast motion of the crack tip, *fast fracture mechanics* . In both cases, additional influences compared to quasi-static cases have to be considered: The high speed of deformation introduces stress waves in

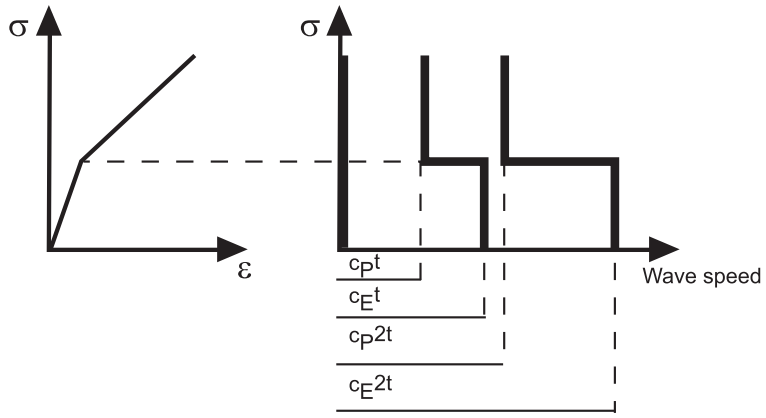

Figure 2: Propagation of a disturbance of magnitude σ from the end of a bar of an elastic-linear plastic material at two different times, t and $2t$ [73]

the structure. Inertia effects become significant and can affect the energy absorption of the structure. Strain rate increases the flow stress and influences the strain hardening of metals. And the local temperature increase due to adiabatic heating reduces the flow strength and counteracts the strain rate hardening.

In general, flow stress in a uni-axial tension case can be expressed as:

$$\sigma = \sigma(\epsilon, \dot{\epsilon}, \Theta) \tag{9}$$

where ϵ and $\dot{\epsilon}$ are strain and strain rate, respectively and Θ is the temperature.

In the following subsections, each of these influences are discussed in more details.

2.1 Stress waves propagation and inertia effects

Consider a straight bar influenced by impact loading at one end. The stress wave propagation in the bar is expressed as:

$$\frac{\partial^2 u}{\partial x^2} = \frac{1}{c_0^2}\frac{\partial^2 u}{\partial t^2} \tag{10}$$

where $c_0 = \sqrt{\frac{E'}{\rho}}$ is the characteristic longitudinal wave velocity in the uniform bar and E' is the Young's modulus of the material. Whether the material is elastic or plastic, the wave speed is different. Figure 2 shows how plastic stress wave is slower than elastic one.

When the longitudinal stress wave is moving in the bar, another wave is introduced normal to the longitudinal direction because of poisson's ratio which is called dilatational wave with the velocity of c_d. It can also lead to a shear or transverse wave propagation with velocity c_s. For the elastic case, the mentioned wave velocities can be presented as [73]:

$$C_d = \sqrt{\frac{E(1-\nu)}{\rho(1+\nu)(1-2\nu)}}, \quad C_s = \sqrt{\frac{G}{\rho}} = \sqrt{\frac{E}{2\rho(1+\nu)}} \tag{11}$$

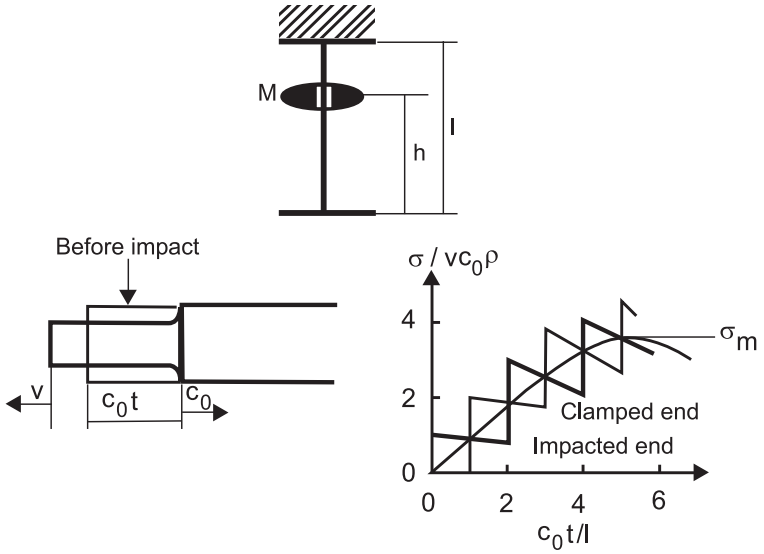

Figure 3: Dynamic loading of a wire of mass m and impulsive amplitude created by the shock in the case of elastic behavior of the wire [124]

The other stress wave introduced in structures is Rayleigh surface wave, C_R, e.g. see Freund [45]:

$$C_R = C_s \frac{0.862 + 1.14\nu}{1 + \nu} \tag{12}$$

To evaluate how these waves induce stress in a structure, consider a wire of mass m with cross section A impacted by heavy mass M (Fig. 3). For elastic behavior, we will have:

$$Mg(h + \delta l) = \frac{1}{2}\frac{\sigma_m^2}{E} Al \tag{13}$$

and for $h >> \delta l$:

$$\sigma_m = \rho V c_0 \sqrt{\frac{M}{m}} \tag{14}$$

Figure 3 shows that the stress waves in two ends of the wire have time difference and σ_m is obtained after some time. It can also be shown that the stress initially transmitted to the wire is proportional to the speed, not the mass. The value of elastic stress wave in the continua is:

$$\sigma_m = \rho V c_0 \tag{15}$$

Therefore, the stress wave introduced is not only a function of material density (inertia effect), but also the speed of the load. Since a uniaxial stress wave can introduce multiaxial stresses with different speeds, Eqs. 11 and 12, the stress state at a crack tip, whether it is a fast running crack or a crack under high speed of loading, is a function of time and is different from quasi-static cases. For example, these multiaxial stress waves can lead

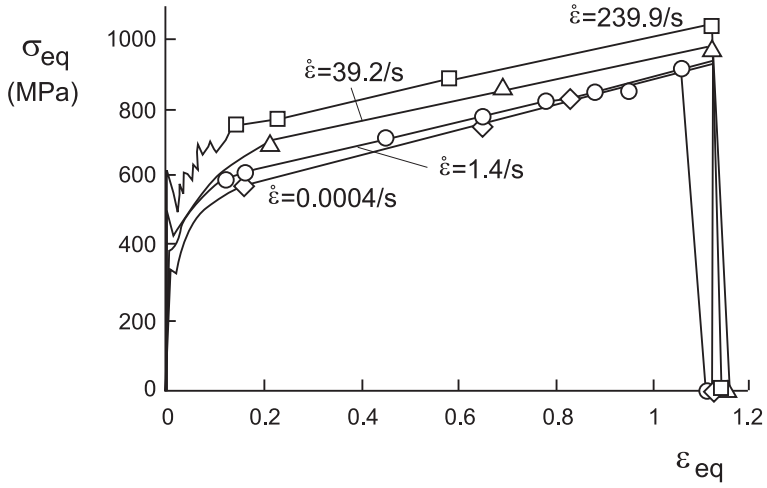

Figure 4: Equivalent stress-strain curves for mild steel [4]

to crack closure [126] and local unloading at the crack tip or produce lateral tensile or compressive stresses in the structure [40]. Inertia can also affect localization in structures. For example, when long tensile bars are loaded by high speed deformation, more than one necking can happen [22, 90].

2.2 Strain rate sensitivity and thermal effect

A material is rate sensitive if the stress-strain curve changes with the rate of loading. A sample of this phenomenon is shown in Fig. 4.

El-Magd et al. [41] showed that applying static stress-strain curve in crash analysis of aluminum car structures would cause a wrong prediction of fracture, and that it is necessary to consider rate sensitivity of the material. Many studies on ductile dynamic fracture [16, 17, 39, 53, 71, 85, 87, 93, 143] are based on strain rate viscoplastic solid as follow [98]:

$$\dot{\bar{\epsilon}}^{pl} = \dot{\epsilon}_0 \left(\frac{\bar{\sigma}}{g\left(\bar{\epsilon}, \Theta\right)} \right)^{(1/m)} \tag{16}$$

where $\dot{\bar{\epsilon}}^{pl}$ and $\dot{\epsilon}_0$ are the plastic and a reference strain rate, respectively. m is a rate exponent and $m \to 0$ means rate-independent material. g function is defined as:

$$g\left(\bar{\epsilon}, \Theta\right) = \sigma_0 \left[1 - \beta\left(\Theta - \Theta_0\right)\right] \left[1 + \frac{\bar{\epsilon}}{\epsilon_0}\right]^N \tag{17}$$

where N is the strain hardening of the material and β is known as thermal softening coefficient. Θ_0 and σ_0 are reference temperature and stress, respectively and $\bar{\epsilon}$ is the equivalent plastic strain. If there is no temperature change due to adiabatic heating or

material is insensitive to temperature change, Eq. 17 is simplified to:

$$g\left(\bar{\epsilon}\right) = \sigma_0 \left[1 + \frac{\bar{\epsilon}}{\epsilon_0}\right]^N \tag{18}$$

Although Eqs. 16 and 18 have widely been used in the literature, ABAQUS finite element code [1] uses Cowper-Symonds law [33] named "overstress power law" as:

$$\dot{\bar{\epsilon}}^{pl} = D(\Theta, f_i)\left(\frac{\bar{\sigma}}{\sigma_0} - 1\right)^{p(\Theta, f_i)} \tag{19}$$

where $D(\Theta, f_i)$ and $p(\Theta, f_i)$ are material parameters that can be functions of temperature and, possibly, of other predefined state variables. The other parameters are the same as used in Eq. 16 and σ_0 is the same as g function in Eq. 17. It is worth noting that if $\bar{\sigma}$ and σ_0 are considered to be the yield strength of the material at a certain strain rate and at quasi-static conditions, respectively, and D and p are constant, Eq. 19 is reduced to pure isotropic hardening case in which viscosity, i.e. time dependent effects, are not considered.

When the rate of deformation in a structure is high and failure intends to happen in a short time, the material does not have enough time to transfer the heat induced caused by plastic dissipation to the environment. Therefore, the structure heats up locally. The phenomenon is called adiabatic heating and can result in a decrease of flow stress of the material. The effect of temperature on flow stress has been included in Eq. 17. The heat increase can be calculated by this equation:

$$\rho c_p \frac{\partial \Theta}{\partial t} = \eta \boldsymbol{\sigma} : \dot{\boldsymbol{\epsilon}}^{pl} \tag{20}$$

where Θ is the temperature, $\boldsymbol{\sigma} : \dot{\boldsymbol{\epsilon}}^{pl}$ is the inner product of stress and plastic strain rate tensors, ρ is density, c_p is the heat capacity, and η defines the fraction of plastic strain energy converted to heat and its typical value for metals is 0.9 [125].

2.3 Dynamic J integral

In a cracked body under quasi-static loading, the conservation of energy reads:

$$\frac{d}{da}\left(F - U - W\right) = 0 \tag{21}$$

or

$$\frac{d}{da}\left(F - U\right) = \frac{dW}{da} \tag{22}$$

where F and U are the work done by the applied load and the strain energy stored in the structure, respectively. W is the energy required for the fracture and da is the crack extent. Fracture will occur when enough energy can be delivered to provide for the fracture energy. $\frac{dW}{da}$ is the energy release rate.

In dynamic fracture, kinetic energy due to the dynamic deformations and inertia needs to be considered which reads:

$$\frac{dW}{da} = \frac{d}{da}(F - U - K) \tag{23}$$

Therefore, the energy release rate for a steady state dynamically propagating crack in a plate can be expressed as:

$$G = \frac{1}{B}\left(\frac{dF}{da} - \frac{dU}{da} - \frac{dK}{da}\right) = \frac{1}{B.V}\left(\frac{dF}{dt} - \frac{dU}{dt} - \frac{dK}{dt}\right) \tag{24}$$

where B is the plate thickness, K is the kinetic energy stored in the plate, and V is the speed of the crack growth. Similar to quasi-static cases, to obtain macroscopic behavior and fracture toughness in dynamic case, dynamic J integrals should be defined based on the energy release rate. Nishioka and Atluri [92] presented path-independent elastodynamic J-integral and later Atluri, Nishioka and Nakagaki [14] derived the general form of path-independent integral for nonlinear dynamic fracture mechanics and called it T^*.

Dynamic J integral formulation for numerical simulations was also presented by Nakamura et al. [79] and Moran and Shih [76] who added more terms to Nakamura's equation which involves an area integral as well as a line integral. It is important to consider that the integral is not path-independent like quasi-static cases and does not necessarily serve as a characteristic parameter, see Needleman and Tvergaard [85]. They showed that J is path-independent only in early stages of crack blunting and decreases smoothly as plastic flow becomes more extensive and the value of the area integral is typically 8 to 10 percent of the total J value. On the other hand, Basu and Narashimhan [17] showed numerically that similar to quasi-static loading, J integral is not the only parameter to characterize the dynamic elastic-plastic crack tip fields. Therefore, they considered Q parameter in their analyses and showed that constraint effect under dynamic loading can be considerably different and even more important than quasi-static cases. They also showed that Q is a function of both J and its time derivative.

2.4 Scales in dynamic fracture

In general, dynamic fracture is important when the inertia of relatively large pieces of material is large enough to balance the energy of fracture required, including the kinetic energy. For a propagating crack, dynamic effects are important when the crack tip speed is considerable compared to stress wave velocities. This is the necessary condition for macroscopic dynamic fracture, otherwise, all fractures are dynamic at some scale [34]. For example, at the atomic scale, the most fundamental for understanding crack propagation is the inertia of individual atoms even when the crack at the macroscopic scale appears to be advancing quasi-statically. Atomic studies, largely represented by molecular dynamics simulations, have been used significantly to date to provide fundamental understanding of underlying basic physical processes of dynamic fracture, rather than being predictive or specific to a particular material.

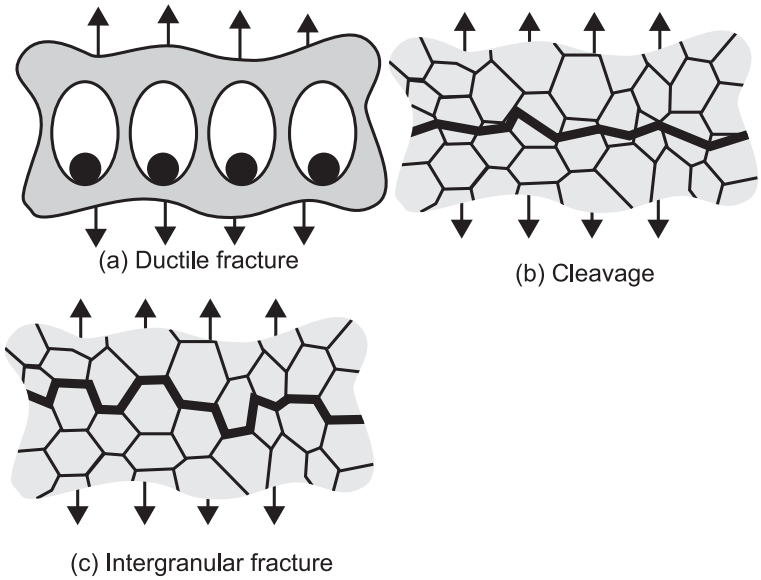

Figure 5: Different micromechanisms of fracture in metals under monotonic loading conditions [5]

In addition to macroscopic and microscopic scales, geological scales and atomic scales are important in dynamic fracture regarding their applications in different fields. For example, earthquake modeling is concerned with dynamic shear cracks under slow loading. Although the load is slow, it is shown that there is a complex phenomenon of dynamic cracking under such conditions [20].

For a comprehensive review of the different scales on dynamic fracture, see [34].

In the present thesis, microscopic and macroscopic scales have been in focus. In this way, mechanisms of nonlinear damage at microscopic scale are simulated and the analyses are performed for an appropriately defined problem in macroscopic fracture.

3 Fracture mechanisms in metals - local approaches

In order to obtain a good understanding of fracture process and simulating crack initiation or growth, it is necessary to understand what happens in the material at micro scale under slow or fast loading conditions. Under the influence of monotonic loading, the most common fracture mechanisms in metals and alloys are ductile fracture, cleavage and intergranular fracture, Fig. 5. Ductile materials usually fail as the result of nucleation, growth and coalescence of microscopic voids that initiate at the inclusions and second phase particles. Cleavage fracture involves separation along specific crystallographic planes. Intergranular fracture occurs when the grain boundaries are the preferred fracture path in the material. This article reviews only ductile fracture as the main fracture mechanism for aluminum alloys at room temperature.

The limitations regarded to analytical and macroscopic fracture mechanics approaches were briefly explained in the previous sections. Because of the limitations of macroscopic approaches, another approach has been developed since the 80s called "local approach" to model the fracture based on the local fracture criteria (see e.g. [21, 77, 101, 102, 109]). The general advantage with these approaches is that the parameters of the respective models depend only on the material, and not on the geometry. Therefore, by using these approaches, it is possible to transfer fracture criteria from specimens to structures over a wide range of geometries and dimensions as long as the fracture mechanisms are the same.

The first approaches [21, 77], used a conventional behavior for the material supplemented by models of local fracture processes to model brittle fracture. In later studies, softening due to the micromechanical mechanisms of damage was introduced locally to model ductile fracture [52, 104, 109]. In these models, an equation for the evolution of damage variables and a correlation between damage variables and stress and strain are needed to be established. For that purpose, a representative volume element (RVE) is used as a volume element of the material. In an RVE, the microscopic properties and mesoscopic quantities are linked in order to generate a macroscopic constitutive equation for the material damage. A material element can have its complexity regarding microstructural damage and with increasing this complexity, the possibility to obtain an analytical constitutive equation decreases. In practice, using relatively simple unit cells can be used to simulate ductile damage mechanism. For example, Koplik and Needleman [62] used a plastically deforming matrix containing a spherical void to model void growth and coalescence with respect to Gurson model [52]. In addition to micromechanically based models, there are phenomenological models for material separation introduced as material elements surrounded by elastic-plastic non failure material. The most widely known of the former approach is the Gurson model, which was later improved by Tvergaard [133] and Tvergaard and Needleman [140] known as Gurson-Tvergaard-Needleman or GTN model. The most well-known phenomenological model is cohesive zone model. Each of these models are described in the following.

3.1 Gurson type model

Ductile crack growth consists of three main steps: Void initiation from second phase inclusions, void growth, and finally, void coalescence. To obtain the related constitutive equation for damage in this case, not only equivalent stress, but also hydrostatic stress is important. Maybe the most well known work in this regard was performed by Gurson [52] in 1977. He examined different material unit cells including isolated voids. He considered the material surrounding the void to be rigid-plastic and obtained a constitutive equation for cylindrical and spherical void shapes. The following approximate yield function is the result of his work:

$$\Phi = \frac{\sigma_e^2}{\bar{\sigma}^2} + 2f cosh\left(\frac{3\sigma_h}{2\bar{\sigma}}\right) - 1 - f^2 = 0 \tag{25}$$

where $\bar{\sigma}$ is the matrix yield strength, f is the void volume fraction and is defined as the volume of void divided by volume of the cell. With $\boldsymbol{\sigma}$ the stress tensor and $\mathbf{I}$ the second

order identity tensor, σ_h and σ_e will be:

$$\sigma_h = \frac{1}{3} trace(\boldsymbol{\sigma}), \quad \sigma_e = \sqrt{\frac{3}{2}\mathbf{S}:\mathbf{S}}, \quad \mathbf{S} = \boldsymbol{\sigma} - \sigma_h \mathbf{I} \tag{26}$$

Tvergaard [133] modified Gurson model by adding three additional parameters:

$$\Phi = \frac{\sigma_e^2}{\bar{\sigma}^2} + 2q_1 f cosh\left(\frac{3q_2\sigma_h}{2\bar{\sigma}}\right) - 1 - q_3 f^2 = 0 \tag{27}$$

He suggested that $q_1 = 1.5$, $q_2 = 1$ and $q_3 = q_1^2$. Details on how to find q values are explained elsewhere [135].

The Gurson model presented by Eq. 25 does not contain any separate coalescence criterion. To facilitate coalescence predictions by the Gurson model, Tvergaard and Needleman [140] proposed an effective void volume fraction f^* as follows:

$$f^* = \begin{cases} f & , f \leq f_c \\ f_c + \frac{f_u^* - f_c}{f_f - f_c}(f - f_c) & , f > f_c \end{cases} \tag{28}$$

where f_f and f_c denote the void volume fraction at failure and at a critical situation at which f starts to deviate from f^*. f_u^* is the value of f^* at fracture. The combination of Eqs. (27) and (28) is known as Gurson-Tvergaard-Needleman or GTN model.

In general, the evolution of void volume fraction results from growth of the existing voids and nucleation of new voids. Chu and Needleman [28] presented the following void nucleation rate criteria whether they are strain or stress controlled as:

$$\dot{f}^n_{nucleation} = \frac{f_N^n}{S_N^s\sqrt{2\pi}}\ exp\left[-\frac{1}{2}\left(\frac{\epsilon^p - \epsilon_N}{S_N^n}\right)^2\right]\dot{\epsilon}^p \tag{29}$$

$$\dot{f}^s_{nucleation} = \frac{f_N^s}{S_N^s\sqrt{2\pi}}\ exp\left[-\frac{1}{2}\left(\frac{\sigma_{eq} + \sigma_m - \sigma_N}{S_N^s}\right)^2\right](\dot{\sigma}_{eq} + \dot{\sigma}_m) \tag{30}$$

where f_N^n and f_N^s are the volume fractions of void nucleating particles, S_N^n and S_N^s are the standard stress deviations, and ϵ_N and σ_N are the mean nucleation strain and nucleation stress respectively. The strain controlled nucleation can be used for small particles and the stress controlled nucleation is proper for large inclusions [71].

The application of the approach in dynamic cases will be reviewed in section 4.1.

3.1.1 Complete Gurson model

Zhang et al. [154] presented another version of the Gurson model which they called "complete Gurson model". They used Thomason's coalescence criteria [128] combined with the Gurson model and succeeded to eliminate critical void volume fraction (in Eq. 28) which works well only for low stress triaxiality cases, and slightly worse for high stress triaxiality cases [62]. They also proposed final void volume fraction to be a function of initial void volume fraction. The research has been done for quasi-static loading only and no investigation has been performed in dynamic cases as yet.

3.2 Models of ductile fracture micromechanisms under dynamic loading

The ductile fracture micromechanisms in quasi-static cases, Gurson type model and also the macroscopic influences of dynamic loading have been explained briefly in the previous sections. To develop Gurson constitutive equations in dynamic cases, two subjects need to be considered: (i) how to consider the effect of strain rate, inertia and temperature increase in the constitutive equations and (ii) how and if the Gurson parameters are influenced.

It was shown in the previous section that void nucleation formulations, Eqs. 29 and 30, are defined as the functions of changes of stress and/or strain versus time. A similar set of equations can be used for dynamic cases, see e.g. [85].

During the last decades, many investigations have been performed on void expansion simulation under dynamic loading. The first step in this regard is to consider the stress in the constitutive equation not only as a function of strain but also strain rate and temperature. A pioneering work on considering the effect of material rate sensitivity in Gurson type equations was performed by Pan et al. [98] and was developed by Needleman and Tvergaard [85] to consider the void nucleation and temperature increase in addition to rate sensitivity. Whether the deformation is slow or fast, the rate of the increase of void volume fraction for an incompressible matrix material is:

$$\dot{f}_{growth} = (1-f)\dot{\boldsymbol{\epsilon}}^{pl} : \mathbf{I} \tag{31}$$

In rate-dependent representation of Gurson constitutive equation, Φ serves as a plastic potential [98] and the plastic part of the rate of deformation is taken normal to the flow potential as:

$$\dot{\boldsymbol{\epsilon}}^{pl} = \dot{\Lambda}\frac{\partial \Phi}{\partial \boldsymbol{\sigma}} \tag{32}$$

By setting the rate of the plastic work equal to the matrix dissipation, we will have:

$$\boldsymbol{\sigma} : \dot{\boldsymbol{\epsilon}}^{pl} = (1-f)\bar{\sigma}\dot{\bar{\epsilon}} \tag{33}$$

and the plastic work proportionality factor, $\dot{\Lambda}$ is determined as:

$$\dot{\Lambda} = \frac{(1-f)\bar{\sigma}\dot{\bar{\epsilon}}}{\boldsymbol{\sigma} : \frac{\partial \Phi}{\partial \boldsymbol{\sigma}}} \tag{34}$$

The effect of temperature increase and the strain rate on stress-strain curve of the matrix material can be calculated by the equations shown in section 2.2.

Finally, the rate of deformation (total strain rate) will be calculated as the sum of an elastic part, a plastic part and a part due to thermal straining. Based on the Hooke's law, the Jaumann stress rate will then be calculated as:

$$\dot{\boldsymbol{\sigma}} = \mathbf{C} : \left(\dot{\boldsymbol{\epsilon}} - \dot{\Lambda}\frac{\partial \Phi}{\partial \boldsymbol{\sigma}} - \alpha\dot{\Theta}\mathbf{I}\right) \tag{35}$$

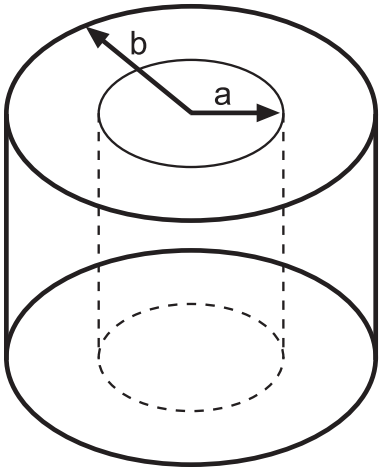

Figure 6: Long circular cylindrical cell model [53]

where $\mathbf{C}$ is the modulus of elasticity tensor and α is the thermal expansion coefficient of the material.

For details on how to implement the above formulations to a numerical finite element code like ABAQUS, see [78].

In the formulations obtained above, the influence of micro-inertia in a single RVE has been ignored. The inertia effect on crack growth can be considered in macroscale in the form of transient dynamic analysis performed for a structure containing elements which obey dynamic Gurson type constitutive equations. The application of dynamic Gurson type models in simulating fast fracture or impact fracture will be reviewed in section 4.1. To consider the micro-inertia effects in a Gurson constitutive equation, Hao and Brocks [53] combined Eq. 35 and the momentum balance equations for a long cylindrical cell model, Fig. 6. The resulting radial stress was then obtained as sum of two parts, one part related to viscoplasticity of the material and the second part due to the inertia effects. The mesoscopic yield function they developed was not only a function of temperature, strain rate and material properties like thermal expansion coefficient and rate sensitivity, but also the cell outside diameter, $2b_0$, which the spacing of void nucleation sites, and density of the matrix material:

$$\Phi = \frac{\sigma_e^2}{\sigma_{Y1}^2} + 2q_1 f cosh\left(\frac{3q_2\sigma_h}{2\sigma_{Y2}}\right) - 1 - q_3 f^2 \tag{36}$$

where σ_{Y1} and σ_{Y2} are functions of porosity (f), strain rate, temperature, cell outside radius, visco plastic strain and the matrix material properties (for example, the effect of material density is considered in σ_{Y2}).

The importance of micro-inertia on the expansion rate and coalescence of the voids depends on the rate of deformation, spacing of the voids, material porosity and density. Johnson [58] considered a hollow sphere of inner and outer initial radii as b_0 and a_0 respectively for the cell model, Fig. 7. He considered an incompressible perfectly plastic material with mass density of ρ, and succeeded to obtain a relationship between the stress σ_b and

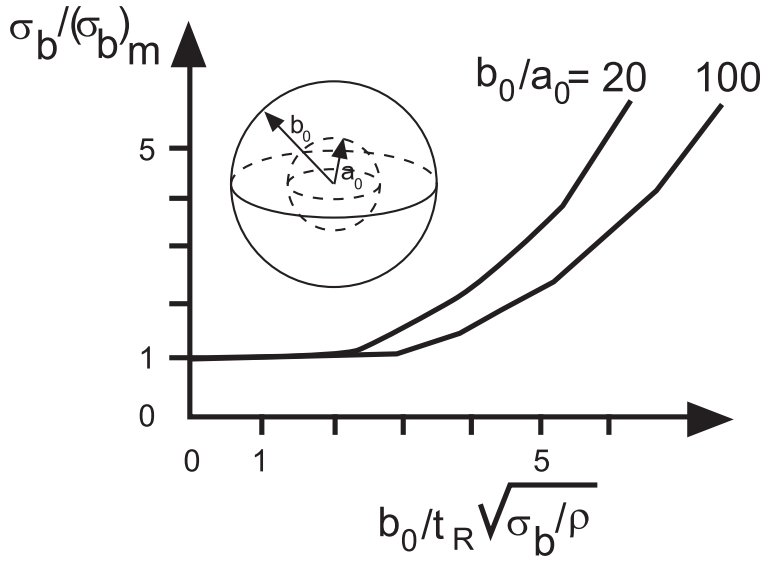

Figure 7: Relation between the normalized tensile stress applied on the outer surface of the sphere and the time to rupture. a_0,b_0: inner and outer radius of unit cell. t_R: time to rupture, ρ: material density. [58]

the time to rupture t_R as shown in Fig. 7. The figure shows that if $\frac{b_0}{t_R\sqrt{\sigma_0/\rho}}$ is larger than 2, which means t_R is less than $\frac{1}{2}\frac{b_0}{\sqrt{\sigma_0/\rho}}$, the effect of the inertia of individual voids is important. In this case, if we consider the crack growth speed as $\frac{2b_0}{t_R}$, it means that crack speed must be more than $4\sqrt{\sigma_0/\rho}$. Based on these results, the inertia effect is important when the crack speed is higher than 1200 m/s in high strength steel (σ_0=790 MPa, ρ=7720 kg/m3) and higher than 1100 m/s for aluminum alloy 6XXX series (σ_0=225 MPa, ρ=2710 kg/m3). A similar result had been obtained by Glennie [49] in 1972 who considered dynamic growth of void in a plastic material subjected to a far-field starin rate and mean normal stress. He concluded that micro-inertia is important when $3\sigma_0 \approx \frac{3}{2}\rho\left(\frac{b_0}{t_R}\right)^2$ or $2\frac{b_0}{t_R} \approx 4.83\sqrt{\frac{\sigma_0}{\rho}}$. Curran et al. [36] considered rate sensitive material for a hollow sphere of internal radius a subjected to internal constant pressure P_0. The considered material was rigid, perfectly plastic with a viscosity coefficient. Numerical investigation for aluminum alloy (Fig. 8) showed that the inertia effect becomes important for quite large voids larger than 10 μm and for a wide range of radii a, maximum rate governs by the viscous regime only. Klöcker and Montheillet [60] studied the effect of hydrostatic load and inertia on the expansion of a spherical void subjected to an axisymmetric deformation similar to a notched round bar for the case where stress flow obeys the rule $\sigma = \sigma_0 + \nu\dot{\epsilon}_{eq}$ and showed the important effect of inertia when $\dot{\epsilon}$ >1000 s^{-1}. They showed that triaxiality and inertia are both important parameters in the void expansion rate.

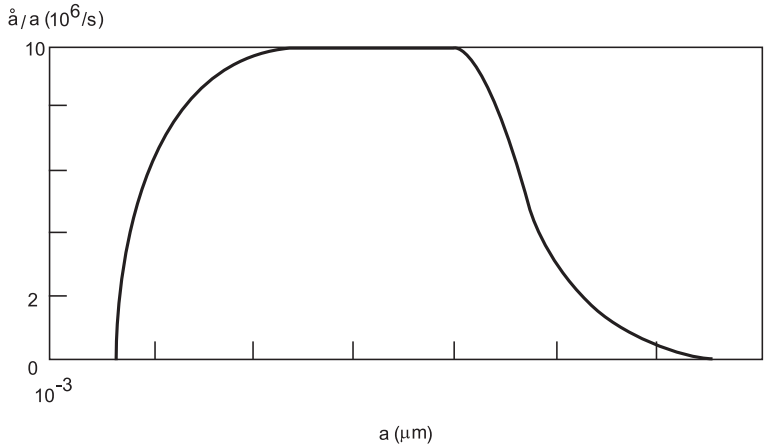

Figure 8: Void expansion rate as a function of void radius in aluminum under a hydrostatic tensile stress [36]

In all of the references mentioned up to now, the void and cell shapes are either spherical or cylindrical. There have been researchers who have considered other shapes in micromechanisms based constitutive equations, e.g. [47, 50]. In this overview, only Liu's [69] investigation is shortly presented. He developed a dynamic void growth model including strain rate, void shape, and inertia effect as a combined set. The void shape he considered was ellipsoidal. He used elastic rigid plastic rate sensitive material and combined the constitutive equations developed by Gåråjeu et al. [47] and Molinari and Mercier [75]. His model is reduced to Gåråjeu's model when the inertia effect is neglected and returns to Molinari's model when the void shape effect is ignored (spherical void and cell shape). Obviously, the model decreases to Gurson model, when both of the mentioned parameters are ignored. He concluded that higher initial void volume fraction decreases the effect of inertia. He also showed that void shape can influence inertia effect remarkably only when the triaxiality is low, but when the triaxiality is high, spheroidal shape will change to spherical. He also demonstrated that increasing strain rate will increase the inertia effect, but this effect is significant only when the strain rate is over 10000 $1/s$ for aluminum alloy.

The other complicating factor in developing ductile fracture process, whether it is slow or fast, is that voids can join by mechanism other than simple expansion up to coalescence. Fracture surfaces often show evidence of plastic strain localization in ligaments between voids resulting in coalescence by shearing of the ligament [135]. These shear bands can be divided into two types; those in which thermal softening role is negligible which are called isothermal shear bands and those in which thermal softening is very effective which are called adiabatic shear bands. Localization of deformation in a narrow band makes a thermo-plastic instability. Plastic shear gives rise to adiabatic heating in the band and therefore the flow stress decreases in that region. Because of this flow stress decrease and the geometry of the band, very high local strains exist in that region. These bands propagate similar to mode II fracture and are formed preferably in compressive zones and at

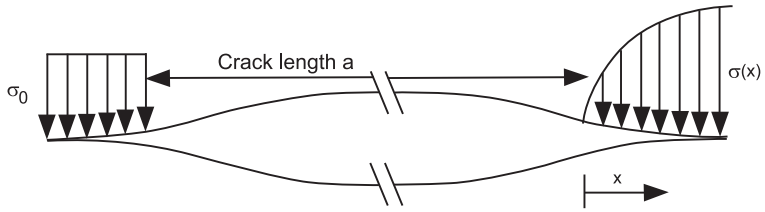

Figure 9: Strip-yield models, Dugdale (left) and Barenblatt (right). σ_0 and $\sigma(x)$ are the resisting stresses (cohesive stresses) at the crack tip

high strain rates. Adiabatic shear banding is prominent at large local strains (order of 5 to 10), high shear strain rate (order of $10^4 - 10^6 s^{-1}$) and high local temperature (increase of order $500^o C$) [73]. Under adiabatic deformation condition, the equation of energy conservation is the same as Eq. 20. Such discussions arise the question that how much the coalescence criterion and parameters recommended in a GTN model are influenced by the rate of loading. Doing cell calculations and comparing them with GTN model calculations for rate and temperature dependency values of steel, Brocks et al. [25] showed that loading rate has little effect on critical void volume fraction (f_c) in the GTN model. This low effect of rate of loading on critical void volume fraction was also shown by Sun et al. [122] through comparison of simulations and test on Charpy-V and SENB specimens.

3.3 Cohesive zone model (CZM)

A phenomenological local approach used for the numerical simulation of crack propagation is known as the cohesive zone model. The idea is based on the pioneering work by Dugdale [38] and Barenblatt [15] who introduced the strip-yield model. Both authors divided the crack into two parts as shown in Fig. 9: One corresponds to the physical length of the crack, which is stress free, and the other one is the fracture process zone, where yielding and degradation of the material occur and which is loaded by a finite stress named cohesive stress. Later developments of cohesive models, particularly in combination with finite element method, e.g. [55, 80, 100, 135], considered the cohesive stress as a function of material separation and not of the distance from the crack-tip as Barenblatt did. In finite element representation of cohesive zone models, cohesive elements are introduced as interface between continuum elements and damage occurs only in the interface elements which obey a constitutive equation named traction separation law (TSL), Fig. 10. Separation in these elements is calculated from the difference of the displacements of the continuum elements adjacent to them. The maximum opening at which the cohesive element completely fails is called critical separation, δ_0, and is one of the fracture parameters. The other fracture parameter is the maximum traction or cohesive strength, S. The area under the TSL is the

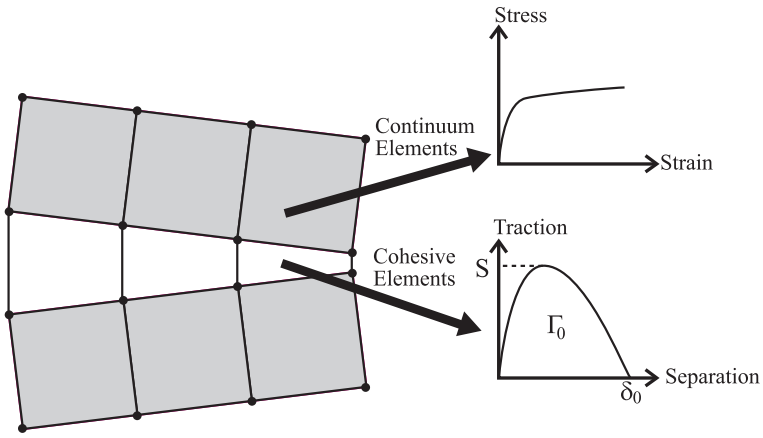

Figure 10: Cohesive zone obeying a TSL and the surrounding undamaged elastic-plastic material

energy absorbed by the cohesive element and is known as the cohesive energy, Γ_0:

$$\Gamma_0 = \int_0^{\delta_0} T(\delta) d\delta \tag{37}$$

where δ is the opening and $T(\delta)$ is the traction of cohesive element as a function of the opening. If the shape of a TSL is known or presumed, having two of the aforementioned parameters is enough to define the cohesive law. Note that δ is not only a normal opening, but it can be a combination of normal and tangential openings. In 3D case, there are one normal and two tangential displacements and of course three tractions. Further discussions on this subject, related to mixed-mode conditions, will be presented in section 3.3.4.

3.3.1 Shape of traction separation law

Since the cohesive model is known as a phenomenological model, authors have introduced a variety of formulations for defining the shape of TSL and the cohesive values. For example, Needleman [80] considered the following function:

$$T(\delta) = \frac{27}{4} S \frac{\delta}{\delta_0} \left(1 - \frac{\delta}{\delta_0}\right)^2 \tag{38}$$

where δ is the opening. The form of the function is shown in Fig. 11(a).

Needleman [81] also proposed another function as exponential form to simulate ductile crack growth:

$$T(\delta) = zSe \frac{\delta}{\delta_0} exp\left(-z\frac{\delta}{\delta_0}\right) \tag{39}$$

where $e = exp(1)$ and $z = 16e/9$. The form of the function is shown in Fig. 11(b). Note that in this model, the traction is not zero at $\delta = \delta_0$.

The model represented in Fig. 11(c) was proposed by Hillerborg et al. [55] for brittle materials, e.g. rocks. The models shown in Fig. 11(d) were proposed by Bazant [18] and Guinea et al. [51].

Another model has been proposed by Scheider [111, 113] as shown in Fig. 11(e). The model covers the area in which the traction is constant and does not change with opening. Besides, changing the values of δ_1 and δ_2 parameters, one can obtain various behaviors from the introduced model to make it closer to Needleman's cubic model or to Hilleborg's model. A similar model had already been introduced by Tvergaard and Hutchinson [138] as shown in Fig. 11(f), but the main difference in Scheider's model is that the obtained curve is continuously differentiable to avoid numerical problems. Traction as a function of opening in this definition is:

$$T = S \begin{cases} 2\left(\frac{\delta}{\delta_1}\right) - \left(\frac{\delta}{\delta_1}\right)^2 & ,0 \leq \delta \leq \delta_1 \\ 1 & ,\delta_1 \leq \delta \leq \delta_2 \\ 2\left(\frac{\delta-\delta_2}{\delta_0-\delta_2}\right)^3 - 3\left(\frac{\delta-\delta_2}{\delta_0-\delta_2}\right)^2 + 1 & ,\delta_2 \leq \delta \leq \delta_0 \end{cases} \tag{40}$$

Although it has been claimed that the shape of TSL does not have or has very little influence on crack growth behavior [66, 81, 120, 138], there are a few works that show higher effects of the shape [44, 112, 151]. For example, Scheider and Brocks [112] showed numerically that not only the shape of TSL can affect load-displacement behavior, but also the different TSL shapes that make the same results in one specimen, might make different results in another fracture specimen (Fig. 12). Falk et al. [44] showed that if the TSL is initially rigid, the model can not capture crack branching using a regular finite element mesh. They discuss that it is possible to capture branching when the TSL has initial elasticity, although initial elasticity of the cohesive elements alerts the linear elastic response of the body containing these elements.

Uncertainties like these arises the question if it is possible to give a physically meaningful TSL for cohesive elements. The discussions are presented in the next section.

3.3.2 Micromechanism based cohesive law

Considering Eq. 22 with a simple reordering and separating the total strain energy into elastic and plastic parts, we will have:

$$\frac{dF}{da} = \frac{dU^{el}}{da} + \frac{dU^{pl}}{da} + \frac{dW}{da} \tag{41}$$

Turner [131,132] introduced total energy dissipation rate, R, as a non-recoverable dissipated energy to be:

$$R = \frac{dU_{diss}}{da} = \frac{d}{da}\left(F - U^{el}\right) = \frac{dU^{pl}}{da} + \frac{dW}{da} = R^{pl} + \Gamma_0 \tag{42}$$

where R^{pl} is the plastic strain energy fraction of the dissipation rate and can be calculated by elastic-plastic finite element analysis. To separate the dissipated energy into the plastic

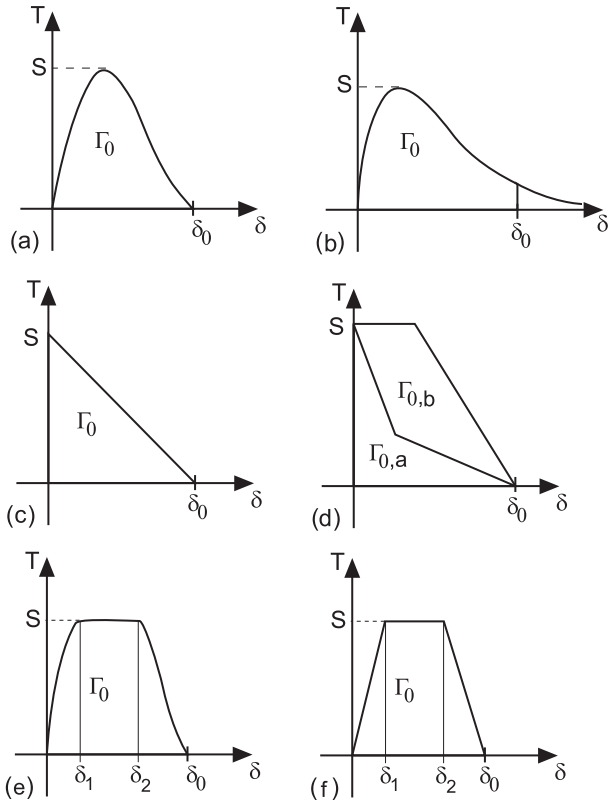

Figure 11: Various shapes of TSL [24]. δ_N: normal opening, T_N: normal traction, Γ_0: cohesive energy

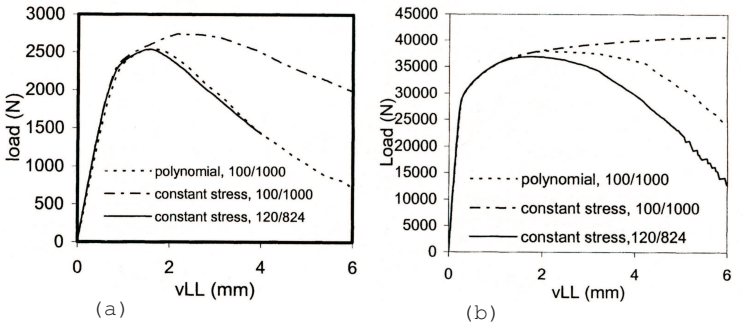

Figure 12: The effect of TSL shape on the mechanical behavior of fracture specimens. (a) C(T)specimen, (b) M(T) specimen. Numbers inside the charts are the ratio of cohesive energy to cohesive strength [112]

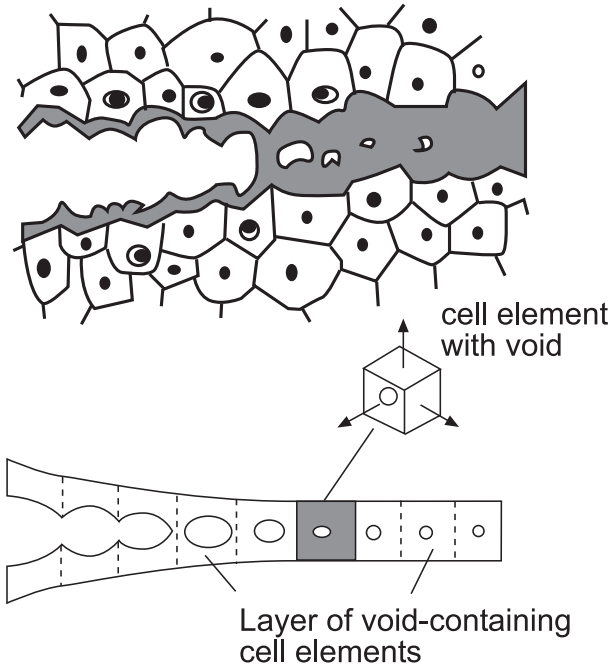

Figure 13: simulating ductile crack growth by a layer of cell elements at the ligament

dissipation energy and the energy of separation, Γ_0, local approaches can be used. In the finite element representation of ductile fracture, crack growth can be simulated by one or more layers of elements at the crack tip area obeying constitutive equations for porous metal plasticity like a GTN model (Fig.13), see e.g. [110, 146]. If we suppose that each of these elements (cells) contain reasonably sufficient information about crack growth in the material, we can apply tensile loading on a single element to obtain its cohesion-decohesion behavior. The area under the cohesion-decohesion curve is regarded as the energy of separation and the curve can be considered as TSL for cohesive elements. Cohesive elements with the obtained TSL can be used for CZM as explained in sec. 3.3. Figure 14 shows schematically how a cell model is used to obtain TSL for a representative cohesive element and the use of cohesive elements in the ligament. By using cell elements to obtain cohesive element properties it is possible to calculate the effect of local variables, e.g. stress triaxiality and strain rate on TSL. This statement is valid as long as the constitutive equations of the cell model has the capability to capture these variables properly.

The mechanical work dissipated per crack growth increment in one finite element with dimensions w, b and h as width, thickness and height respectively is expressed as:

$$\Delta U_{diss} = \bar{u}_{diss} \Delta V \tag{43}$$

where element volume is $\Delta V = wbh$ and $\bar{u}_{diss}$ is the average dissipated energy in the element. The energy release rate per crack extension increment or work of separation is

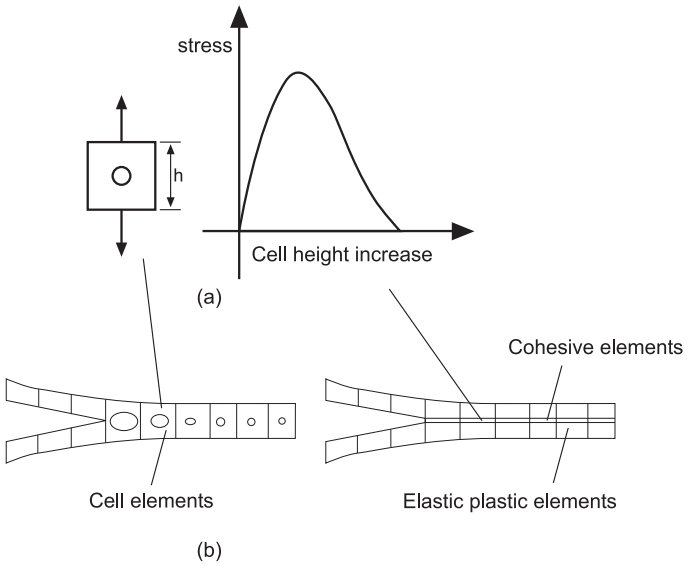

Figure 14: (a) Cohesion-decohesion behavior obtained from single element calculations and used as a TSL (b)Cohesive elements at the ligament to simulate ductile crack growth

then calculated as:

$$\Gamma_0 = \frac{\bar{u}_{diss}\Delta V}{\Delta A} = \frac{\bar{u}_{diss}\Delta V}{b\Delta a} \propto h \tag{44}$$

Variable h is the characteristic length scale in damage models. Therefore if a single cell element with unit height is used for obtaining TSL, the calculated area under the cohesion-decohesion curve must be divided by h in order to be a correct representative of Γ_0 for the cohesive elements, see [118].

3.3.3 Unloading and reverse loading

Local unloading or reverse loading can happen because of global unloading, elastic waves or crack branching. To study this phenomenon in cohesive elements, one has to divide the separation into normal and shear separation and also to ductile and cleavage fracture, see Fig. 15. As it is expected, when unloading happens in cleavage fracture, there is no plastic strain remained in the element, Fig. 15(c). It is similar in the shear loading with the difference that the resistance to opening can exist on reverse loading and therefore the stress-displacement behavior obeys the original shape of TSL but in the opposite direction, Fig. 15(d). Unloading for ductile cohesive elements is different. Load growth and inelastic local separation are irreversible and therefore the unloading will be purely elastic with the same elastic stiffness for loading [107], Fig. 15(a). Unloading in shear direction for ductile fracture is similar to normal direction, but reverse shear is different since damage is due to

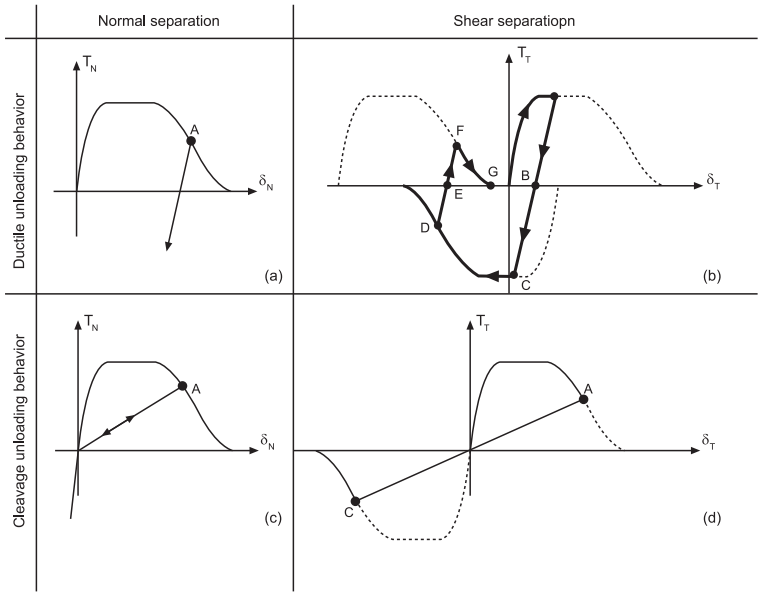

Figure 15: TSL behavior at unloading for normal and shear loading [111]

increase in both directions, Fig. 15(b). In this case, the stress-displacement behavior will be similar to the loading TSL but in the opposite direction.

Even after the failure of the cohesive elements, reverse loading can happen. In this case a TSL is applicable which simulates contact elements in a finite element model. For shear loading, a TSL is applicable which simulates friction behavior for fracture surfaces.

3.3.4 Mixed mode fracture

It was mentioned before that δ in a cohesive element or a cohesive zone is not only a normal opening, but it can be a combination of normal and tangential openings which is the case for mixed-mode fracture. In 3D case, there are one normal and two tangential displacements and of course three tractions. In these cases, shear damage can reduce ductility in normal direction and vise versa. Therefore it is necessary to define traction separation laws which reproduce this behavior.

Since the cohesive model is phenomenological, it is possible to define the TSL under mixed mode in various ways. It should be noted that using RVE or cell models to obtain mixed mode behavior is not well covered yet.

Tvergaard [134] defined a non-dimensional parameter λ as the equivalent dimensionless displacement:

$$\lambda = \left[\left(\frac{\delta_N}{\delta_{N,0}} \right)^2 + \left(\frac{\delta_T}{\delta_{T,0}} \right)^2 \right]^{\left(\frac{1}{2}\right)} \tag{45}$$

and normal and tangential tractions are defined as:

$$T_N = \frac{\delta_N}{\delta_{N,0}} F(\lambda) \quad T_T = \alpha \frac{\delta_T}{\delta_{T,0}} F(\lambda) \tag{46}$$

where $F(\lambda)$ is a polynomial cohesive law. Subscripts N and T represent the normal and tangential components, respectively.

A more general form of interaction between shear and normal separation can be defined as [111]:

$$D = \left[\left(\frac{\delta_N}{\delta_{N,0}} \right)^{\rho} + \left(\frac{\delta_T}{\delta_{T,0}} \right)^{\rho} \right]^{(1/\rho)} \tag{47}$$

where D is the damage parameter ($D = 1$ is equivalent to fully damaged element). For $\rho = 2$, Eq. 47 will become the same as Eq. 45.

Camacho and Ortiz [26] considered different weights for the traction components by weight factor β_T:

$$\sigma^{eff} = \sqrt{\beta_T^2 \tau^2 + \sigma^2} \tag{48}$$

Keller et al. [59] represented a cohesive model named generalized cohesive zone model (GCZM) in which TSL and the cohesive energy are related to mixed model propagation probability. In their model, triaixlaity and the mode of crack growth are related. If triaxiality is higher, failure mode I becomes more dominant. The importance of mixed mode failure increases with decreasing triaxiality. The dependence of interface fracture toughness and triaixality values on the degree of more mixity is discussed by Tvergaard [137], too.

Another way to consider the influence of tangential opening on normal one, is to define the traction in each direction not only as a function of opening in the the same direction but also the other directions as proposed by Scheider [113]:

$$T_N = T_N(\delta_N, \delta_T) = S_N \, f(\delta_N) \; g(\delta_{T,0}) \;\; , \;\; T_T = T_T(\delta_T, \delta_N) = S_T \, f(\delta_T) \; g(\delta_{N,0}) \tag{49}$$

where

$$f(\delta) = \begin{cases} 2\left(\frac{\delta}{\delta_1}\right) - \left(\frac{\delta}{\delta_1}\right)^2 & , 0 \le \delta \le \delta_1 \\ 1 & , \delta_1 \le \delta \le \delta_2 \\ 2\left(\frac{\delta-\delta_2}{\delta_0-\delta_2}\right)^3 - 3\left(\frac{\delta-\delta_2}{\delta_0-\delta_2}\right)^2 + 1 & , \delta_2 \le \delta \le \delta_0 \end{cases} \tag{50}$$

and

$$g(\delta) = 2\left(\frac{\delta}{\delta_0}\right)^3 - 3\left(\frac{\delta}{\delta_0}\right)^2 + 1 \tag{51}$$

In most of the simulations performed in the present investigation, only normal displacement and traction have been considered. It is only in Paper III [10] that normal and shear properties for TSL have been considered due to the mixed mode crack growth in the welded structure. The formulation used in that article is based on Eqs. 49 to 51.

It should be noted that the crack growth behavior in mixed mode not only depends on the relation between TSL of tangential and normal directions, but also on the modeling and orientation of cohesive elements when the interface elements are not considered randomly in the model [113].

3.4 Rate-dependent cohesive model

Considering the relation between cohesive zone modeling and micromechanism of crack growth in ductile materials, it is concluded that the rate of deformation might affect the energy of separation. This means that the TSL considered for a fast running crack simulation can be rate dependent. This rate dependency can be the rate of opening, strain rate, temperature rate or even the rate of traction.

Although most of the investigations performed for rate dependency are for brittle or semi brittle materials like ceramics, polymers and hard composites, there are a few works, e.g. [120, 151], that show the importance of rate dependency in ductile fracture.

Rate dependency in CZM can be considered in both finite element analyses and analytical approaches.

3.4.1 Rate-dependent cohesive elements

There are various approaches to consider rate dependency of cohesive elements because of phenomenological property of the model.

Corigliano and Ricci [30] considered the displacement in the interface to be the sum of elastic and viscoplastic displacements. For the elastic part, traction-displacement relationship is linear time independent and for the viscoplastic part, Perzyna [99] law of viscoplasticity has been used for multiaxial loading cases. The viscoplastic interface model response to different displacement velocities is shown in Fig. 16. It is observed that increasing velocity increases the strength and also the critical displacement and that the curves are parallel in the cohesion and decohesion parts.

Xu et al. [147] used standard linear solid (SLS) model that consists of a spring in parallel to a Maxwell element which consists of a second spring and a dashpot in series. In their consideration, the critical separation is taken to be constant and independent of the rate. For the SLS considered, the equivalent modulus (or time dependent cohesive strength over rate independent strength) becomes constant if the separation rate is either low or high relative to the reference rate. At intermediate rates, the equivalent modulus depends on the separation rate (Fig. 17). Similar assumptions were used in the rate-dependent cohesive elements considered by Liechte and Wu [65]. In their investigation, they considered nonlinear Kelvin unit (nonlinear spring and dashpot in parallel) for the rate-dependent cohesive element. The rate-dependent cohesive force was then expressed as the sum of the non-dissipative force (spring) and the dissipative force (dashpot):

$$f = f_s(\delta) + f_d(\dot{\delta}) \tag{52}$$

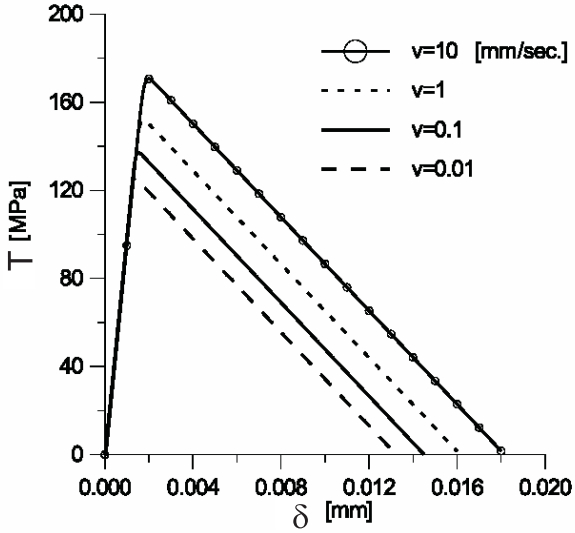

Figure 16: Viscoplastic interface model: response in pure mode at varying displacement discontinuity velocity. $u3$ and $t3$ are opening and traction of the cohesive element, respectively. [30]

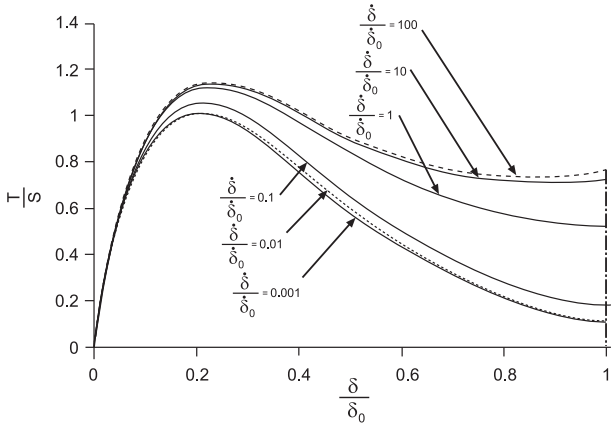

Figure 17: Traction-separation response at different normalized material separation rates [147]

The rate-dependent force was characterized by an increasing trilinear representation:

$$f_d = \begin{cases} c_1\dot{\delta} & ,0 \le \dot{\delta} \le \dot{\delta}_1 \\ f_d\left(\dot{\delta}_1\right) + c_2\left(\dot{\delta} - \dot{\delta}_1\right) & ,\dot{\delta}_1 \le \dot{\delta} \le \dot{\delta}_2 \\ f_d\left(\dot{\delta}_2\right) + c_3\left(\dot{\delta} - \dot{\delta}_2\right) & ,\dot{\delta}_2 \le \dot{\delta} \end{cases} \tag{53}$$

Rahul-Kumar et al. [103] considered visco-elastic cohesive elements in which the rate-dependent normal traction is:

$$T_{nr} = T_n\left(\delta\right)\left[1 + \left(\frac{\dot{\delta}}{\dot{\delta}_0}\right)^n\right] \tag{54}$$

where $\dot{\delta_0}$ and n are the characteristic of the dominant damage mechanism and T_n is the rate independent traction law and can be defined by any rate-independent TSL. They used this idea and defined the stress change in the cohesive element by a function G as:

$$\sigma(t) = \sigma(\epsilon)\int_0^t G\left(t - t^{'}\right)\frac{d\epsilon}{dt^{'}}dt^{'} \tag{55}$$

In this way, the evolution of these cohesive tractions are coupled to the response of the surrounding bulk material.

To consider the effect of temperature change on TSL, Estevez et al. [43] recommended the viscoplastic separation as:

$$\dot{\delta}^{vp} = \dot{\delta}_0 exp\left[\frac{-A^c\sigma^c}{\Theta}\left(1 - \frac{T}{S_0}\right)\right] \tag{56}$$

where Θ is the temperature and A^c and σ^c are the model parameters. T and S_0 are traction and a reference traction, respectively. The total displacement is defined as:

$$\delta = \delta^{el} + \delta^{vp} \tag{57}$$

It is worth noting that most of the research in this field are for semi-brittle material and visco-plastic cases.

3.4.2 Rate-dependent cohesive zone

In this approach, analytical models are presented for process zone, rather than cohesive finite elements, where cohesive stresses are applied on an area at the crack tip.

To avoid 'noise' problems existing in finite element solution of dynamic crack propagation problems, Costanzo and Walton [31, 32] proposed a numerical solution strategy to solve systems of integro-differential equations (similar to the equations used in finite element analysis and finite difference method) for cohesive zone under the conditions of dynamic crack growth. The bulk material was considered to be elastic. They studied both

rate-independent and rate-dependent cohesive zones. They concluded that for the rate-independent cohesive zone, whether linear or nonlinear, there is no limitation for crack growth rate up to Rayleigh wave speed. They also examined two rate-dependent cohesive models one of which has the form:

$$T_{rd} = S + \nu\dot{\delta} \tag{58}$$

where T_{rd} stands for rate-dependent cohesive stress, S is the rate-independent cohesive strength and ν is viscosity coefficient. In the second model, there is a critical value for displacement. When the opening displacement reaches this critical value, the cohesive stress vanishes:

$$T_{rd} = \left(S + \nu\dot{\delta}\right)\left(1 - \frac{\delta}{\delta_0}\right) \tag{59}$$

The discussions on the effect of rate sensitivity on crack growth behavior are postponed to section 4.

Kubair et al. [63] used the following rate-dependent cohesive model for mode III fracture in elastic medium:

$$T_{rd} = T_{ri}\left(1 + \nu\frac{\dot{\delta}}{c_s}\right) \tag{60}$$

where c_s is the characteristic wave speed in the material and T_{ri} is the linear damage-dependent rate independent cohesive stress:

$$T_{ri} = S\left(1 - \frac{\delta}{\delta_0}\right) \tag{61}$$

Equation 60 was first introduced by Glennie [48]. Solving the related analytical equations with different numerical methods, they concluded that numerical difficulties while solving the steady-state problem mentioned previously by Langer and Lobkovsky [64] were due to the solution method employed and did not depend on the choice of the cohesive model.

Zhang et al. [151] considered viscoplastic solids and analyzed mode I steady-state dynamic crack growth under small scale yielding conditions. In the plastic region, the cohesive law was assumed to be both strain hardening and rate dependent. The process zone was divided into two regions, plastic region in which the cohesive law is assumed to be both strain hardening and rate dependent; and the damage region which is cohesive zone, and was considered linear viscose with different viscosity coefficient. The plastic area constitutive equation is:

$$\sigma = \sigma_{pl}\left(\frac{\delta}{\delta_c}\right)^N\left(1 + \nu_n\dot{\delta}\right) \tag{62}$$

where N is the hardening exponent, σ_{pl} is the ultimate strength and ν_n is viscosity coefficient for plastic area. Similarly, the rate dependency for cohesive zone was presented by:

$$T = S\left(1 - \frac{\delta}{\delta_c}\right)^m\left(1 + \nu_m\dot{\delta}\right) \tag{63}$$

where m is softening index, ν_m is viscosity coefficient, δ_c is critical opening displacement, S is ultimate tensile strength for the damage zone. In their analyses, the cohesive area has no elastic (reversible) part. It is maximum stress (strength) and then decohesion. In this way, the energy dissipated by plastic deformation is captured by the plastic deformation mechanism. Crack growth in ductile material is governed by the competition between damage and plastic flow. Both contribute to the fracture energy, but compete against each other. The results of their parametric studies will be reviewed in section 4.

3.5 The status of cohesive zone modeling

Perhaps the most important development in computational fracture mechanics in the last decade has been the introduction and refinement of the cohesive element methods [34].

General advantages of cohesive modeling compared to the other well-known fracture mechanics approaches are as follow:

1. Due to its phenomenological character, a cohesive model is applicable to different types of material and fracture mechanisms.

2. The model can be applied for the simulation of both crack propagation and crack initiation.

3. There is not, in principle, any problem with transferring the fracture parameters from small specimens to large components. Transferability of fracture parameters is possible as long as the fracture mechanisms are similar between the specimen and the component. It also requires similar constraint, e.g. stress triaxiality, at the crack tip between the specimen and the component. In cases where the influence of constraint on crack growth behavior is high, triaxiality dependent cohesive elements as proposed e.g. in [119] or in the present investigation are applicable.

4. The number of parameters in defining a cohesive law is low compared to many other damage approaches.

5. Cohesive laws can be extended to time-dependent material behavior.

6. By using cohesive elements as interface between non-damage continuum elements in a finite element model, it is possible to split the energy dissipated by plastic deformation and the energy dissipated by separation.

7. Length scale is inherent in the definition of fracture energy, which eliminates mesh dependency in the finite element models.

8. Cohesive models can be used in a variety of analyses like fatigue (e.g. [117,150]) and environmental embrittlement (e.g. [115]).

9. Cohesive models have shown to be an efficient approach for simulation of crack initiation and growth in functional graded materials (e.g. [57, 152]).

Like any other approach, the cohesive zone models have drawbacks and uncertainties which need more research and investigation:

1. The phenomenological nature of the model causes some uncertainties with respect to the physics of the process under consideration.

2. Interaction of normal and shear separation in a mixed mode fracture and multiaxial effects in a process zone are not yet established with sufficient evidence.

3. Simulation of arbitrary crack growth is far from being an established method. Although models which have cohesive elements in different orientations, e.g. [113, 148] and also non-ordered mesh models, e.g. [130] help in simulation of arbitrary crack propagation, they are still not efficient enough since the crack is bounded to move on the boundary of continuum elements. In addition, these models suffer from loss of uniquness of the equilibrium path and stability by introducing a high number of cohesive elements in the model [129].

4. Convergence problems related to snap-back instability in numerical solutions is a general challenge.

5. It is observed that the shape of traction-separation law can affect crack branching whether to happen or not [44].

6. To overcome the problems related to mesh dependency, a new class of cohesive elements has been developed in which the crack allows to propagate on any surface within an element, rather than only along the element boundaries, see e.g. [19, 37, 74]. These approaches are still under development.

4 Local approaches and simulation of fast running cracks

This section addresses the application of local approaches previously reviewed and the important aspects in numerical simulation of fast running cracks.

First, the application of Gurson type models in finite element dynamic fracture analysis are addressed and then cohesive zone modeling in numerical dynamic fracture will be discussed in more details.

4.1 Application of Gurson type models in dynamic fracture

By using Gurson type models, it is possible to simulate crack growth simulation free from any fracture criteria. Ahmad et al. [2] showed that even for rapid crack propagation in a high strength steel, the effect of crack tip plasticity is significant, so that a conventional elastodynamic analysis is not sufficient. Considering this fact and remembering that local approaches give strong numerical tools to simulate fracture mechanics and crack growth were the motivation for many researchers to use nonlinear rate-dependent Gurson type model in their finite element dynamic analyses.

A pioneering work on using Gurson type model to simulate dynamic fracture was performed by Tvergaard and Needleman in 1986 [141]. The formulations they used for rate-dependent bulk material are the same as the equations shown in section 2.2. The aim was to check numerically the influence of strain rate on competing failure mechanisms (ductile and cleavage) in Charpy V-notch test. The numerical results showed that in the transition regime, the porosity in the notch tip region plays a role in the fracture process even when

failure occurs by cleavage. Quite interestingly, once the transition of failure mode from cleavage to ductile rupture has occurred, the energy absorbed at low rates is greater than that absorbed at higher rates. Sun et al. [122] used dynamic GTN model for simulating Charpy V-notch test, too. To evaluate the effect of stress state at the crack tip, they modeled the specimen by plane stress, plane strain and a combination of 3D/plane stress elements. In 2D models, the simulation results were far from test due to the absence of side grooves in the models. To achieve proper stress triaxiality for such cases, they showed that a combined 3D/2D model (3D elements in the area close to the crack tip and 2D elements for the rest of the model) gives a proper solution for the load-displacement curve compared to the test results.

Needleman and Tvergaard [85] performed similar work to [141] in order to consider ductile fracture and to account the effect of adiabatic heating using GTN model in a double edge cracked steel specimen under dynamic loading. In the analyses, waves did not have enough time to be reflected back to the crack front because failure occurred at a very short time. In their model, void nucleation was considered and they concluded that for the plane strain specimen analyzed, only large inclusions (stress controlled) affected the results. Hence, stress and stress triaxiality can be regarded as the most important phenomena affecting the failure. In addition, higher void nucleation stresses (σ_N in Eq. 30) make the crack growth initiation happen earlier, but has very little effect on crack growth speed. The only curve that was insensitive to the speed of loading is Δa-CTOD. They also showed that in their case study, although temperature rise is about 300^oC, these thermal effects did not greatly affect the crack growth behavior, because porosity had the dominant softening effect.

Opposite to Needleman and Tvergaard [85], Tvergaard and Needleman [142] showed that in dynamic loading of notched round bars, the effect of thermal softening was higher than porosity. This is due to the fact that in the former case, the high hydrostatic tension at the crack tip drives the void to coalescence at smaller accumulated plastic strains.

Alves and Jones [4] investigated on steel round bars under dynamic loading numerically (they did not use Gurson model) and experimentally and recommended that for round bars, a relationship between the stress triaxiality and the plastic strain might determine the actual location where failure commences. This is somehow revealed in [84] that for plane strain round bars, the crack can start at the sharp notch root where the plastic strain is high.

Xia and Shih [145] showed that in a dimensional analysis, the resistance to fracture or the fracture energy is defined as:

$$\Gamma\left(\Delta a\right) = h\sigma_0 F\left(\frac{\Delta a}{l_c}, \frac{\sigma_0}{E}, N, \nu, f_0, f_E, \frac{T}{\sigma_0}\right) \tag{64}$$

This means a length scale parameter, h, that can be element height in a finite element analysis is important, see also sec. 3.3.2. In other words, using Gurson type model is mesh dependent. They recommended that the spacing between large inclusions can act as the length scale which controls the crack growth.

Needleman and Tvergaard [86] reported similar discussions and conclusions for a crack growth simulation using elastic-viscoplastic GTN model under dynamic loading. They reported that crack growth predictions in cases where the large-scale voids dominated showed practically no mesh sensitivity, whereas cases dominated by the small-scale voids showed a clear mesh sensitivity. They also showed that for initially sharp cracks the initiation of crack growth was quite sensitive to the mesh. However, for initially blunt cracks the mesh sensitivity of the initiation time was removed. Comparing tests and simulations, Sun et al. [122] showed that h is independent of strain rate. Therefore the length scale value obtained from a quasi-static simulation can be used for dynamic simulations, too.

The mentioned literature above and similar investigations show that dynamic GTN models are powerful tools for simulating dynamic ductile crack growth but it is important to notice that mesh dependency is an important issue in such simulations. In cases that it is necessary to use very fine meshes for large structures or for simulating large amount of crack growth, mesh dependency for dynamic simulations can result in very time consuming analyses. It should be noted that transient dynamic solutions in general are relatively time consuming compared to static solutions.

4.2 Application of cohesive zone models in dynamic fracture

The most straightforward way to simulate dynamic crack growth by finite element analysis and cohesive elements is to choose some interface elements having constant properties placed between continuum elements, where the properties can be related to dynamic loading. To capture the inertia effect and wave effects, one needs to solve the model using transient dynamic solution techniques, see e.g. [1, 35].

Siegmund and Needleman [120] performed full transient dynamic analysis on a center cracked plane strain specimen. They used one array of cohesive elements in the ligament, so the crack was restricted to grow along the initial crack line (Mode I). The effect of temperature rise was ignored. Two strain rate hardening calculations were considered for the bulk material, pure power law and enhanced strain rate hardening as shown in Fig. 18. $(\sigma_0)_{qs}$ in the vertical axis is the same as g used in Eqs. 16 and 17 with the simplification that in their analyses, temperature effect was not considered. The enhanced strain hardening which has exponential form was basically recommended by Zhou et al. [155] for high strength steel under high rates of loading. As it is shown in Fig. 18, the model is applicable for strain rates of more than 5000 1/s. For each analysis, they considered constant properties for the cohesive elements. For all the analyses, cohesive characteristic length was fixed at 2 μm, but cohesive strength and consequently the work of separation were varied in different analyses. They showed numerically that having rate sensitive bulk material increased the crack velocity under the same load speed. The crack speed is even higher for the enhanced rate sensitivity. They also considered the effect of temperature by having variety of cohesive strength and strain rate sensitivities and discussed that plastic straining has an essential effect on the crack speed and also the mode of fracture or brittle to ductile transition due to the temperature change.

To check the mesh dependency effect, Needleman [83] considered the same center

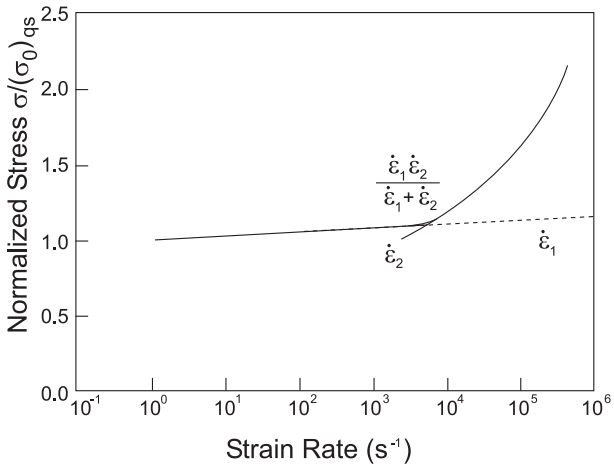

Figure 18: Dependence of the normalized flow strength on plastic strain rate [120]

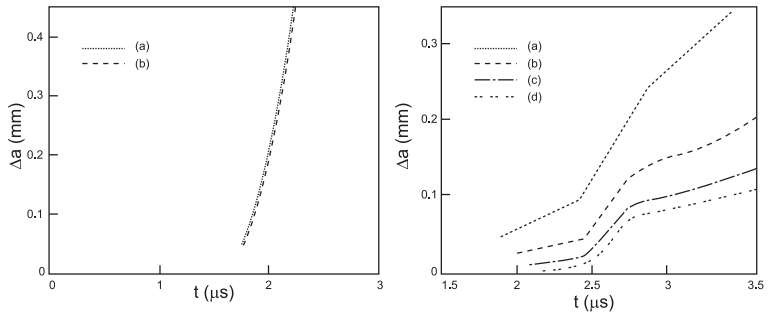

Figure 19: Crack extension vs. time for left:elstic material and right:elastic-viscoplastic material with different mesh refinements [83]

cracked specimen for elastic and elastic-viscoplastic material with four different mesh refinements. Figure 19 shows how mesh refinement can affect the crack velocity. It is observed that for the elastic material, mesh size is not important, but for the elastic-viscoplastic solid, it is very important. The curves do not deny length scale independency or mesh independency of cohesive zone approach that is related to the fact that the cohesive zone formulation includes work of separation per unit length or unit area. The curves show that mesh dependency has occurred because large elements do not have the capability of calculating plastic stress and strain distribution accurately. The difference is less in the initiation of crack growth until large scale plastic flow takes place. These discussions prove again that plastic dissipation plays a major role in crack growth behavior.

Arata and Needleman [13] showed again the importance of plasticity on dynamic crack growth behavior, this time for a bimaterial case. They chose a center cracked specimen, elastic material containing a preexisting crack, and viscoplastic material on two sides.

Each part had different cohesive properties, while there was a line between them in which interface elements existed. The finite element model was based upon linear displacement elements arranged in crossed triangular quadrilaterals. They chose mixed mode cohesive elements with the stress ratio of normal to shear cohesive strength equal to 2.33 and normal cohesive energy equal to shear cohesive energy. Their analyses showed that for weak interface (the cohesive energy of interface is 0.15 times of the cohesive energy of the viscoplastic part), in all cases, the crack deflected into elastic part. Quite interestingly, when the interface was stronger (the cohesive energy of interface is 0.25 times the cohesive energy of the viscoplastic part), in all quasi-static cases, the crack still deflected to elastic part, but in the dynamic cases when the elastic cohesive strength was high, the crack could penetrate the interface and grow into the elastic-plastic solid. This fact proves again that not only cohesive properties, but also the plasticity distribution can affect the crack growth behavior and they explained that crack deflection is promoted into the interface because the increased cohesive strength in the elastic-viscoplastic solids leads to increased plastic flow.

In all of the aforementioned references, the cohesive elements properties were considered constant during the crack growth. The effect of parameters like strain rate and temperature on crack behavior and energy absorption of the specimen analyzed were obtained by having different analyses with various cohesive properties. But in reality, constraint changes during crack growth which means the cohesive element properties can change. The constraint defined as stress triaxiality was considered for cohesive elements (or cohesive zone) by e.g. Siegmund and Brocks [118, 119], Wnuk and Legat [144] and also Broberg [23]. Tvergaard [136] considered stress triaxiality as constraint too, but commented that the stress triaxiality inside the narrow band of porous material might not be equal to the stress triaxiality outside of the band. He recommended continuity in normal and tangential strains and obtaining stress triaxiality in the interface elements from the strain values. Broberg [23] also discussed that the competition between decohesion and macroscopic plastic flow depends on the ratio between cohesive and yield strength, but is also influenced by the T-stress. For example, when the ratio of cohesive strength to the yield strength is low (less than 1.7 for T-stress=0), only process region (cohesive region) exists and no plastic region exists (Fig.20).

One of the major problems with FE cohesive elements is the numerical convergence. Because of displacement jump in cohesive elements, there might be an elastic snap-back instability which is higher when the decohesion part happens in a shorter opening. Chaboche et al. [27] showed that using viscous cohesive elements can highly solve the problem, but it affects the results. Therefore, if there is not any real viscosity for the cohesive zone, the results will not match the experimental results. In a similar discussion, Gao and Bower [46] showed that viscous cohesive elements result in a better rate of convergence. This means that performing dynamic analysis with rate-dependent cohesive elements can favor convergence compared to quasi-static rate independent analyses. O'Day and Curtin [94] used this idea and added a small amount of viscous damping to the interface constitutive description to avoid convergence problems.

There are also a few works in the literature with cohesive zone rate dependency.

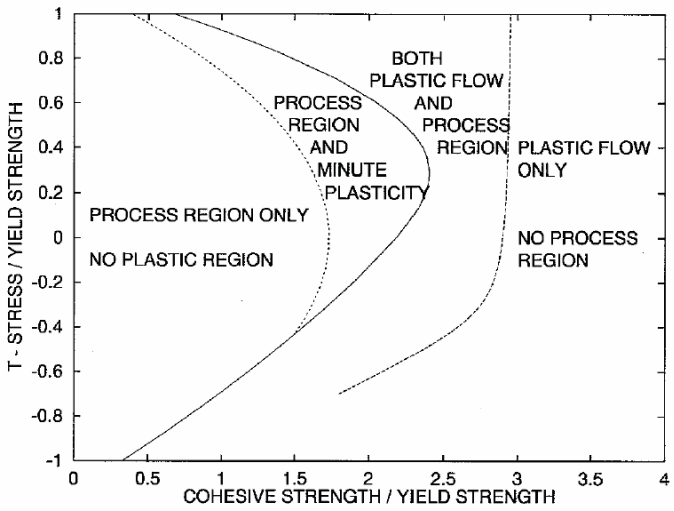

Figure 20: The effect of strength ratio of cohesive elements to continuum elements on the competition between decohesion and macroscopic plastic flow [23]

Costanzo and Walton [31] showed that rate independent models are intrinsically unable to account for the experimental evidence available from the literature. They used Eqs. 58 and 59 for rate dependent cohesive zone and showed that the key to control the crack tip velocity is the inclusion of rate dependence into the cohesive zone constitutive behavior although rate dependency itself does not allow one to correct all the other shortcomings of rate independent models. They also showed that in order to calculate proper crack tip velocity, it is necessary to have limitations for cohesive stresses and a critical crack opening displacement. Kubair et al. [63] discussed that the effect of rate dependency in cohesive zone is to increase the fracture toughness with increase in crack speed. Zhang et al. [151] did parametric studies and showed that for rate-dependent materials, the maximum cohesive stress depends not only on the cohesive material parameters, but also on the crack propagation rates. They also showed that the traction increases with crack growth velocity, but in the decohesion part, the TSLs are the same, Fig. 21. The similar behavior exists for rate dependency so that with increasing rate dependency (viscosity coefficient in this article), normalized crack opening decreases slightly, but traction increases more and also this rate dependency does not affect the decohesion part behavior. These results show that for fast running cracks, more energy is dissipated in the damage zone. They also discussed that the increase of crack-tip constraints can be related to an increase in crack growth rate and rate-sensitivity factors. One should remember that crack speed is not an independent parameter, but it is influenced by material properties and loading rate. In their discussions, higher crack speed is showing higher crack opening in the zone considered and also higher strain rate in the surrounding material.

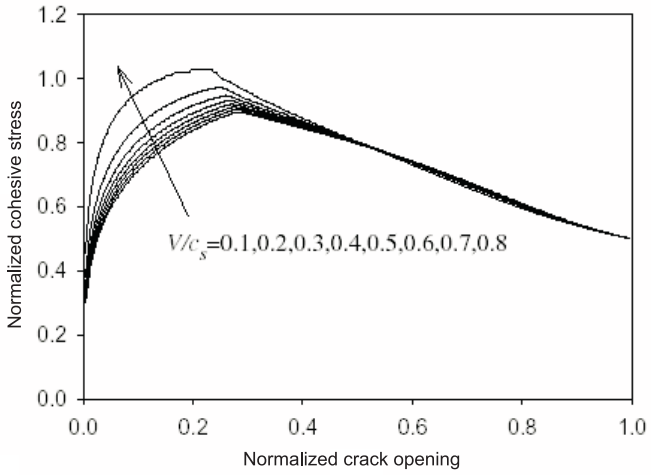

Figure 21: Normalized traction along the cohesive zone at various crack speeds [151].

5 Aluminum alloys and weldment

Increasing use of aluminum alloy in car body construction has promoted the need to have a better understanding of aluminum joining technique and the material properties of the weldments. Joining aluminum sheets with spot weld is more costly and less reliable than spot welding steel sheets. Therefore alternative methods of joining aluminum components/sheets have been developed which include self-piercing rivets, MIG (metal-inner-gas) and laser welding [123]. Laser welding of aluminum alloys has a wide application in aerospace industry, too. For example, it has been specifically used for body construction of Airbus A318 aircrafts. Its application in construction of the XXL generation of Airbus aircrafts has saved 15% of the aircrafts' weight [108].

Weldment is considered as a source of geometric and material discontinuity in the analysis of structures. When two metal parts are welded, the new structure does not consist of single material, but the joint area has a high gradient of material properties. Distinct microstructural regions occur in fusion welds as a result of the effects of heat. At the weld centerline is the fusion zone (FZ). Outside the FZ is the partially melted zone (PMZ), where the temperature of the alloy is below the liquidus but above the solidus. Outside the PMZ is the heat affected zone (HAZ), where the temperatures are lower, but still high enough to cause observable microstructural changes due to solid-phase transformations. At some further distance from the weld centerline is the unaffected base material (BM), where the temperature rise is too low to cause any noticeable microstructural changes [72]. In a beam laser welded joint, there is no metal injection and the joint can be ideally divided into FZ, HAZ and BM. In addition to different microstructural and elastoplastic properties in a welded joint, welding can leave residual stresses on the structure and affect the stress distribution.

In fracture analysis (quasi-static or dynamic) of a welded joint, parameters like mechanical properties difference e.g. yield stress between BM, WM and HAZ, the properties and length of HAZ, the crack location, and residual stresses are important. These kinds of joints can be modeled in finite element method as a mismatch case. When a crack exists on the interface of mismatch, the normal and shear stresses are the same in both materials, but the parallel stress components are different. This jump in the stress components results in a different stress triaxiality and constraint for the interface compared to any of the single materials. The mismatch can cause the crack to grow in one of the materials and results in mixed mode fracture, see e.g. [88, 97, 136]. Thaulow et al. [127] considered different strength mismatches and presented an extra parameter in fracture analysis of welded joints compared to two parameter approaches (J-Q theory). Using finite element method, they showed that the difference field of material mismatch constraint is self-similar and can be scaled by a mismatch constraint parameter called M. Therefore, they presented a new approach which they called "J-Q-M approach". It should be noted that the material models they chose did not have porosity and they used von-Mises failure criteria. They also did the analyses for only stationary cracks. Later, Zhang et al. [153] used the Gurson model in the static analysis of welded aluminum structures. To have a better microstructure property of HAZ, they used a software named WELDSIM, which simulates HAZ thermally.

Tvergaard and Needleman [143] performed analyses on welded plane strain specimens under dynamic loading and showed that the transition temperature (ductile-brittle) and work of fracture is highly different between different strength mismatch cases. They also showed that the worst location of the notch is not the same in the overmatch ($(\sigma_0)_{WM} > (\sigma_0)_{BM}$) and undermatch ($(\sigma_0)_{WM} < (\sigma_0)_{BM}$) cases. This is true if the mismatch difference is more than 20% [87]. It is worth noting that during dynamic loading, different values of strength mismatch can change even the mode of failure [6]. Needleman and Tvergaard [87] showed that the flow stress and width of HAZ have a large influence on the transition temperature of a welded structure during dynamic loading. The importance of the width of HAZ in also quasi-static cases was shown to be high by Liu and Lademo [70], although they showed that changing HAZ shape does not highly influence the fracture behavior. Besides, Zhang et al. [153] showed that the dimensions of HAZ primarily determine the shape of load-displacement curves, while the strength of HAZ influences the loading level.

Although residual stresses can significantly affect fracture behavior of welded structures [116], none of the previously mentioned articles consider this effect. This influence is mostly considered in brittle fracture and fatigue analysis of weldments.

Although there are a number of investigations in the application of cohesive zone models in crack growth simulation in mismatch cases, e.g. [67, 81, 82, 139, 149], there are not many publications reporting the application of the model under dynamic loading conditions. Besides, most of the publications are performed for steel due to its wide application in industry. Aluminum alloys are different in some aspects compared to steel alloys. The level of anisotropy and/or inhomogeneity that can affect localization and consequently the mode of failure [135] are different between steel and aluminum. Besides, aluminum has a different strain rate sensitivity compared to steel. On the other hand, the effect of adiabatic

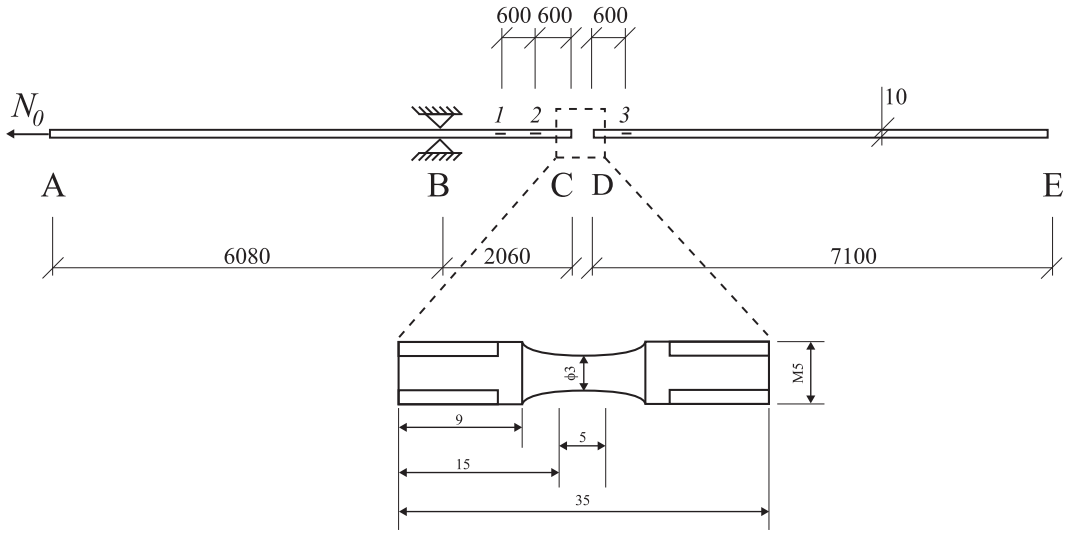

Figure 22: The split-Hopkinson Tension Bar setup at SIMLab of NTNU. The smooth specimen tested is indicated. Measures are in mm.

heating can be different for these alloys. Aluminum weldments will often include soft zone whereas a steel weldment will usually be overmatched.

6 Split-Hopkinson tension bar (SHTB)

Split-Hopkinson bar technique, first introduced by Kolsky [61], is the most widely used method to study material behavior at deformation rates between 100 1/s and 10000 1/s. In this setup, a short sample made of the material under study is placed between two long bars made of high strength steel. The specimen is loaded by the stress wave generated in one of the bars named input bar. When the load reaches the specimen, part of the wave is transferred into the other bar, output bar, and the other part reflects to the input bar. The loading bars are chosen long enough to ensure that the specimen breaks before the waves are reflected into the sample again. The loading bars are supposed to be deformed elastically to ensure precise calculations on elastic waves. By measuring the strain values in the loading bars and application of stress wave theories, the load and deformation in the specimen are monitored. This technique was initially used for compression loading of the specimen, and has been modified for tension and torsion loadings.

Among the various methods introduced to generate tension load with a short rising time in the specimen, e.g. [3, 54, 68, 89, 121], the SHTB used in the present thesis is identical to the one introduced by Albertini and Montagnani [3]. In this technique, tension force is directly applied on the input bar and a clamp is designed to ensure sufficient pressure on the bar and a short fracture time. Figure 22 shows the schematic view of the test rig and the specimen tested. The specimen to be tested is placed between input bar (AC) and output bar (DE). The experiments consist of two phases. First, the locking mechanism

prevents point B to move while a tension force N_0 is applied to part AB. After that, the lock is suddenly removed and a released stress wave moves toward point C. The stress wave is partly transmitted to bar DE and partly reflected back in CBA. The stress, strain and strain rate are determined by the use of one-dimensional stress wave theory and the strains measured at strain gauges 1, 2 and 3. The general formulations to calculate the engineering stress, strain and strain rates in the specimen based on the traction and reflected measured waves are:

$$\sigma_s = \frac{E_0 A_0}{A_s} \epsilon_T \tag{65}$$

$$\epsilon_s = -2 \frac{c_0}{L_s} \int_0^t \epsilon_R d\tau \tag{66}$$

$$\dot{\epsilon}_s = -2 \frac{c_0}{L_s} \epsilon_R \tag{67}$$

Subscript 0 refers to the bars and subscript s refers to the specimen. Subscripts T and R refer to transmitted and reflected waves respectively. E is the modulus of elasticity and A is the cross section. L_s is the parallel length of the specimen. The strains measured in this way are valid for smooth specimens up to necking. For notched specimens and also for obtaining true stresses and strains, it is necessary to measure diameter reduction in the specimen by a high speed digital camera synchronized with the test rig. For a comprehensive reference on the theory, formulations and application of SHTB, see [29].

References

[1] ABAQUS. *ABAQUS theory manual- Version 5.8.* Hibbitt, Karlsson & Sorensen, 1998.

[2] J. Ahmad, J. Jung, C.R. Barnes, and M.F. Kanninen. Elastic-plastic finite element analysis of dynamic fracture. *Engineering Fracture Mechanics*, 17:235–246, 1983.

[3] C. Albertini and M. Montagnini. Wave propagation effects in dynamic loading. *Nuclear Engineering and Design*, 37:115–124, 1976.

[4] M. Alves and N. Jones. Influence of hydrostatic stress on failure of axisymmetric notched specimens. *Journal of the Mechanics and Physics of Solids*, 47:643–667, 1999.

[5] A.L. Anderson. *Fracture mechanics, fundamentals and applications.* CRC Press, 2^{nd} edition, 1995.

[6] K. Angamuthu, B. Guha, and D.R.G. Achar. Investigation of dynamic fracture toughness behavior of strength mis-matched Q & T steel weldments using instrumented charpy impact testing. *Engineering Fracture Mechanics*, 64:417–432, 1999.

[7] M. Anvari, J. Liu, and C. Thaulow. Dynamic ductile fracture in aluminum round bars: Experiments and simulations. *International Journal of Fracture*, 143(4):317–332, 2007.

[8] M. Anvari, I. Scheider, and C. Thaulow. Ductile fracture under dynamic loading using a strain-rate dependent cohesive model. In B.H.V. Topping and C.A. Mota Soares, editors, *Proceedings of the* 7^{th} *International Conference on Computational Structures Technology*, Lisbon, Portugal, September 2004. Technical University of Lisbon and National Laboratory for Civil Engineering (LNEC), Civil-Comp Press, Stirling, Scotland.

[9] M. Anvari, I. Scheider, and C. Thaulow. Simulation of dynamic ductile crack growth using strain-rate and triaxiality-dependent cohesive elements. *Engineering Fracture Mechanics*, 73:2210–2228, 2006.

[10] M. Anvari and C. Thaulow. Crack extension in aluminum weldment using rate-dependent cohesive elements. In J. Besson, D. Moinereau, and D. Steglich, editors, *Local Approach to Fracture -* 9^{th} *European Mechanics of Materials Conference*, pages 211–215, Moret-sur-Loing, France, May 2006. European Mechanics Society and French Society for Mechanics of Materials, École des Mines de Paris.

[11] M. Anvari, C. Thaulow, and J. Liu. Simulation of ductile fracture in round bars using cohesive elements. In B. Skallerud and H.I. Andersson, editors, *Proceedings*

of the 3^{rd} *National Conference on Computationl Mechanics, MekIT05*, pages 61–73, Trondheim, Norway, May 2005. Nowegian University of Science and Technology, NTNU.

[12] M. Anvari, C. Thaulow, and I. Scheider. A dynamic crack growth simulation using cohesive elements. In *Proceedings of ECF16 - Symposium on cohesive models of fracture*, Alexandroupolis, Greece, July 2006. European Structural Integrity Society.

[13] J.J.M. Arata and A. Needleman. The effect of plasticity on dynamic crack growth across an interface. *Internation Journal of Fracture*, 94:383–399, 1998.

[14] S.N. Atluri, T. Nishioka, and M. Nakagaki. Incremental path-independent integrals in inelastic and dynamic fracture mechanics. *Engineering Fracture Mechanics*, 20(2):209–244, 1984.

[15] G.I. Barenblatt. The mathematical theory of equilibrium cracks in brittle fracture. *Advances in Applied Mechanics*, 7:55–129, 1962.

[16] S. Basu and R. Narashimhan. Finite element simulation of mode I dynamic, ductile fracture initiation. *International Journal of Solids and Structures*, 33(8):1191–1207, 1996.

[17] S. Basu and R. Narashimhan. A numerical investigation of loss of crack tip constraint in a dynamically loaded ductile specimen. *Journal of the Mechanics and Physics of Solids*, 48:1967–1985, 2000.

[18] Z.P. Bazant. Current status and advances in the theory of creep and interaction with fracture. In Z.P. Bazant and I. Carol, editors, *Proceedings of the* 5^{th} *International RILEM Symposium on Creep and Shrinkage of Concrete*, pages 291–307, E & FN Spon, London-New York, 1993.

[19] T. Belytchko, H. Chen, J.X. Xu, and H. Zi. Dynamic crack propagation based on loss of hyperbolicity and a new discontinuous enrichment. *International Journal of Numerical Methods in Engineering*, 58:1873–1905, 2003.

[20] Y. Ben-zion and J.R. Rice. Dynamic simulations of slip on a smooth fault in an elstic solid. *Journal of Geophysics Research*, 102:771–784, 1997.

[21] F.M. Beremin. A local criterion for cleavage fracture of a nuclear pressure vessel steel. *Metallurgical Transactions A*, 14:2277–2287, 1983.

[22] K.B. Broberg. The cell model of materials. *Computational Mechanics*, 19:447–452, 1997.

[23] K.B. Broberg. Influence of T-stress, cohesive strength and yield strength on the competition between decohesion and plastic flow in a crack edge vicinity. *International Journal of Fracture*, 100:133–142, 1999.

[24] W. Brocks, A. Cornec, and I. Scheider. Computational aspects of nonlinear fracture mechanics. In R. de Borst and H.A. Mang, editors, *Comprehensive Structural Integrity*, number 3, chapter 3.03, pages 127–209. Elsevier Ltd., 2003.

[25] W. Brocks, D.Z. Sun, and A. Hönig. Verification of the transferability of micromechanical parameters by cell model calculations for visco-plastic materials. *International Journal of Plasticity*, 11:971–989, 1995.

[26] G.T. Camacho and M. Ortiz. Computational modeling of impact damage in brittle materials. *International Journal of Solids and Structures*, 33(20-22):2899–2938, 1996.

[27] J.L. Chaboche, F. Feyel, and Y. Monerie. Interface debonding models: a viscous regularization with a limited rate dependency. *Intenation Journal of Solids and Structures*, 38:3127–3160, 2001.

[28] C.C. Chu and Needleman A. Void nucleation effects in bi-axially stretched sheets. *Journal of Engineering Materials and Technology*, 102:249–256, 1980.

[29] A.H. Clausen and T. Auested. Split-Hopkinson tension bar, experimental set-up and theoretical considerations. Technical report, SIMLab internal report no. R-16-02, 2002.

[30] A. Corigliano and M. Ricci. Rate-dependent interface models: formulation and numerical applications. *International Journal of Solids and Structures*, 38:547–576, 2001.

[31] F. Costanzo and J.R. Walton. Numerical simulations of a dynamically propagating crack with a nonlinear cohesive zone. *International Journal of Fracture*, 91:373–389, 1998.

[32] F. Costanzo and J.R. Walton. A numerical solution technique for a class of integrodifferential equations in elastodynamic crack propagation problems. *Computer Methods in Applied Mechanics and Engineering*, 162:19–48, 1998.

[33] G.R. Cowper and P.S. Symonds. Strain hardening and strain rate effects of cantilever beams. Technical report, Brown University Applied Mathematics Report, 1958.

[34] B.N. Cox, H. Gao, D. Gross, and D. Rittel. Modern topics and challenges in dynamic fracture. *Journal of the Mechanics and Physics of Solids*, 53:565–596, 2005.

[35] M.A. Crisfield. *Non-linear finite element analysis of solids and structures, Vol.2: Advanced Topics*. John Wiley and Sons, 1997.

[36] D.R. Curran, L. Seaman, and D.A. Shockey. Dynamic failure of solids. In *Physics Reports*, number 147, pages 253–388. North Holland, Amsterdam, 1987.

[37] R. deBorst. Some recent issues in computational failure mechanics. *International Journal of Numerical Methods in Engineering*, 52:63–95, 2001.

[38] D.S. Dugdale. Yielding of steel sheets containing slits. *Journal of the Mechanics and Physics of Solids*, 8:100–104, 1960.

[39] A. Eberle, D. Klingbeil, and J. Schicker. The calculation of dynamic JR-curves from the finite element analysis of a charpy test using a rate-dependent damage model. *Nuclear Engineering and Design*, 198:75–87, 2000.

[40] E. El-Magd and M. Brodmann. Influence of precipitates on ductile fracture of aluminum alloy AA7075 at high strain rates. *Materials Science and Engineering*, A307:143–150, 2001.

[41] E. El-Magd, H. Gese, R. Tham, H. Hooputra, and H. Werner. Fracture criteria for automobile crashworthiness simulation of wrought aluminum alloy components. *Materialwissenschaft und Werkstofftechnik*, 32:712–724, 2001.

[42] J.D. Eshelby. Calculation of energy release rate. In *Prospects of fracture mechanics*, pages 69–84, Noordhoff, 1974.

[43] R. Estevez, M.G.A. Tijssens, and E. Van der Giessen. Modeling of the competition between shear yielding and crazing in glassy polymers. *Journal of the Mechanics and Physics of Solids*, 48(12):2585–2617, 2000.

[44] M. Falk, A. Needleman, and J.R. Rice. A critical evaluation of cohesive zone models of dynamic fracture. *Journal de Physique IV*, 11:43–50, 2001.

[45] L.B. Freund. *Dynamic fracture mechanics*. Cambridge University Press, 1998.

[46] Y.F. Gao and A.F. Bower. A simple technique for avoiding convergence problems in finite element simulations of crack nucleation and growth on cohesive interfaces. *Modelling and Simulation of Material Science and Engineering*, 12:453–463, 2004.

[47] M. Gåråjeu, J.C. Michel, and P. Suquet. A micromechanical approach of damage in viscoplastic materials by evolution in size, shape and distribution of voids. *Computer Methods in Applied Mechanics and Engineeing*, 183:223–246, 2000.

[48] E.B. Glennie. A strain-rate dependent crack model. *Journal of the Mechanics and Physics of Solids*, 19(5):255–272, 1971.

[49] E.B. Glennie. The dynamic growth of a void in a pastic material and application to fracture. *Journal of the Machanics and Physics of Solids*, 20:415–429, 1972.

[50] M. Gologanu, J.B. Leblond, and J. Devaux. Approximate models for ductile metals containing non-spherical voids - case of axisymmetric oblate ellipsoidal cavities. *ASME Journal of Engineering Materials and Technology*, 116:290–297, 1995.

[51] G.V. Guinea, J. Planas, and M. Elices. A general bilinear fit for the softening curve of the concrete. *Materials and Structures*, 27:99–105, 1994.

[52] J. Gurson. Continuum theory of ductile rupture by void nucleation and growth. part I-yield criteria and flow rules for porous ductile media. *Journal of Engineering and Materials Technology*, 99:2–15, 1977.

[53] S. Hao and W. Brocks. The Gurson-Tvergaard-Needleman model for rate and temperature-dependent materials with isotropic and kinematic hardening. *Computational mechanics*, 20:34–40, 1997.

[54] J. Harding, E.O. Wood, and J.D. Campbell. Tensile testing of materials at impact rates of strain. *Journal of Mechanical Engineering and Science*, 2:88–96, 1960.

[55] A. Hillerborg, M. Modéer, and P.E. Petersson. Analysis of crack formation and crack growth in concrete by means of fracture mechanics and finite elements. *Cement and Concrete Research*, 6:773–782, 1976.

[56] J.W. Hutchinson. Singular behavior at the end of a tensile crack tip in a hardening material. *Journal of the Mechanics and Physics of Solids*, 16:13–31, 1968.

[57] Z.H. Jin, G.H. Paulino, and R.H. Dodds Jr. Finite element investigation of quasi-static crack growth in functionally graded materials using a novel cohesive zone fracture model. *ASME Journal of Applied Mechanics*, 69:370–379, 2002.

[58] J.W. Johnson. Dynamic fracture and spallation in ductile solids. *Journal of Applied Physics*, 52(4):2812–2825, 1981.

[59] K. Keller, S. Weihe, T. Siegmund, and B. Kröplin. Generalized cohesive zone model: incorporating triaxiality dependent failure mechanisms. *Computational Materials Science*, 16:267–274, 1999.

[60] H. Klöcker and F. Montheillet. Influence of flow rule and inertia on void growth in a rate sensitive material. In *Journal the Physique IV, DYMAT 3^{rd} International Conference on Mechanical and Physical Behaviour of Materials under Dynamic Loading*, volume 1, pages 733–738, Strasbourg, 1991.

[61] H. Kolsky. An investigation of the mechanical properties of materials at very high rates of loading. *Proceedings of Royal Society of London*, pages 676–700, 1949.

[62] J. Koplik and A. Needleman. Void growth and coalescence in porous plastic solids. *International Journal of Solids and Structures*, 24:835–853, 1988.

[63] D.V. Kubair, P.H. Geubelle, and Y.Y. Huang. Analysis of rate-dependent cohesive model for dynamic crack propagation. *Engineering Fracture Mechanics*, 70:685–704, 2003.

[64] J.S. Langer and A.E. Lobkovsky. Critical examination of cohesive zone models in the theory of dynamic fracture. *Journal of the Mechanics and Physics of Solids*, 46:1521–1556, 1998.

[65] K.M. Liechte and J.D. Wu. Mixed-mode, time-dependent rubber/metal debonding. *Journal of the Mechanics and Physics of Solids*, 49:1039–1072, 2001.

[66] G. Lin, A. Cornec, and K.H. Schwalbe. Three-dimensional finite element simulation of crack extension in aluminum alloy 2024FC. *Fatigue and Fracture of Engineering Materials and Structures*, 21:1159–1173, 1998.

[67] G. Lin, X.G. Meng, A. Cornec, and K.H. Schwalbe. The effect of strength mismatch on mechanical performance of weld joints. *International Journal of Fracture*, 96:37–54, 1999.

[68] U.S. Lindholm and L.M. Yeakley. High strain-rate testing: Tension and compression. *Experimental Mechanics*, 8:1–9, 1968.

[69] J. Liu. *A new dynamic void growth model*. Norwegian University of Science and Technology, 2004. Doctoral thesis.

[70] J. Liu and Lademo O.G. Finite element simulations of cross weld specimens without weld defects. Technical report, SINTEF, 2002.

[71] K.K. Mathur, A. Needleman, and V. Tvergaard. Three dimensional analysis of dynamic ductile crack growth in a thin plate. *Journal of the Mechanics and Physics of Solids*, 44(3):439–464, 1996.

[72] R.W. Messler Jr. *Principles of Welding: Processes, Physics, Chemistry, and Metallurgy*. John Wiley & Sons, Inc. New York, NY, 1999.

[73] D.P. Miannay. *Time-dependent fracture mechanics*. Springer-Verlag, 2001.

[74] N. Möes, J. Dolbow, and T. Belytchko. A finite element method for crack growth without remeshing. *International Journal of Numerical Methods in Engineering*, 46:131–150, 1999.

[75] A. Molinari and S. Mercier. Micromechanical modeling of porous materials under dynamic loading. *Journal of the Mechanics and Physics of Solids*, 49:1497–1516, 2001.

[76] B. Moran and C.F. Shih. Crack tip and associated domain integrals from momentum and energy balance. *Engineering Fracture Mechanics*, 27:615–642, 1987.

[77] F. Mudry. A local approach to cleavage fracture. *Nuclear Engineering and Design*, 105:65–76, 1987.

[78] U. Mühlich, T. Siegmund, and W. Brocks. A user-material subroutine of the modified gurson-tvergaard-needleman model of porous metal plasticity for rate and temperature dependent hardening. Technical report, GKSS internal report no. WMG/98/1, 1998.

[79] T. Nakamura, C.F. Shih, and L.B. Freund. Analysis of a dynamically loaded three-point bend ductile fracture specimen. *Engineering Fracture Mechanics*, 25:323–339, 1986.

[80] A. Needleman. A continuum model for void nucleation by inclusion debonding. *Journal of Applied Mechanics*, 54:525–531, 1987.

[81] A. Needleman. An analysis of decohesion along an imperfect interface. *International Journal of Fracture*, 42:21–40, 1990.

[82] A. Needleman. An analysis of tensile decohesion along an interface. *Journal of the Mechanics and Physics of Solids*, 38:289–324, 1990.

[83] A. Needleman. Numerical modeling of crack growth under dynamic loading conditions. *Computational Mechanics*, 19:463–469, 1997.

[84] A. Needleman and V. Tvergaard. An analysis of ductile rupture in notched bars. *Journal of the Mechanics and Physics of Solids*, 32(6):461–490, 1984.

[85] A. Needleman and V. Tvergaard. An analysis of dynamic, ductile crack growth in a double edge cracked specimen,. *International Journal of Fracture*, 49:41–67, 1991.

[86] A. Needleman and V. Tvergaard. Mesh effects in the analysis of dynamic ductile crack growth. *Engineering Fracture Mechanics*, 47(1):75–91, 1994.

[87] A. Needleman and V. Tvergaard. A micromechanical analysis of the ductile-brittle transition at a weld. *Engineering Fracture Mechanics*, 62:317–338, 1999.

[88] P. Négre, D. Steglich, and W. Brocks. Crack extension in aluminium welds: a numerical approach using the Gurson-Tvergaard-Needleman model. *Engineering Fracture Mechanics*, 71(71):2365–2383, 2004.

[89] T. Nicholas. Tensile testing of materials at high rates of strain. *Experimental Mechanics*, 21:177–185, 1981.

[90] K. Nilsson. Effects of inertia on dynamic neck formation in tensile bars. *European Journal of Mechanis A/Solids*, 20:713–729, 2001.

[91] T. Nishioka. Computational dynamic fracture mechanics. *International Journal of Fracture*, 86:127–159, 1997.

[92] T. Nishioka and S.N. Atluri. A numerical study of the use of path independent integrals in elasto-dynamic crack propagation. *Engineering Fracture Mechanics*, 18(1):1–22, 1983.

[93] A.K. Noor, A. Needleman, and J.M. Peters. Sensitivity analysis for failure and damage in dynamically loaded tensile bars. *Computer Methods in Applied Mechanical Engineering*, 151:461–478, 1998.

[94] M.P. O'Day and W.A. Curtin. Bimaterial interface fracture: A discrete dislocation model. *Journal of the Mechanics and Physics of Solids*, 53(2):359–382, 2005.

[95] N.P. O'Dowd and C.F. Shih. Family of crack-tip fields characterized by a triaxiality parameter-I. structure of fields. *Journal of the Mechanics and Physics of Solids*, 39:898–1015, 1991.

[96] N.P. O'Dowd and C.F. Shih. Family of crack-tip fields characterized by a triaxiality parameter-II. fracture applications. *Journal of the Mechanics and Physics of Solids*, 40:939–963, 1992.

[97] E. Østby. *Numerical simulations of material mismatch and ductile crack growth.* Norwegian University of Science and Technology, 2002. Doctoral thesis.

[98] J. Pan, M. Saje, and A. Needleman. Localization of deformation in rate sensitive porous plastic solids. *Internation Journal of Fracture*, 21:261–278, 1983.

[99] P. Perzyna. *Fundamental problems in visco-plasticity. Recent Advaces in Applied Mechanics.* Academic Press, New York, 1966.

[100] P.E. Petersson. Crack growth and development of fracture zones in plain concrete and similar matrials. Technical report, Report LUTVDG/TVBM-1006, Lund Institute of Technology, 1981.

[101] A. Pineau. Review of fracture mecahnisms and a local approach to predicting crack resistance in low strength steels. In D. Francois, editor, *Advances in Fracture Research, ICF5*, pages 553–577, Oxford, UK, 1982. Pergamon.

[102] A. Pineau and P. Joly. Local versus global approaches to elastic-plastic fracture mechanics: Application to ferritic steels and a cast duplex stainless steel. In J.G. Blauel and K.H. Schwalbe, editors, *Defect Assessment in Components - Fundamentals and Applications, ESIS/EGF9*, pages 381–414, London, UK, 1991. Mechanical Engineering Publications.

[103] P. Rahul-Kumar, A. Jagota, S.J. Bennison, S. Saigal, and S. Muralidhar. Polymer interface fracture simuations using cohesive elements. *Acta Material*, 47(15):4161–4169, 1999.

[104] J. Rice and D.M. Tracey. On the ductile enlargement of voids in triaxial stress fields. *Journal of the Machanics and Physics of Solids*, 17:201–219, 1986.

[105] J.R. Rice. A path independent integral and the approximate analysis of strain concentration by notches and cracks. *Journal of Applied Mechanics*, 35:371–386, 1968.

[106] J.R. Rice and G.F. Rosengren. Plain strain deformation near a crack tip in a power-law hardening material. *Journal of the Mechanics and Physics of Solids*, 16:1–12, 1968.

[107] K.L. Roe and T Siegmund. An irreversible cohesive zone model for interface fatigue crack growth simulation. *Engineering Fracture Mechanics*, 70:209–232, 2003.

[108] I. Rötzer. Laser-beam welding makes aircraft lighter. *Fraunhafer magazine*, 1:36–37, 2005.

[109] G. Rousellier. Ductile fracture models and their potential in local approach of fractutre. *Nuclear Engineering and Design*, 105:97–111, 1987.

[110] C. Ruggieri, T.L. Pantonin, and R.H. Dodds. Numerical modeling of ductile crack growth in 3d using computational cell elements. *International Journal of Fracture*, 82:67–95, 1996.

[111] I. Scheider. Cohesive model for crack propagation analyses of structures with elastic-plastic material behavior. foundations and implimentation. Technical report, GKSS internal report no. WMS/2000/19, 2000.

[112] I. Scheider and W. Brocks. The effect of the traction separation law on the results of cohesive zone crack propagation analyses. *Key Engineering Materials*, 251:313–318, 2003.

[113] I. Scheider and W. Brocks. Simulation of cup-cone fracture using the cohesive model. *Engineering Fracture Mechanics*, 70:1943–1961, 2003.

[114] I. Scheider and W. Brocks. Cohesive elements for thin-walled structures. *Computational Material Science*, 37:101–109, 2006.

[115] S. Serebrinsky, E.A. Carter, and M. Ortiz. A quantum-mechanically informed continuum model of hydrogen embrittlement. *Journal of the Mechanics and Physics of Solids*, 52:2403–2430, 2004.

[116] K. Shankar and W. Wu. Effect of welding and weld repair on crack propagation behavior in aluminum alloy 5083 plates. *Materials & Design*, 23(2):201–208, 2002.

[117] T. Siegmund. A numerical study of transient fatigue crack growth by use of an irreversible cohesive zone model. *International Journal of Fatigue*, 26:929–939, 2004.

[118] T. Siegmund and W. Brocks. Predictions of the work of separation and implications to modeling. *International Journal of Fracture*, 99:97–116, 1999.

[119] T. Siegmund and W. Brocks. A numerical study on the correlation between the work of separation and the dissipation rate in ductile fracture. *Engineering Fracture Mechanics*, 67:139–154, 2000.

[120] T. Siegmund and A. Needleman. A numerical study of dynamic crack growth in elastic-viscoplastic solids. *International Journal of Solids and Structures*, 34:769–787, 1997.

[121] G.H. Staab and A. Gilat. A direct-tension split hopkinson bar for high strain-rate testing. *Experimental Mechanics*, 31:232–235, 1991.

[122] D.Z. Sun, A. Hönig, W. Böhme, and W. Schmitt. Application of micromechanical models to the analysis of ductile fracture under dynamic loading. In F. Erdogan and R.J. Hartranft, editors, *Fracture Mechanics: 25th Symposium, ASTM STP 1220*, pages 343–357, Philadelphia, 1994. American Society for Testing and Materials, ASTM.

[123] D. Tang, D. Loosle, and B. Barthelemy. Laser and mig weld modeling method for aluminum structure crash analysis. *SAE paper #2002-01-2019*, IBAT2002, 2002.

[124] G.I. Taylor. The testing of materials at high rates of loading. *Proceeding of Institute of Civil Engineers*, 26(8):486–519, 1946.

[125] G.I. Taylor and H. Quinney. The latent energy remaining in a metal after cold working. *Proceedings of the Royal Society of London*, 143:307–326, 1934.

[126] C. Thaulow and W. Burget. The emission of rayleigh waves from brittle fracture initiation, and the possible effect of the reflected waves on crack arrest. *Fatigue and Fracture of Engineering Materials and Structures*, 13(4):327–346, 1990.

[127] C. Thaulow, Z.L. Zhang, Ø. Renestad, and M. Hauge. J-Q-M approach for failure assessment of fusion line cracks: two material and three material models. In *Fatigue and Fracture Mechanics, ASTM STP 1360*, number 30, pages 1–16. ASTM, 1998.

[128] P.F. Thomason. *Ductile fracture of metals*. Pergamon Press, Oxford, 1990.

[129] M.G.A. Tijssens, L.J. Sluys, and E. van der Giessen. Numerical simulation of quasi-brittle fracture using damaging cohesive surfaces. *European Journal of Mechanics A/Solids*, 19:761–779, 2000.

[130] M.G.A. Tijssens, E. van der Giessen, and L.J. Sluys. Modeling quasi-static fracture of heterogeneous materials with the cohesive surface methodology. In K.J. Bathe, editor, *Computational Fluid and Solid Mechanics, First MIT conference*, volume 1, pages 509–512, Amsterdam and London, 2001. Elsevier.

[131] C.E. Turner. A re-assessment of ductile tearing resistance, part I: The geometry dependence of J-R curves in fully plastic bending. In D. Firraro, editor, *ECF 8*, volume II, pages 933–949, EMAS, Warley, Turin, 1990.

[132] C.E. Turner. A re-assessment of ductile tearing resistance, part II: Energy dissipation rate and associated R-curves on normalized axes. In D. Firraro, editor, *ECF 8*, volume II, pages 951–968, EMAS, Warley, Turin, 1990.

[133] V. Tvergaard. On localization in ductile materials containing spherical voids. *International Journal of Fracture*, 18:237–252, 1982.

[134] V. Tvergaard. Effect of fibre debonding in a whisker-reinforced metal. *Materials Science and Engineering*, pages 203–213, 1990.

[135] V. Tvergaard. Material failure by void growth to coalescence. *Advances in applied mechanics*, 27:83–151, 1990.

[136] V. Tvergaard. Crack growth predictions by cohesive zone model for ductile fracture. *Journal of the Mechanics and Physics of Solids*, 49:2191–2207, 2001.

[137] V. Tvergaard. Prediction of mixed mode interface crack growth using a cohesive zone model for ductile fracture. *Journal of the Mechanics and Physics of Solids*, 52:925–940, 2004.

[138] V. Tvergaard and J.W. Hutchinson. The relation between crack growth resistance and fracture process parameters in elastic-plastic solids. *Journal of the Mechanics and Physics of Solids*, 40:1377–1397, 1992.

[139] V. Tvergaard and J.W. Hutchinson. The influence of plasticity on mixed mode interface toughness. *International Journal of Solids and Structures*, 41:1119–1135, 1993.

[140] V. Tvergaard and A. Needleman. Analysis of the cup-cone fracture in a round tensile bar. *Acta Metallurgica*, 32:157–169, 1984.

[141] V. Tvergaard and A. Needleman. Effect of material rate sensitivity on failure modes in the charpy V-notch test. *Journal of the Mechanics and Physics of Solids*, 34:213–241, 1986.

[142] V. Tvergaard and A. Needleman. Ductile failure modes in dynamically loaded notched bars. In J.W. Ju, D. Krajcinovic, and H.L. Schreyer, editors, *Damage Mechanics in Engineering Materials*, pages 117–128. ASME, 1990.

[143] V. Tvergaard and A. Needleman. Analysis of charpy V-notch test for weld. *Engineering Fracture Mechanics*, 65(6):627–643, 2000.

[144] P.W. Wnuck and J. Legat. Work of fracture and cohesive stress distribution resulting from triaxiality dependent cohesive zone model. *International Jornal of Fracture*, 114:29–46, 2002.

[145] L. Xia and C.F. Shih. Ductile crack growth I. a numerical study using computational cells with microstructurally-based length scales. *Journal of the Mechanics and Physics of Solids*, 43(2):233–259, 1995.

[146] L. Xia and C.F. Shih. Ductile crack growth II. void nucleation and geometry effects on macroscopic fracture behavior. *Journal of the Mechanics and Physics of Solids*, 43(12):1953–1981, 1995.

[147] C. Xu, T. Siegmund, and K. Ramini. Rate-dependent crack growth in adhesives I. modeling approach. *International Journal of Adhesion & Adhesives*, 23:9–13, 2003.

[148] X. Xu and A. Needleman. Numerical simulations of fast crack growth in brittle solids. *Journal of the Mechanics and Physics of Solids*, 42:1397–1434, 1994.

[149] X. Xu and A. Needleman. Numerical simulations of dynamic interfacial crack growth allowing for crack growth in brittle solids. *International Journal of Fracture*, 74:253–275, 1995.

[150] B. Yang, S. Mall, and K. Ravi-Chandar. A cohesive zone model for fatigue crack growth in quasibrittle materials. *International Journal of Solids and Structures*, 38:3927–3944, 2001.

[151] X. Zhang, Y.W. Mai, and R.G. Jeffrey. A cohesive plastic and damage zone model for dynamic crack growth in rate-dependent materials. *International Journal of Solids and Structures*, 40:5819–5837, 2003.

[152] Z.J. Zhang and G.H. Paulino. Cohesive zone modeling of dynamic failure in homogeneous and functionally graded materials. *International Journal of Plasticity*, 21:1195–1254, 2005.

[153] Z.L. Zhang, J. Ødegård, O.R. Myhr, and H. Fjær. From microstructure to deformation and fracture behavior of aluminum welded joints-a holistic modeling approach. *Computational Materials Science*, 21:429–435, 2001.

[154] Z.L. Zhang, C. Thaulow, and J. Ødegård. A complete Gurson model approach for ductile fracture. *Engineering Fracture Mechanics*, 67:155–168, 2000.

[155] M. Zhou, A. Needleman, and R.J. Clifton. Finite element simulations of shear localizations in plate impact. *Journal of the Mechanics and Physics of Solids*, 42:423–458, 1993.

Paper I

M. Anvari, I. Scheider, and C. Thaulow

Simulation of dynamic ductile crack growth using strain-rate and triaxiality-dependent cohesive elements

Published in

Engineering Fracture Mechanics

Vol. 73, pp. 2210-2228, 2006

Available online at www.sciencedirect.com
ScienceDirect
Engineering Fracture Mechanics 73 (2006) 2210–2228
Engineering Fracture Mechanics
www.elsevier.com/locate/engfracmech

Simulation of dynamic ductile crack growth using strain-rate and triaxiality-dependent cohesive elements

M. Anvari [a,*], I. Scheider [b], C. Thaulow [a]

[a] Department of Engineering Design and Materials, NTNU, Trondheim, Norway
[b] GKSS Research Center, Geesthacht, Germany

Received 28 June 2005; received in revised form 15 March 2006; accepted 26 March 2006
Available online 12 June 2006

Abstract

Rate-sensitive and triaxiality-dependent cohesive elements are used to simulate crack growth under quasi-static and dynamic loading conditions. The simulations are performed for a middle-cracked tension M(T) specimen made of an aluminum alloy (6XXX series). To consider the effect of stress triaxiality and strain rate on the cohesive properties, a single plane strain element obeying the constitutive equations of a rate-dependent Gurson type model has been used. The single element is loaded under various stress biaxiality ratios and strain rates and the obtained stress–displacement curves are considered as traction separation law for the cohesive elements. These curves are used for analyzing the aluminum M(T) specimen. The qualitative effects of constraint, strain rate, inertia and stress waves on the energy absorption of the specimen and crack growth are discussed.

Keywords: Cohesive zone modeling; Dynamic loading; Rate dependency; Stress triaxiality; Rate-dependent Gurson type model

1. Introduction

When a structure is subject to dynamic loading, some additional phenomena compared to quasi-static cases have to be considered. The high speed of deformation introduces stress waves into the structure. Inertia effects become significant and can affect the energy absorption of the structure. Strain rate increases the flow stress and influences the strain hardening of metals. And last, but not least, high local temperature increase due to adiabatic heating reduces the flow strength and counteracts the strain-rate hardening. Whether it is a stationary crack subject to impact loading, called ''impact fracture'', or it is a fast motion of the crack tip, named ''fast fracture'' [1], the mentioned phenomena can affect the fracture toughness significantly and it is important to have an efficient analysis tool for simulating damage and crack growth including these influences.

Analytical and macroscopic approaches used in fracture mechanics have some limitations with respect to the amount of plasticity allowed at the crack tip, constraint and geometry dependency. As Siegmund and

* Corresponding author.
E-mail address: majid.anvari@immtek.ntnu.no (M. Anvari).

0013-7944/$ - see front matter
doi:10.1016/j.engfracmech.2006.03.016

Brocks [2] point out, to the present, "local approaches" are the only really successful methods for prediction of crack growth resistance. In a local approach, in principle, the parameters of the respective model depend only on the material, and not on the geometry. In this kind of approach, one can simulate ductile fracture either by employing a micromechanical model of damage, which represents the micromechanism of void initiation, growth and coalescence, or by using a phenomenological model for material separation and coupling it to the surrounding undamaged elastic–plastic material. In the former approach, a representative volume element (RVE) or "unit cell" is considered to study the respective mechanism. The most widely known model of this kind for ductile damage calculation is the Gurson–Tvergaard–Needleman or GTN model [3]. Zhang et al. [4] proposed a model called "complete Gurson model" as a combination of GTN and Thomason's coalescence criteria [5]. This model has been used for unit cell calculations in the present article.

A phenomenological local approach used for the numerical simulation of crack propagation is known as the cohesive zone model. The idea is based on the pioneering work by Dugdale [6] and Barenblatt [7] who introduced the strip-yield model. Both authors divided the crack into two parts: One corresponds to the physical length of the crack, which is stress free, and the other one is the fracture process zone, where yielding and degradation of the material occur and which is loaded by a finite stress named cohesive stress. Later developments of cohesive models, particularly in combination with finite element method (e.g. [8–11]), considered the cohesive stress as a function of material separation and not depending on the distance from the crack tip as Barenblatt did. In a finite element representation of cohesive zone models, cohesive elements are introduced as interface between continuum elements and damage occurs only in the interface elements which obey a constitutive equation named traction separation law (TSL) (Fig. 1). Separation in these elements is calculated from the difference of the displacements of the continuum elements adjacent to them. The maximum opening at which the cohesive element completely fails is called critical separation, δ_0, and is one of the fracture parameters. The other fracture parameter is the maximum traction or cohesive strength, S. The area under the TSL is the energy absorbed by the cohesive element and is known as the cohesive energy, Γ_0:

$$\Gamma_0 = \int_0^{\delta_0} T(\delta)\,\mathrm{d}\delta \tag{1}$$

If the shape of a TSL is known or presumed, having two of the aforementioned parameters is enough to define the cohesive law.

By using cohesive zone modeling in a finite element analysis, it is possible to split the total dissipated energy into energy dissipated by plastic deformation in the process zone and the energy of separation. In this way, it is possible to evaluate the damage and deformation processes separately, but coupled. Besides, by entrusting the nucleation, propagation, branching and other aspects of the fracture behavior of materials to a master cohesive law, the amount of phenomenology is considerably reduced compared to theories of distributed damage. Since a characteristic length is included in the TSL (cohesive energy is the work of separation per unit area), the models with cohesive elements are not mesh dependent, which is always an issue for the GTN models [12].

Cohesive elements used in simulating ductile fracture are supposed to represent the mechanism of nucleation, growth and coalescence of microscopic voids that initiate at the inclusions and second phase particles.

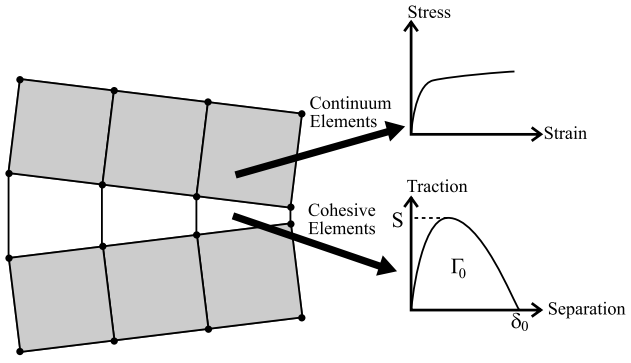

Fig. 1. Cohesive zone obeying a TSL and the surrounding undamaged elastic–plastic material.

The idea of the present contribution is to obtain the cohesive properties by studying the mechanical response of a single element obeying a rate-dependent Gurson type constitutive equation. This sort of mechanism-based cohesive model has also been proposed by other authors, e.g. [12–16]. It is well known that the cohesive strength increases with strain rate [17–19] and this implies an increase in stress triaxiality [20,21]. Using a Gurson type model provides a mean for exploring the effect of stress triaxiality on TSL parameters [12]. Rate sensitivity of the cohesive zone is determined by applying different values of loading speed on the rate-sensitive single element and calculating the cohesive parameters from the mechanical response. A similar procedure is performed by applying different stress ratios on the single element to study the effect of stress trixiality on the TSL parameters. The shape of the TSL, cohesive strength and critical displacement are fitted to meet the results of the single element calculations for various strain rates and triaxialities. The parameters are then used for crack growth simulations of an aluminum middle-cracked tension M(T). In the model, the cohesive elements are both triaxiality and rate dependent. Triaxiality-dependent cohesive elements have already been introduced to cohesive elements by Siegmund and Brocks [2], whereas the effect of dynamics on cohesive parameters is usually written by a separation rate dependency (see e.g. [18]). Even though the implementation of a strain-rate effect is a bit more complicated than a separation rate, it has the advantages that are described in Section 2.3.

Since the measures of strain rate and stress triaxiality are not available in the cohesive elements, they are calculated and transferred from the solid elements adjacent to them, which is performed in a similar way as proposed in [2] for only stress triaxiality values. The technique has also been used for strain-dependent cohesive elements by Tvergaard and Hutchinson [22]. The analyses are performed in quasi-static and dynamic cases. The effects of rate dependency, inertia, constraints and waves on mechanical response of the structure are shown by the load–displacement diagrams and the results are discussed. The influence of the pointed out phenomena on plastic energy dissipation and crack growth are illustrated, too. The influence of adiabatic heating has not been considered in the analyses.

The static and transient dynamic analyses are performed in ABAQUS/Standard non-linear finite element code [23]. The rate-dependent complete Gurson model developed and implemented into ABAQUS as a user defined material (UMAT) subroutine [24] is used for the single element calculations. The cohesive element calculations are performed by a user defined element (UEL) subroutine developed by Scheider [25] and expanded by the present authors for rate and triaxiality-dependent cohesive elements to be used in transient dynamic analysis.

2. Calculations

2.1. Material

Smooth round bars made of aluminum alloy 6XXX series were tested by split-Hopkinson tension bar in SIMLab of NTNU [26]. The experimental stress–strain curves at different strain rates are approximated by the following equation [27] as shown in Fig. 2:

$$\bar{\sigma} = \sigma_0 \left(1 + \frac{\bar{\epsilon}}{\epsilon_0}\right)^N \left(\frac{\dot{\bar{\epsilon}}}{\dot{\epsilon}_0}\right)^m \tag{2}$$

where $\bar{\sigma}$, $\bar{\epsilon}$, σ_0 and ϵ_0 stand for true stress, true plastic strain, yield stress, and a reference strain respectively. $\dot{\bar{\epsilon}}$ and $\dot{\epsilon}_0$ are the strain rate and a reference strain rate, respectively. N is known as strain hardening and m as strain-rate hardening exponent. In this formulation, the strength of the material increases with the increase of strain rate. The constitutive bahavior is based on von Mises plasticity with pure isotropic hardening. Viscous, i.e. time dependent effects are not considered. The values considered for the material tested are: $\sigma_0 = 217$ MPa, $\epsilon_0 = 0.002$, $\dot{\epsilon}_0 = 150\ \mathrm{s}^{-1}$, $N = 0.0526$, $m = 0.05$. Mass density of aluminum, $\rho = 2700\ \mathrm{kg/m}^3$ has been considered in all of the dynamic calculations.

2.2. Single element calculations

For ductile metals, the effective behavior of a unit cell containing a void can be captured by using the Gurson model [28] developed by Tvergaard [29] and Tvergaard and Needleman [3]. The latter, known as

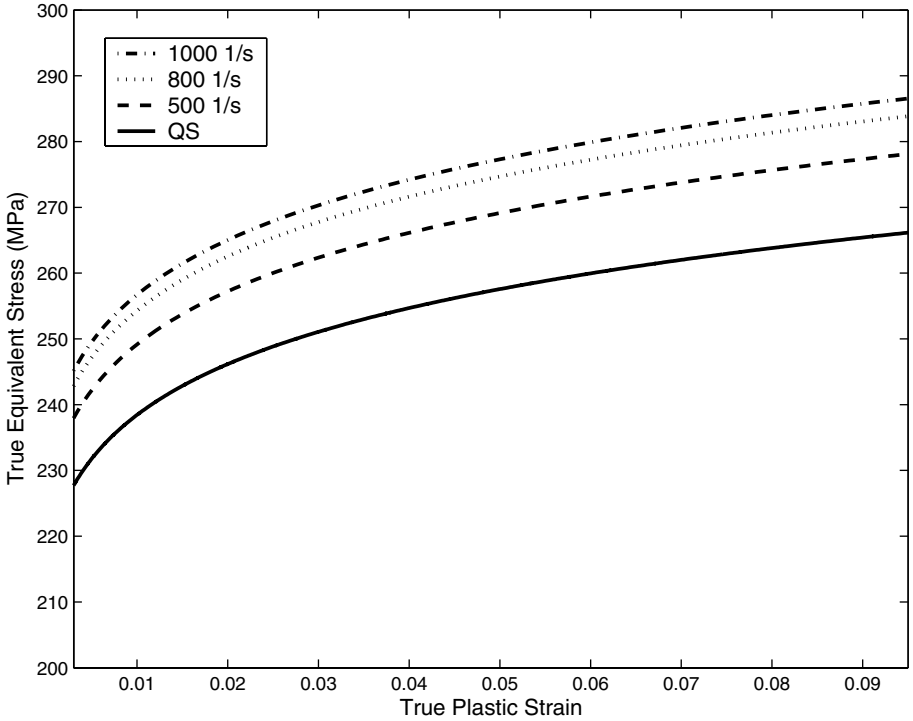

Fig. 2. The experimental stress–strain curves for different strain rates approximated by Eq. (6).

GTN uses a fixed critical void volume fraction, i.e. the point where coalescence starts, as a material parameter. Koplik and Needleman [30] showed that this assumption works well only for low stress triaxiality cases, and slightly worse for high stress triaxiality cases, which is the case in front of a crack tip. Zhang et al. [4] introduced the Thomason's coalescence criteria [5] into the Gurson model so that it can predict void coalescence. In their approach which they called "complete Gurson model", they also proposed final void volume fraction to be a function of initial void volume fraction. In the strain-rate-sensitive version of the model, the flow stress is a function of local strain rate with the same strain-rate hardening exponent as that of the bulk material. Details on the rate-dependent Gurson model is found elsewhere (e.g. [31,32]).

The question that arises is which of the phenomena influencing ductility because of dynamic loading conditions is more important to be considered in modeling a single Gurson type element. Curran et al. [33] considered rate-sensitive material for a hollow sphere of internal radius, a, subjected to internal constant pressure, P_0. The material was considered to be rigid, perfectly plastic with a viscosity coefficient. Their numerical investigation for aluminum showed that the inertia effect becomes important for quite large voids (larger than 10 μm) and for a wide range of radii a, the maximum rate is governed by the viscous regime only. In other words, as far as void size is smaller than a certain value, inertia can be ignored in modeling void growth under dynamic loading. Considering the work done by Johnson [34], it is concluded that the inertia effect is important in void growth only if the speed of crack growth is higher than $4\sqrt{\sigma_0/\rho}$ where σ_0 and ρ are the flow stress and the density of the material, respectively. This value is around 1100 m/s for a typical aluminum alloy. Liu [35] also showed that increasing strain rate will increase the inertia effect, but this effect is significant only when the strain rate is over 10,000 s^{-1}.

Based on these discussions, only rate sensitivity of the material has been considered. The effect of the adiabatic heating is ignored in all of the calculations.

In the present study, a single four node plane strain element with rate-dependent complete Gurson model as constitutive equation is used. The initial void volume fraction of $f_0 = 0.002$ is considered in the calculations as suggested in [36], since no experimental data on micromechanical information is available for this parameter.

The analyses are performed for an element with the initial size of $h \times h$, $h = 1$ mm, for different stress biaxialities β, as shown in Fig. 3:

$$\beta = \frac{\sigma_{11}}{\sigma_{22}} \tag{3}$$

If the material is incompressible, the stress triaxiality which is the ratio between mean normal stress and von-Mises equivalent stress is given by [12]

$$H \approx \frac{1+\beta}{\sqrt{3}(1-\beta)} \tag{4}$$

The constant stress ratios in static loadings were obtained using modified Riks method implemented in ABAQUS. The reason for using Riks method is the instability in load controlled calculations due to softening. Fig. 3 shows the normalized traction separation obtained for different values of triaxiality. Fig. 4 shows the variation of normalized strength and energy obtained from Fig. 3 versus triaxiality. The curves are fitted to the calculated values.

In order to investigate the effect of strain rate on the stress–elongation behavior, quasi-static analyses were performed with a rate-dependent model and high speed loading. Since strain rate was considered, Riks method was not applicable any more. Thus, two linear springs were added to the model and the multi-point constraint (MPC) subroutine in ABAQUS was used to obtain constant stress ratios. For low speed of applied loads, the responses were the same as the Riks method. Fig. 5 shows the normalized traction separation behavior for different triaxialities for a loading rate of 500 mm/s or, in other words, an initial strain rate of 500 s^{-1} for an element of initial length $h = 1$ mm. The figure shows that the effect of triaxiality is similar to the case with rate-independent material behavior, but the values of cohesive strength and consequently cohesive energy are different. To check this, various loading speeds were applied for the same triaxiality of 1.5 ($\beta = 0.44$). Fig. 6 shows that the curves are parallel and only the value of strength changes for the same maximum displacement. Fig. 7 shows the curves fitted to the calculated values of strength and energy for the rate-dependent case at constant loading rate ($V = 500$ mm/s) and different triaxiality values. Comparing this figure with Fig. 4, it is observed that the fitted curves are very similar to the rate-insensitive case.

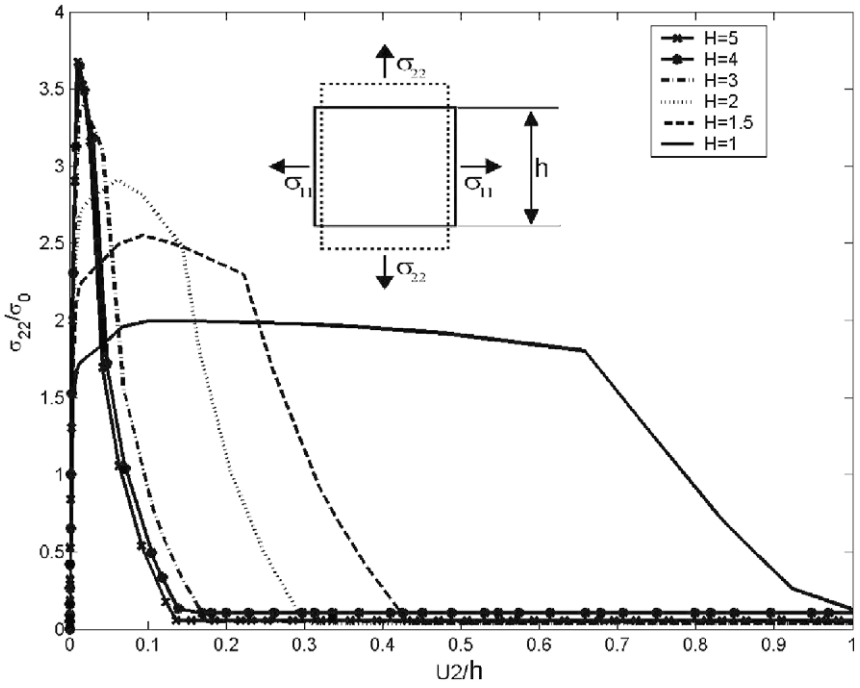

Fig. 3. The effect of triaxiality on the traction separation behavior of a single element obeying complete Gurson model.

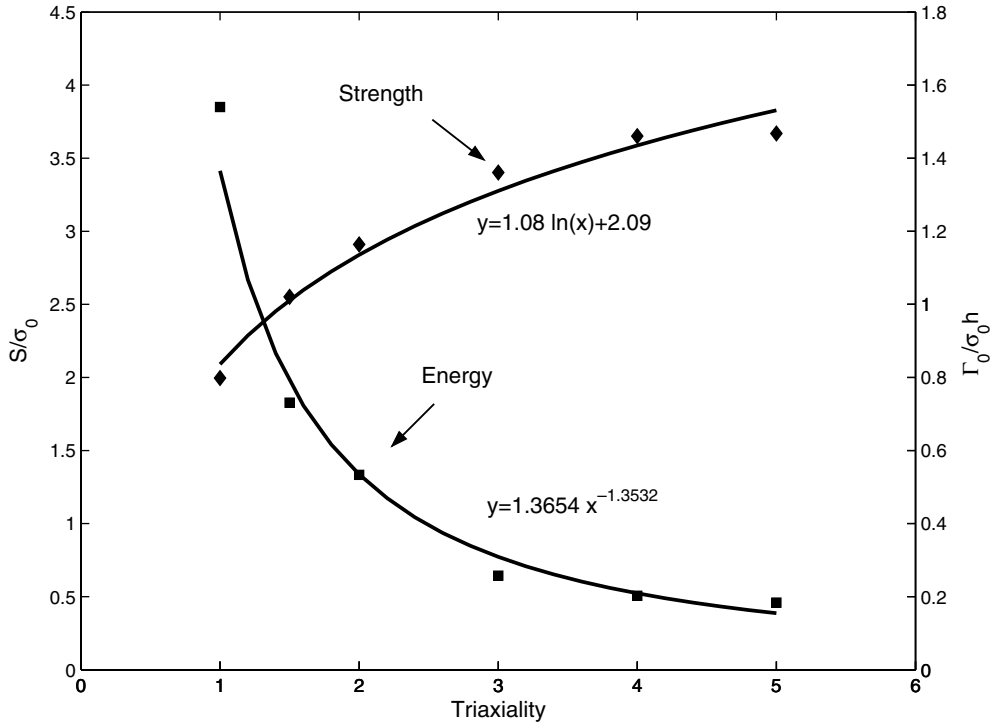

Fig. 4. Variation of normalized cohesive strength and cohesive energy versus applied triaxiality for rate-insensitive material.

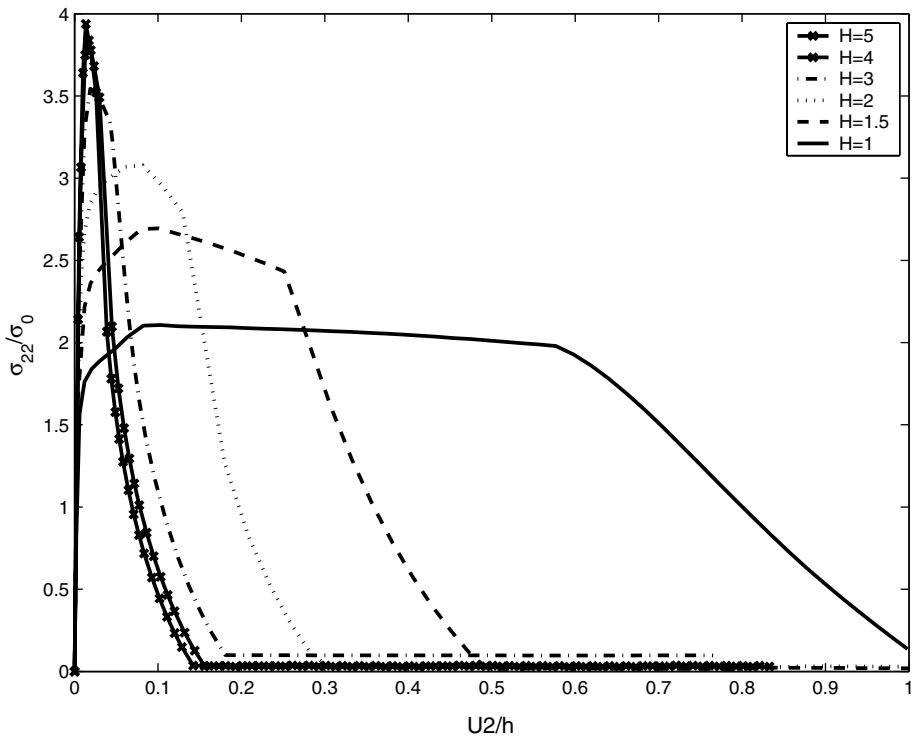

Fig. 5. Normalized traction separation behavior in different triaxialities for a load speed of 500 mm/s (initial strain rate of 500 s^{-1}).

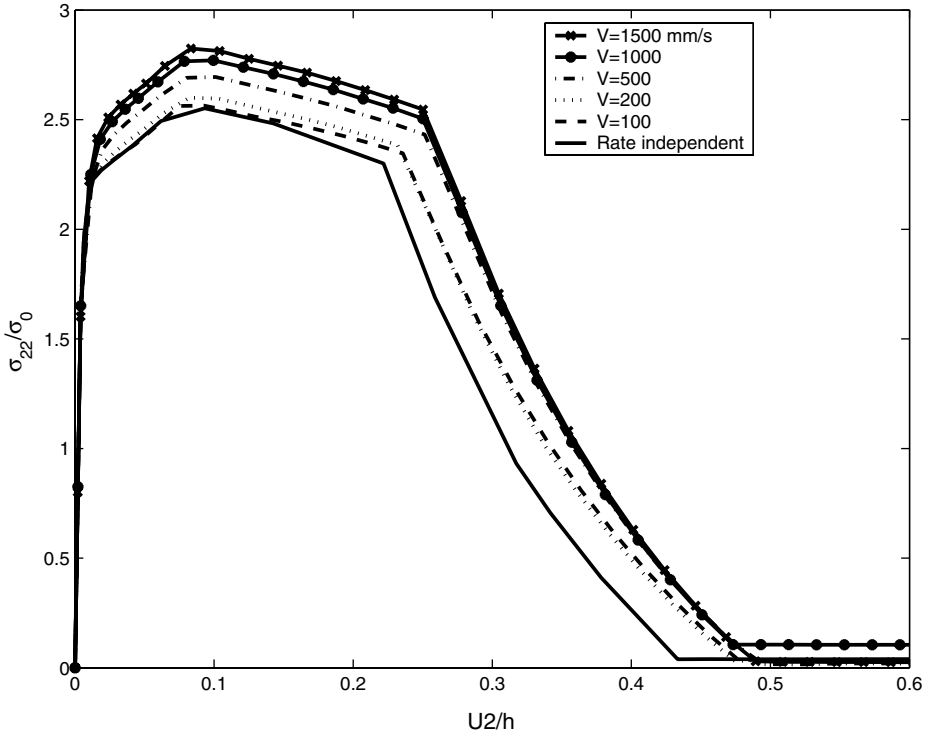

Fig. 6. Normalized traction separation behavior at different load speeds (initial strain rate) and constant triaxiality ($H = 1.5$).

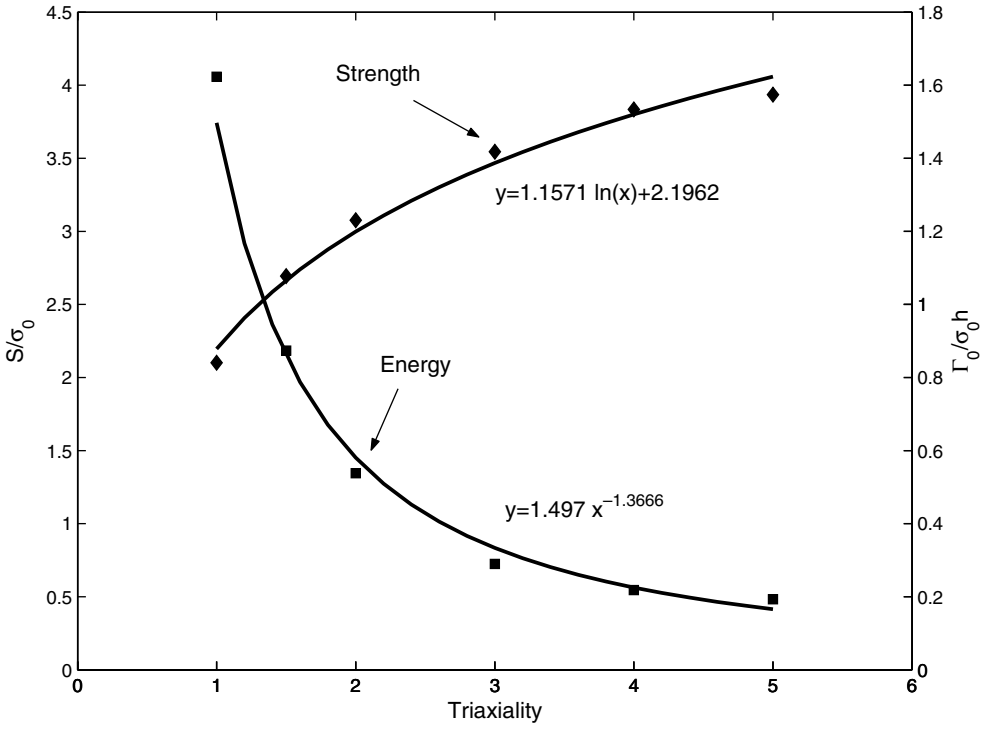

Fig. 7. Variation of normalized cohesive strength and normalized cohesive energy versus different triaxialities in constant load speed of 500 mm/s.

Fig. 8 shows how the values of cohesive strength and cohesive energy change with loading rate for a constant triaxiality of 1.5. As it is shown, the value of the maximum traction changes as a function of the rate-independent case for the same triaxiality multiplied by the relative strain rate to the power of m (strain-rate hardening exponent).

2.3. Traction separation law

Since the cohesive model is a phenomenological model, authors use various formulations for defining the shape of TSL and the cohesive values (e.g. [8,10,37,13,38,39]). Among these definitions, the one introduced by Scheider and Brocks [39] has been used to reproduce the calculated damage and failure of the unit cell by a cohesive element. This TSL has two shape parameters, δ_1 and δ_2, in addition to the cohesive parameters already introduced and consists of three parts: (a) increasing traction or cohesion, (b) constant traction and (c) decreasing traction or decohesion (see Fig. 9). The traction as a function of the separation in this model is

$$T = S\begin{cases} 2\left(\frac{\delta}{\delta_1}\right) - \left(\frac{\delta}{\delta_1}\right)^2, & 0 < \delta < \delta_1 \\ 1, & \delta_1 < \delta < \delta_2 \\ 2\left(\frac{\delta-\delta_2}{\delta_0-\delta_2}\right)^3 - 3\left(\frac{\delta-\delta_2}{\delta_0-\delta_2}\right)^2 + 1, & \delta_2 < \delta < \delta_0 \end{cases} \tag{5}$$

By changing δ_1 and δ_2, one can have a variety of TSL shapes. In this formulation, the maximum separation is

$$\delta_0 = \frac{2\Gamma_0}{S}\frac{1}{1 - \frac{2}{3}\frac{\delta_1}{\delta_0} + \frac{\delta_2}{\delta_0}} \tag{6}$$

Although it has been claimed that the shape of the TSL hardly influences the crack growth behavior [13,37,40,41], there are a few investigations that show higher effects of the shape [19,42,43]. For example,

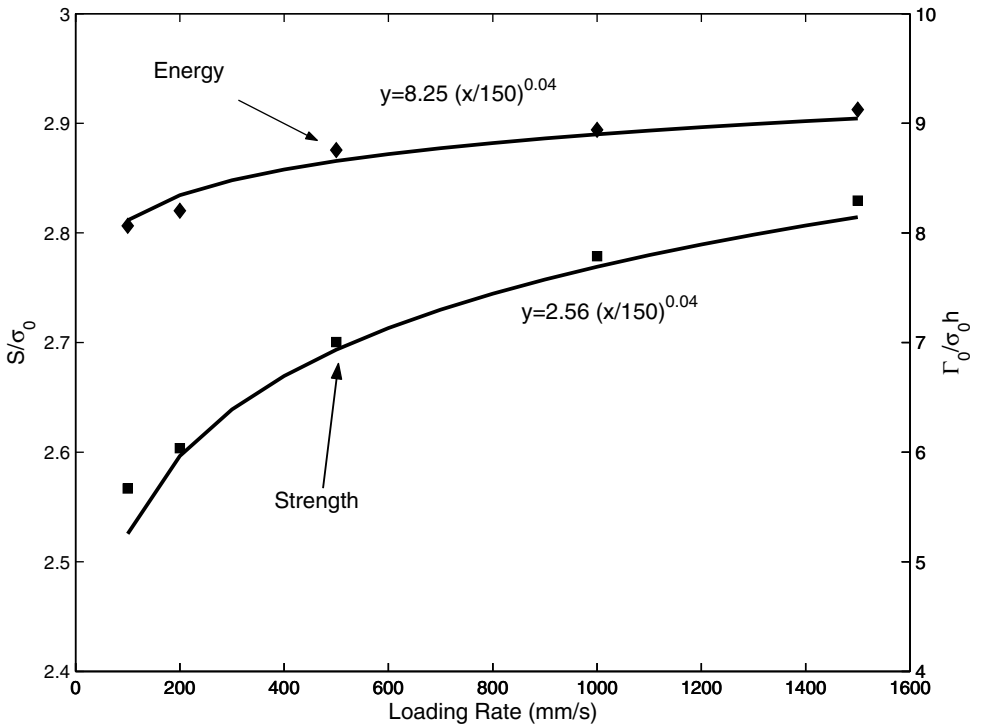

Fig. 8. Cohesive strength and cohesive energy versus load speed for a constant triaxiality of 1.5.

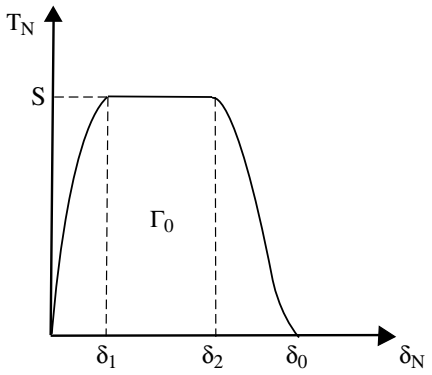

Fig. 9. TSL shape proposed by Scheider and Brocks [39].

Scheider and Brocks [42] showed numerically that not only the shape of the TSL can affect the load–displacement behavior, but also the TSL shapes that make the same results in a fracture specimen, might make different results in another specimen. Falk et al. [43] showed that if the TSL is initially rigid, the model cannot capture crack branching by using a regular finite element mesh and it is possible when the TSL has initial elasticity.

Regarding uncertainties like these, rate-dependent Gurson type model has been used as the basis for obtaining the TSL.

It is possible to obtain the following expressions for the cohesive strength and energy using the mathematical approximations shown in Figs. 4, 7 and 8 as

$$\frac{\Gamma_0}{h} \approx 1.43 H^{-1.36} \sigma_0 \left(\frac{\dot{\bar{\epsilon}}}{\dot{\epsilon}_0} \right)^m \tag{7}$$

$$S \approx (1.1 \ln(H) + 2.1) \sigma_0 \left(\frac{\dot{\bar{\epsilon}}}{\dot{\epsilon}_0} \right)^m \tag{8}$$

The variable h is the characteristic length scale of the Gurson model, which is usually based on the micromechanical structure of the material. A value of $h = 0.1$ mm is chosen in accordance to [44] who also investigated an aluminum alloy of 6XXX series. H is the stress triaxiality. The expression in Eq. (8) is similar to the results obtained analytically by Zhang et al. [19] which show that the curves of normalized traction along the cohesive zone are parallel at various crack speeds and the cohesive strength increases with crack growth rates. It has also been pointed out by Freund [45] that as the crack moves more rapidly, the material is deformed more rapidly and a larger cohesive stress is required in order to achieve the requisite crack tip opening displacement.

Considering e.g. Fig. 5, it is recognizable that the piecewise TSL defined by Eq. (5) and shown in Fig. 5 fits properly to the curves if the shape parameters δ_1 and δ_2 are adjusted accordingly. Combining Eqs. (6)–(8), the critical separation reads

$$\frac{\delta_0}{h} \approx \frac{2.8 H^{-1.36}}{1.1 \ln(H) + 2.1} \frac{1}{1 - \frac{2}{3}\frac{\delta_1}{\delta_0} + \frac{\delta_2}{\delta_0}} \tag{9}$$

The comparison between the stress elongation behavior obtained from rate-dependent Gurson model calculations and the TSL approximation of Eq. (5) with the cohesive parameters from Eqs. (8) and (9) and $\frac{\delta_1}{\delta_0} = 0.07$ and $\frac{\delta_2}{\delta_0} = 0.35$ are shown in Fig. 10 for two different triaxiality values. Since the curves obtained from the single element calculations and those based on Eq. (9) are not exactly the same, the critical displacements are a slightly different for the same cohesive strength and energy, but the differences are reasonable.

It is worth noting that the initial stiffness of the cohesive elements is relatively high. Therefore, the separations are very small in the beginning until the cohesive strength is reached. This is an important indication for the use of a strain rate instead of a separation rate-dependent cohesive model. The cohesive strength is strongly influenced by the rate, and in the beginning most of the deformation takes place in the adjacent

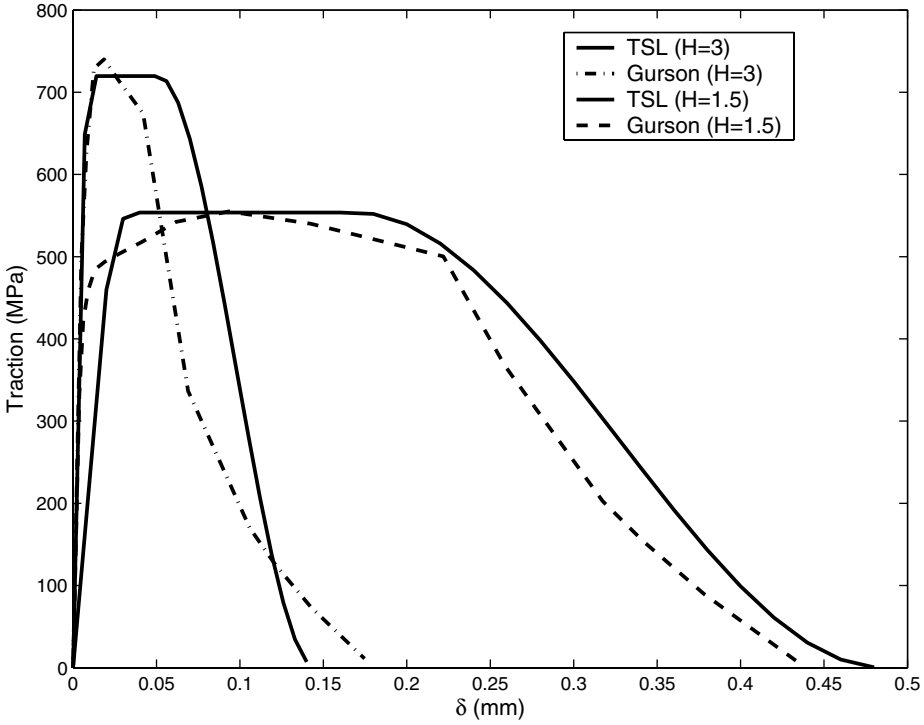

Fig. 10. A comparison between traction separation behavior obtained from Gurson type model and the TSL proposed in Eq. (5).

continuum elements whereas the cohesive elements are still closed. On the other hand, the effect of the rate on the softening branch of the traction separation law is of minor importance since the characteristic of the damage behavior is then more affected by the cohesive energy parameter which is not much dependent on strain rate (see Figs. 6 and 8).

3. Crack growth simulations and results

An M(T) specimen of unit thickness and dimensions of $100 \times 100\ \text{mm}^2$ has been modeled using four node plane strain elements. The ratio of the initial crack length to the specimen's width is $a/W = 0.5$. One row of cohesive elements with initial zero height has been used at the ligament. Because of symmetry, one fourth of the specimen has been modeled. Fig. 11 shows the specimen and the detailed mesh at the crack tip and a part of the ligament. The smallest continuum element size belongs to the elements adjacent to the ligament and it is $0.1 \times 0.1\ \text{mm}^2$.

The surrounding continuum elements behave according to Eq. (2) and the cohesive elements based on Eqs. (5), (7), (8) and (9). Each cohesive element possesses four nodes and two integration points. Because of the symmetry, only the two upper nodes of cohesive elements are shared with the adjacent continuum element and the other two obey the displacement conditions of symmetry. For each cohesive element, the actual values of nodal displacement, triaxiality and strain rate are used to compute the current value of traction and element stiffness. The values of triaxiality and strain rate are calculated in the continuum elements along the ligament at all of the integration points using UVARM subroutine in ABAQUS. The averages of these values are then calculated after the load increment and provided to the respective adjacent cohesive elements in the next increment as shown in Fig. 12. The error of this kind of explicit scheme is accepted since the time increments are always chosen to be small enough.

Material separation process involving void growth and plastic deformation at microlevel are irreversible by nature. This property has been implemented in the cohesive element formulation in a sense that a separation

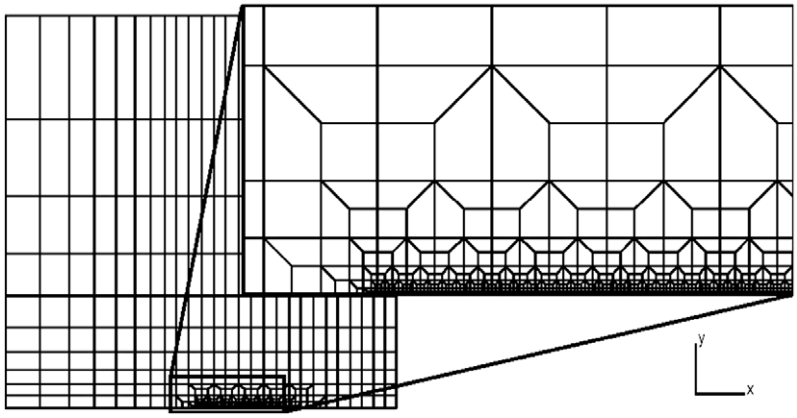

Fig. 11. The M(T) specimen and a detailed finite element model of the crack tip.

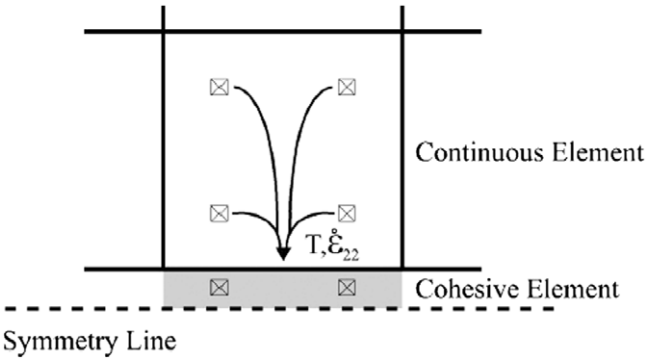

Fig. 12. The triaxiality and strain-rate values are transferred to cohesive elements from the adjacent continuum elements.

already happened to an element remains after local unloading and relaxing the stress [25]. Local unloading can happen because of global unloading, stress waves or crack branching.

The simulations performed are described in Table 1. The aim of the analyses is to check the influence of constraint, rate sensitivity, inertia and elastic waves on the energy absorption of a typical M(T) specimen. In the static simulations, the effect of triaxiality on the energy absorption is studied. In the dynamic analyses, denoted by DYN-xxx, the effects of inertia and elastic waves are investigated as well as the influence of stress triaxiality and rate sensitivity.

Fig. 4 shows that the change of cohesive energy (critical displacement) is very high for triaxiality values of $H < 1.5$. The reason is that for small values of triaxiality, the initial void grows very little and therefore the energy absorbed is mostly related to the plastic deformation and not damage in the cell model. For more detailed discussions on the limitations of the application of cell model and the competition between cohesive

Table 1
Various simulations of M(T) specimen

Case	Analysis	Plasticity	Cohesive zone
QS	Quasi-static	Rate independent	Constant
QS-CTD	Quasi-static	Rate independent	Triaxiality dependent
DYN	Transient dynamic	Rate independent	Constant
DYN-MRD	Transient dynamic	Rate dependent	Constant
DYN-MCRD	Transient dynamic	Rate dependent	Rate dependent
DYN-MCRD-CTD	Transient dynamic	Rate dependent	Rate and triaxiality dependent

process zone and plastic flow (see [20]). It is also known that the M(T) specimen is a low constraint fracture specimen. The analyses show that the stress triaxiality at the crack tip increases while the crack is growing. Regarding these discussions, $H = 1.2$ was considered as an initial stress triaxiality value used in the simulations. Below this value, the cohesive parameters were considered to be constant, i.e.:

$$\frac{\Gamma_0}{h} = \begin{cases} 237.6\left(\frac{\dot{\epsilon}}{\dot{\epsilon}_0}\right)^m, & H < 1.2 \\ \text{Eq. 7}, & H \geqslant 1.2 \end{cases} \tag{10}$$

$$S = \begin{cases} 474\left(\frac{\dot{\epsilon}}{\dot{\epsilon}_0}\right)^m, & H < 1.2 \\ \text{Eq. 8}, & H \geqslant 1.2 \end{cases} \tag{11}$$

The cohesive parameters for $H = 1.2$ were also used for the triaxiality independent analyses.

The load was applied as a prescribed displacement at the upper edge of the specimen. In dynamic cases, the speed of the load was 3.3 m/s. The load and displacements presented in the following diagrams are the values calculated on the boundary of the model.

Fig. 13 shows the load–displacement curves for quasi-static solutions. The figure shows that ignoring triaxiality dependency of interface elements can lead a static crack growth analysis to be highly conservative, because the prediction of the energy absorption is much lower than the constraint (stress triaxiality) dependent case. This shows that the values of triaxiality increase to more than the initial value considered in the analyses.

Fig. 14 shows the load–displacement curves obtained from dynamic analyses. Since transient dynamic solution has been employed, inertia and elastic waves are inherent in the analyses. The existence of oscillations in the curves is inevitable because of the existence of elastic waves. The time that elastic waves travel the length of the specimen is around 20 μs; that is much shorter than the total time of fracture (the shortest time of fracture is 131.8 μs, which is for the case of rate-dependent bulk material). The elastic waves can have two sources, one is the dynamically applied load and the other is the wave induced by broken cohesive elements or, in other

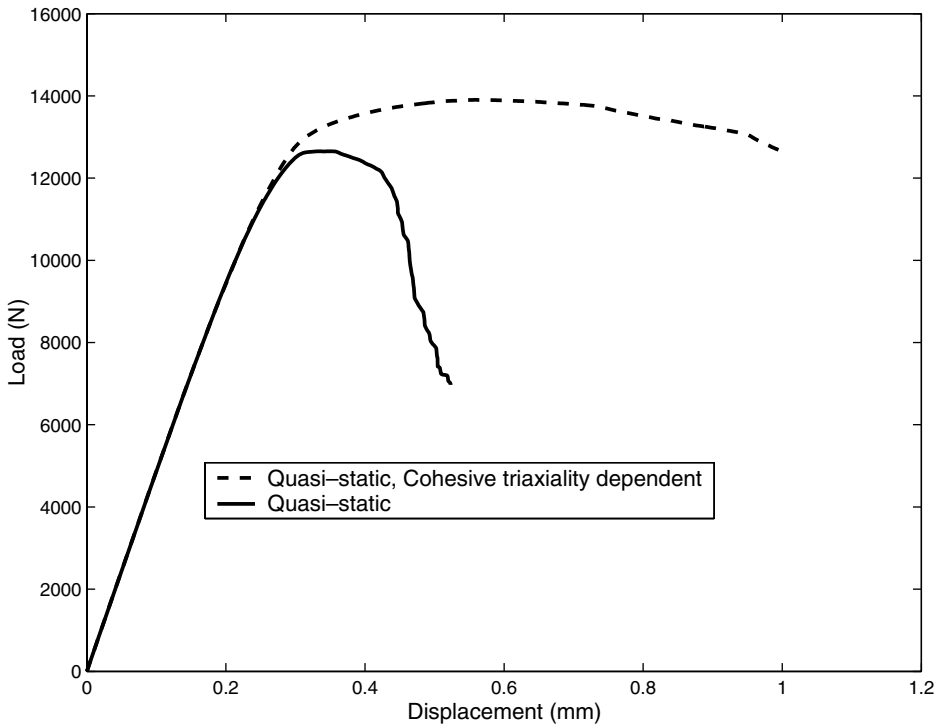

Fig. 13. The effect of constraint on the load–displacement behavior (static analysis).

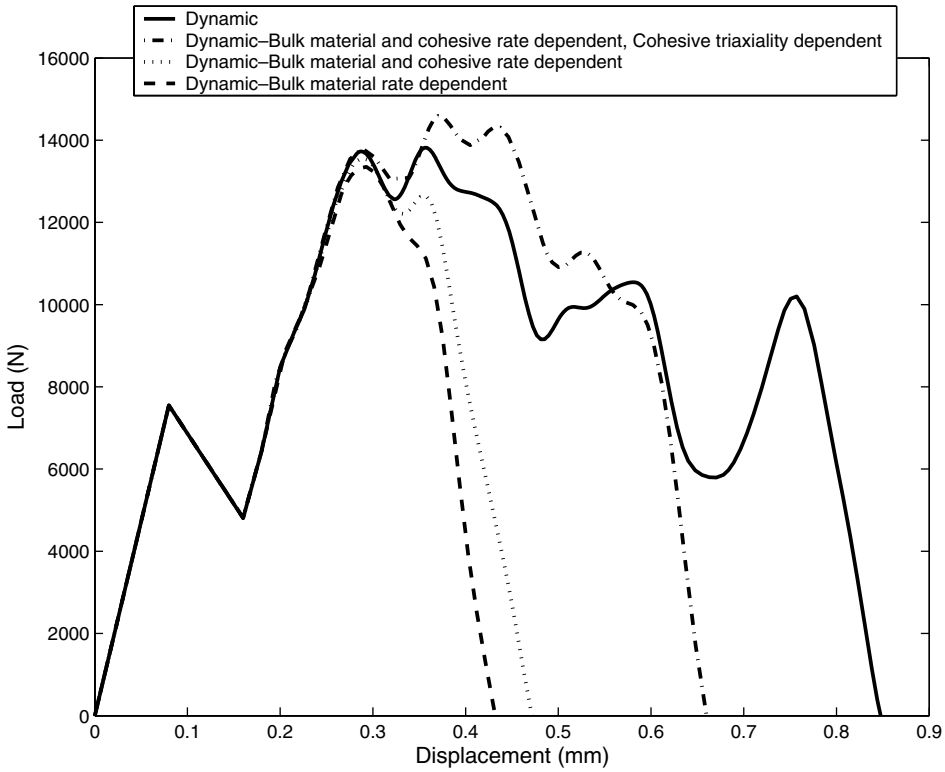

Fig. 14. The effect of strain rate and constraint on the load–displacement behavior (dynamic analysis).

words, the waves induced because of the relatively high speed of the crack growth. Because of the implicit integration used in the dynamic analyses, there is no severe limitation on the time increment chosen. Repeating one of the simulations with very short maximum allowable time increments (0.02 μs instead of 24 μs) showed that the averaged results are similar, but the rate of convergence is very low and the simulation is extremely time consuming.

Dynamic simulation considering the rate dependency only for bulk material leads to the most conservative assumption. Ignoring the effect of strain rate and triaxiality on the behavior of interface elements makes the results unrealistic. Using rate- and triaxiality-dependent cohesive elements results in more energy absorption, although it is less than the simulation which ignores all of these influences.

Fig. 15 shows the crack growth versus time for dynamic simulations. In all of the cases, the crack speed is low in the beginning and then it increases to a somewhat steady state speed. The case with no rate dependency is an exception in it seems that the crack speed is changing during the growth. The figure shows clearly that the steady state speed of the crack growth is highest, about 1430 m/s, for the case in which only bulk material is rate dependent. If an average speed is defined for the case with no rate dependency, the lowest crack growth speed of around 290 m/s is obtained for this case. It should be noted that for the case where both bulk material and cohesive zone are rate dependent, the crack growth initiation happens almost at the same time as for the case with no rate dependency. This is in contrast to the investigations of Basu [46] who numerically showed that strain-rate sensitivity plays a beneficial role on dynamic ductile fracture initiation. This contradiction is related to ignoring triaxiality change even at the first stages of deformation. It is observed in Fig. 15 that when triaxiality dependency is considered, crack growth initiation happens at 69 μs which is higher than the rate-insensitive case. To check if this effect is due to the rate sensitivity of the material, a dynamic case was simulated with triaxiality-dependent cohesive elements while no rate sensitivity was considered. The analysis showed that the crack growth initiation happened at 61.8 μs. This proves that rate sensitivity has postponed crack growth initiation, although after a short time, crack growth speed is higher than the rate-insensitive case.

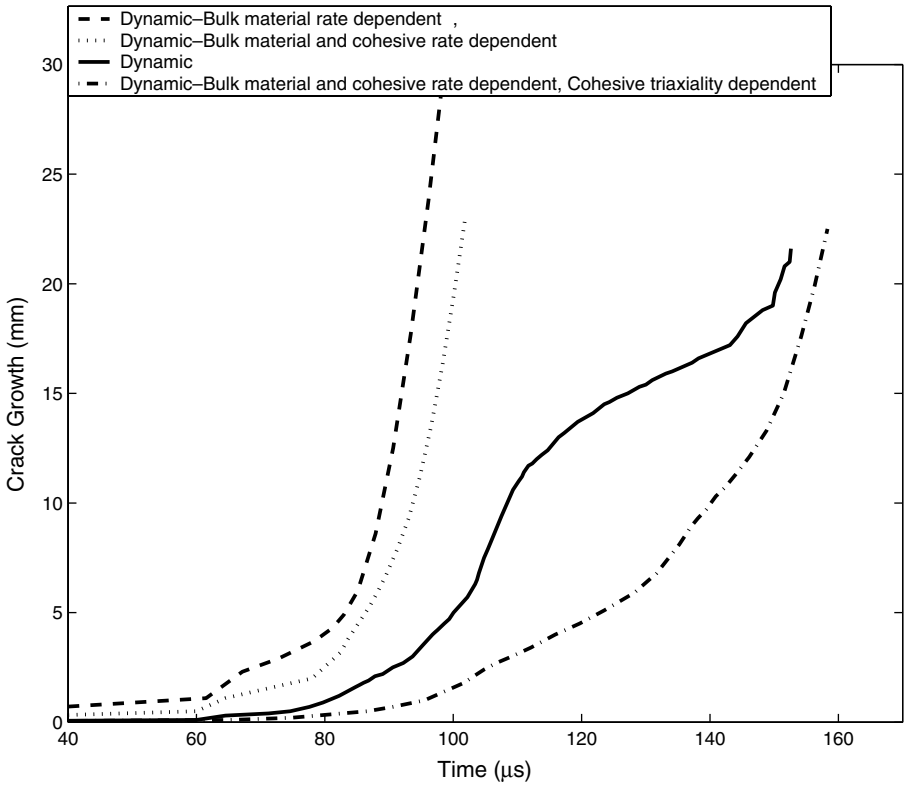

Fig. 15. The effect of strain rate and constraint on crack growth rate (dynamic loading).

It should also be noted that in the case where stress triaxiality change has been ignored, the crack growth velocity becomes so high that the assumption of ductile mechanism of crack growth might be inaccurate. It is worth noting that for the case in which only rate dependency of bulk material has been considered, the crack speed is around 1400 m/s. In this case, the inertia effect on fracture energy is important, but it has been ignored in the calculation. Regarding these discussions and back to Fig. 14, it is well understood why the load in the triaxiality- and rate-dependent case is higher in the beginning and drops very fast after some time. This is qualitatively compatible with Freund's finding [45]. He used a rate-sensitive cohesive zone and showed analytically, with some assumptions on the amount of plasticity and material behavior, that for high speed of crack growth (more than about 20% of shear wave propagation velocity), "as the crack tip speed increases for some fixed level of viscosity (rate sensitivity), the local stress is elevated and a smaller applied stress intensity factor is required for crack growth". He also showed that for lower crack speeds or smaller viscosities, however, the criteria is reversed.

The reason why crack speed is much higher in the case of rate-dependent plasticity is that the material hardens due to high loading rate and opens the crack (cohesive elements) more easily. Fig. 16 shows the ratio of dissipated plastic energy to the external work versus crack growth. This figure shows that for the rate-sensitive material, the percentage of the energy absorbed by the plastic deformation is less compared to the rate-insensitive case and the difference increases with crack growth. When the cohesive zone is rate dependent, the cohesive strength is increased at high loading rates and this causes more energy dissipated by plasticity in the surrounding material. Although the stresses needed for crack propagation are higher compared to the case with rate-independent cohesive parameters, the cohesive strength, S, is not high enough to decrease the crack growth rate as much as for the rate-insensitive case. The reason is that with increasing plasticity, the crack opening speed decreases, so the local strain rate and consequently the cohesive strength decrease again. Besides, stress triaxiality increases initially, but because of inertia it decreases while the crack is growing [47]. This means that the decrease of the cohesive strength is related to the inertia. Fig. 17 shows the change

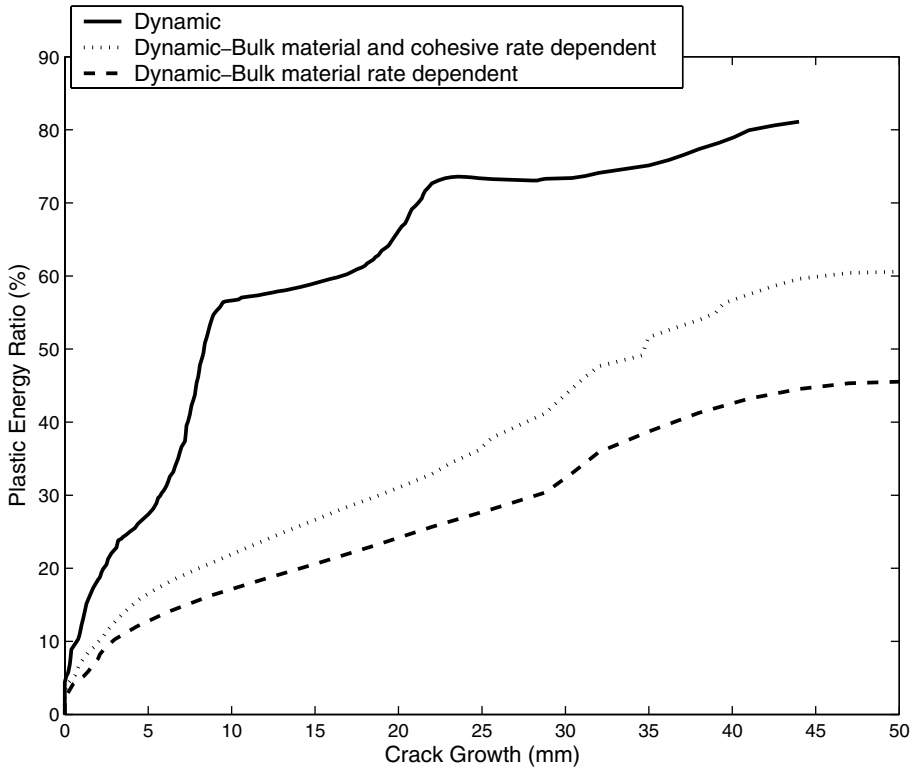

Fig. 16. The effect of strain-rate sensitivity on percentage of energy dissipated by plastic deformation during crack growth.

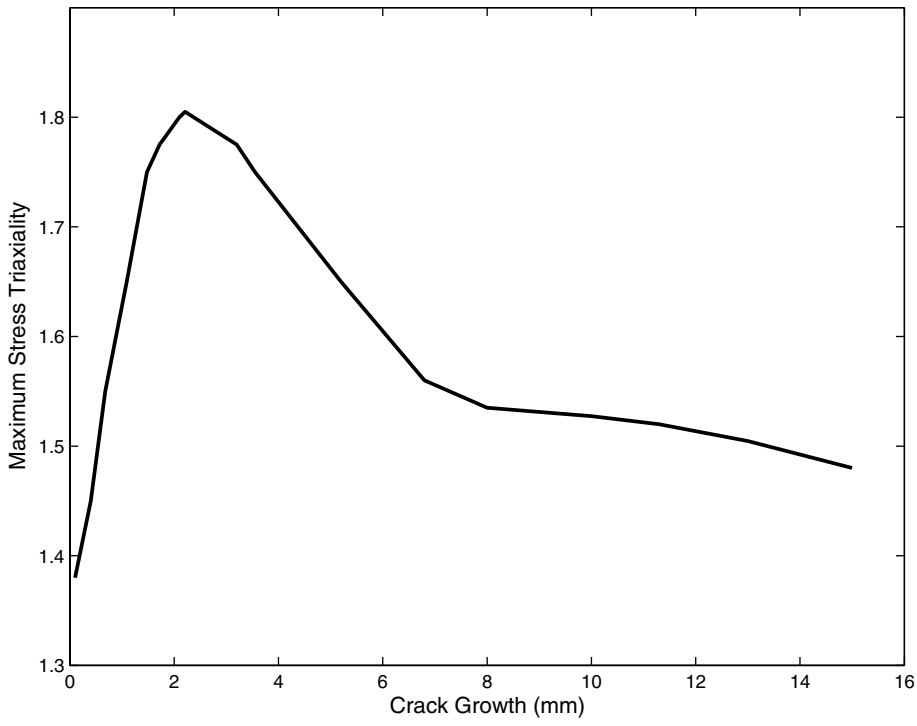

Fig. 17. The change of stress triaxiality during crack growth under dynamic loading conditions.

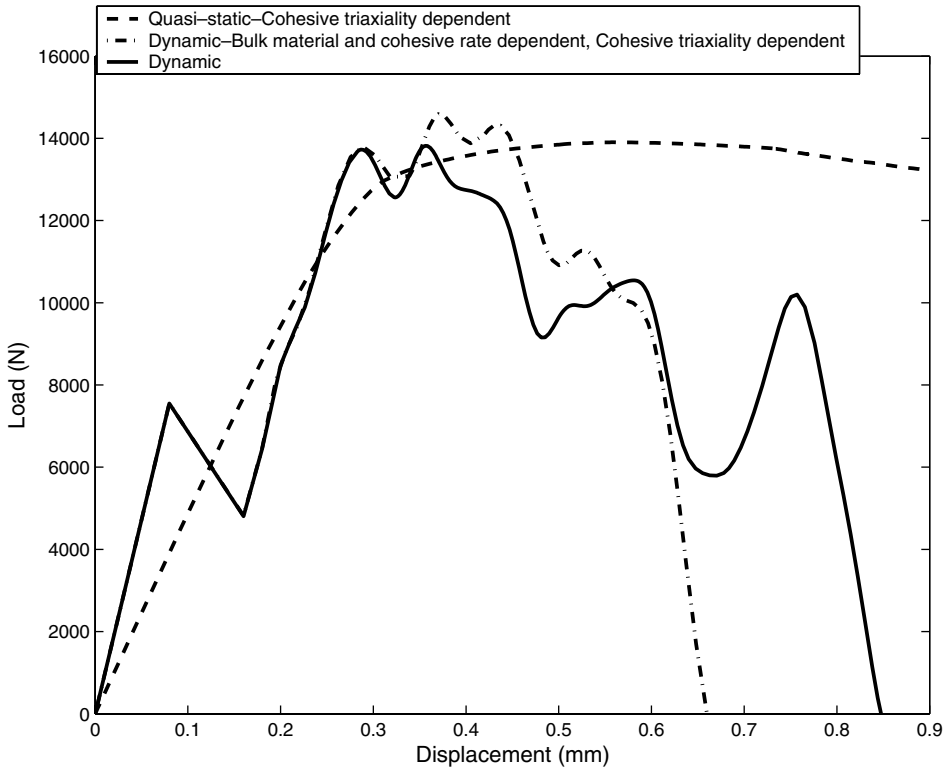

Fig. 18. A general comparison between quasi-static and dynamic cases.

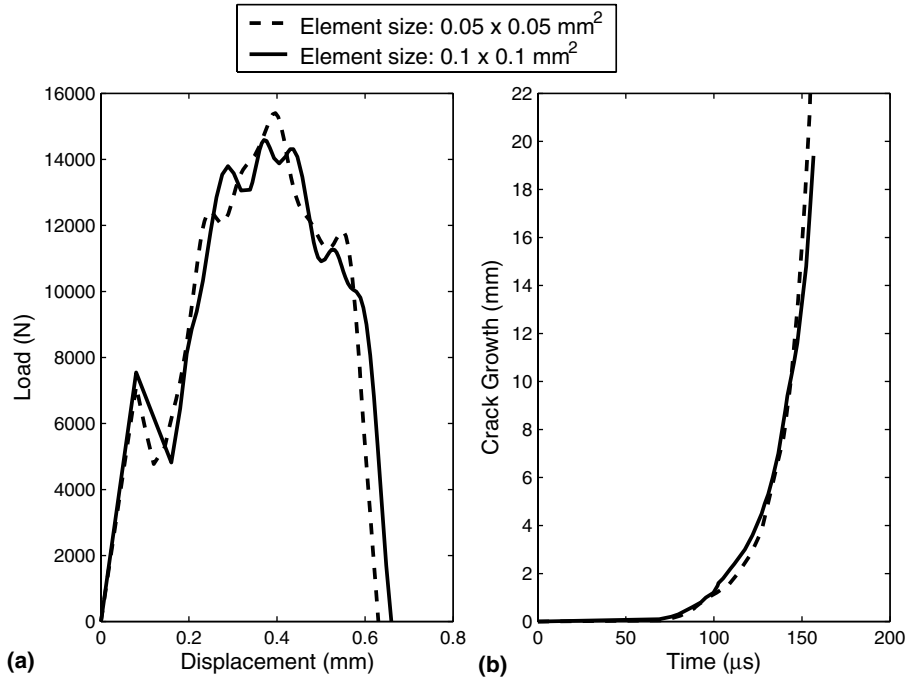

Fig. 19. The effect of element size on (a) load–displacement curve, (b) crack growth.

of triaxiality value during crack growth for the case in which rate dependency and triaxiality have been considered for the cohesive elements.

Fig. 18 shows how the phenomena mentioned in the introduction part affect the mechanical response of the structure and makes it clear that the effect of the combination of them is not easily predicted. It demonstrates that although rate dependency and inertia can increase the maximum load in a displacement-controlled loading, rate dependency decreases the total energy absorption of the specimen. This is in contrast to an uncracked specimen in which rate-dependent plasticity and inertia increase the energy absorption under dynamic loading.

It was already mentioned that models with cohesive elements are mesh independent, but since an average of field variables is calculated in the adjacent continuum element, this average may depend on the element size. To check the influence of rate-sensitive cohesive elements on the mesh dependency of the model, the specimen was also modeled by element size of $0.05 \times 0.05\ \text{mm}^2$ for the continuum elements adjacent to the ligament. Fig. 19(a) shows the load–displacement curves for the two models. It is observed that the effect is insignificant and only exists in the last part of the deformation. Fig. 19(b) shows that the crack growth rates are similar up to some time and then the crack growth speed is slightly higher in the model with finer mesh. With the element sizes considered in the present models, mesh density is not very important, especially for the global energy absorption predicted. It should be noted that although cohesive zone models are theoretically mesh independent, the mesh must not be so coarse that the calculation of local plastic strain field is imprecise or mesh dependent [48].

4. Conclusion

The effect of triaxiality and strain rate on cohesive properties has been considered simultaneously in a finite element dynamic crack growth simulation. Cohesive strength increases with strain rate and this implies an increase in stress triaxiality. Taking into account the interaction between these influences to solve dynamic crack growth problems in a closed form is not an easy task to do. The change of cohesive properties with these variables has been obtained through calculations on a cell model obeying rate-dependent Gurson constitutive equation. The results of the calculations have been used in crack growth simulations of a center-cracked specimen under static and dynamic loading. The procedure has the ability to take into account the effect of stress triaxiality, strain rate and inertia in a proper and relatively simple way. The general results are:

(1) In a quasi-static loading, triaxiality increases with crack growth, but in dynamic cases it increases initially whereas inertia leads to its decrease during crack growth.
(2) Although strain-rate sensitivity makes a ductile crack initiation to be postponed, it leads to a faster crack growth due to a decrease in the amount of plasticity at the crack tip area. In other words, although the energy absorption increases initially, it drops very fast after a short crack growth. This is in contrast with a dynamically loaded uncracked specimen, where positive strain-rate sensitivity always makes the specimen absorb more energy.
(3) In the dynamic analyses performed, the presumption of ductile fracture will be inaccurate if the change of triaxiality is ignored.
(4) Considering strain rate in the dynamic simulations while ignoring the stress triaxiality leads to a high underestimation of the toughness.
(5) The global energy absorption of the specimen with rate-sensitive cohesive elements is not highly mesh dependent. This is valid as long as the mesh is fine enough to calculate plastic stress distribution correctly.

These results are compatible with other studies in this field which have used different approaches.

Acknowledgements

The authors from NTNU would like to acknowledge Hydro Aluminium and the Research Council of Norway for their support through the NorLight project. The first author appreciates the scientific and friendly

atmosphere in WMS department at GKSS research center during his stay. He also gives his special thanks to professor Wolfgang Brocks for his precious support and advises.

References

[1] Nishioka T. Computational dynamic fracture mechanics. Int J Fract 1997;86:127–59.
[2] Siegmund T, Brocks W. A numerical study on the correlation between the work of separation and the dissipation rate in ductile fracture. Engng Fract Mech 2000;67:139–54.
[3] Tvergaard V, Needleman A. Analysis of the cup-cone fracture in a round tensile bar. Acta Metall 1984;32:157–69.
[4] Zhang ZL, Thaulow C, Ødegård J. A complete Gurson model approach for ductile fracture. Engng Fract Mech 2000;67:155–68.
[5] Thomason PF. Ductile fracture of metals. Oxford: Pergamon Press; 1990.
[6] Dugdale DS. Yielding of steel sheets containing slits. J Mech Phys Solids 1960;8:100–4.
[7] Barenblatt GI. The mathematical theory of equilibrium cracks in brittle fracture. Adv Appl Mech 1962;7:55–129.
[8] Hillerborg A, Modéer M, Petersson PE. Analysis of crack formation and crack growth in concrete by means of fracture mechanics and finite elements. Cem Concr Res 1976;6:773–82.
[9] Petersson PE. Crack growth and development of fracture zones in plain concrete and similar materials. Technical report, Report LUTVDG/TVBM-1006, Lund Institute of Technology. 1981.
[10] Needleman A. A continuum model for void nucleation by inclusion debonding. J Appl Mech 1987;54:525–31.
[11] Tvergaard V. Material failure by void growth to coalescence. Adv Appl Mech 1990;27:83–151.
[12] Siegmund T, Brocks W. Predictions of the work of separation and implications to modeling. Int J Fract 1999;99:97–116.
[13] Tvergaard V, Hutchinson JW. The relation between crack growth resistance and fracture process parameters in elastic–plastic solids. J Mech Phys Solids 1992;40:1377–97.
[14] Brocks W, Sun DZ, Hönig A. Verification of the transferability of micromechanical parameters by cell model calculations for visco-plastic materials. Int J Plast 1995;11:971–89.
[15] Broberg KB. The cell model of materials. Comput Mech 1997;19:447–52.
[16] Tvergaard V. Crack growth predictions by cohesive zone model for ductile fracture. J Mech Phys Solids 2001;49:2191–207.
[17] Costanzo F, Walton JR. Numerical simulations of a dynamically propagating crack with a nonlinear cohesive zone. Int J Fract 1998;91:373–89.
[18] Corigliano A, Ricci M. Rate-dependent interface models: formulation and numerical applications. Int J Solids Struct 2001;38:547–76.
[19] Zhang X, Mai YW, Jeffrey RG. A cohesive plastic and damage zone model for dynamic crack growth in rate-dependent materials. Int J Solids Struct 2003;40:5819–37.
[20] Broberg KB. Influence of T-stress, cohesive strength and yield strength on the competition between decohesion and plastic flow in a crack edge vicinity. Int J Fract 1999;100:133–42.
[21] Wnuk MP, Legat J. Work of fracture and cohesive stress distribution resulting from triaxiality dependent cohesive zone model. Int J Fract 2002;114:29–46.
[22] Tvergaard V, Hutchinson JW. Effect of strain-dependent cohesive zone model on predictions of crack growth resistance. Int J Solids Struct 1996;33(20–22):3297–308.
[23] ABAQUS. ABAQUS version 6.4. H.K.S. Inc. Pawtucket, USA. 2003.
[24] Zhang ZL. A practical micro-mechanical model-based local approach methodology for the analysis of ductile fracture of welded T-joints. PhD thesis. Lappeenranta University of Technology, Finland. 1994.
[25] Scheider I. Cohesive model for crack propagation analyses of structures with elastic–plastic material behavior. Foundations and implementation. Technical report, GKSS internal report no. WMS/2000/19. 2000.
[26] Clausen AH, Auested T. Split-Hopkinson tension bar, experimental set-up and theoretical considerations. Technical report, SIMLab internal report no. R-16-02. 2002.
[27] Pan J, Saje M, Needleman A. Localization of deformation in rate sensitive porous plastic solids. Int J Fract 1983;21:261–78.
[28] Gurson J. Continuum theory of ductile rupture by void nucleation and growth. Part I—yield criteria and flow rules for porous ductile media. J Engng Mater Technol 1977;99:2–15.
[29] Tvergaard V. On localization in ductile materials containing spherical voids. Int J Fract 1982;18:237–52.
[30] Koplik J, Needleman A. Void growth and coalescence in porous plastic solids. Int J Solids Struct 1988;24:835–53.
[31] Needleman A, Tvergaard V. An analysis of dynamic, ductile crack growth in a double edge cracked specimen. Int J Fract 1991;49:41–67.
[32] Sun DZ, Hönig A, Böhme W, Schmitt W. Application of micromechanical models to the analysis of ductile fracture under dynamic loading. In: Erdogan F, Hartranft RJ, editors. Fracture mechanics: 25th syp. ASTM STP, vol. 1220. Philadelphia: American Society for Testing and Materials; 1994. p. 343–57.
[33] Curran DR, Seaman L, Shockey DA. Dynamic failure of solids. Phys Rep 1987;147:253–388.
[34] Johnson JW. Dynamic fracture and spallation in ductile solids. J Appl Phys 1981;52(4):2812–25.
[35] Liu J. A new dynamic void growth model. Doctoral thesis. Norwegian University of Science and Technology, Norway. 2004.
[36] Bernauer G, Brocks W. Micro-mechanical modelling of ductile damage and tearing – results of a european numerical round robin. Fatigue Fract Engng Mater Struct 2002;25:384–463.
[37] Needleman A. An analysis of decohesion along an imperfect interface. Int J Fract 1990;42:21–40.
[38] Guinea GV, Planas J, Elices M. A general bilinear fit for the softening curve of the concrete. Mater Struct 1994;27:99–105.

[39] Scheider I, Brocks W. Simulation of cup-cone fracture using the cohesive model. Engng Fract Mech 2003;70:1943–61.
[40] Siegmund T, Needleman A. A numerical study of dynamic crack growth in elastic-viscoplastic solids. Int J Solids Struct 1997;34:769–87.
[41] Lin G, Cornec A, Schwalbe KH. Three-dimensional finite element simulation of crack extension in aluminum alloy 2024-FC. Fatigue Fract Engng Mater Struct 1998;21:1159–73.
[42] Scheider I, Brocks W. The effect of the traction separation law on the results of cohesive zone crack propagation analyses. Key Engng Mater 2003;251–252:313–8.
[43] Falk M, Needleman A, Rice JR. A critical evaluation of cohesive zone models of dynamic fracture. J Phys IV France 2001;11:43–50.
[44] Négre P, Steglich D, Brocks W. Crack extension in aluminium welds: a numerical approach using the Gurson–Tvergaard–Needleman model. Engng Fract Mech 2004;71(71):2365–83.
[45] Freund LB. Dynamic fracture mechanics. Cambridge University Press; 1998.
[46] Basu S, Narashimhan R. Finite element simulation of mode I dynamic ductile fracture initiation. Int J Solids Struct 1996;33(8):1191–207.
[47] Basu S, Narashimhan R. A numerical investigation of loss of crack tip constraint in a dynamically loaded ductile specimen. J Mech Phys Solids 2000;48:1967–85.
[48] Needleman A. Numerical modeling of crack growth under dynamic loading conditions. Comput Mech 1997;19:463–9.

Paper II

M. Anvari, J. Liu, and C. Thaulow

Dynamic fracture in aluminum round bars: Experiments and simulations

Published in
International Journal of Fracture
Vol. 143, pp. 317-332, 2007

Paper II is not included due to copyright.

Paper III

M. Anvari, and C. Thaulow

Crack extension in aluminum weldment using rate-dependent cohesive elements

Published in

Local Approach to Fracture – Proceedings of the 9th European Mechanics of Materials Conference

Editors: J. Besson, D. Moinereau, and D. Steglich

Moret-sur-Loing, France, May 2006

Simulation of Crack Extension in Aluminum Weldment using Rate-Dependent Cohesive Elements

Majid Anvari, Christian Thaulow
Department of Engineering Design and Materials, NTNU, Trondheim, Norway

Abstract

A laser welded compact tension C(T) specimen has been analyzed using finite element method. The loading is dynamic and the crack growth simulation has been performed by employing rate dependent cohesive elements. The cohesive elements are distributed in different orientations, so the crack path is not limited to mode I, but mixed mode fracture is possible. The effect of strength mismatch on maximum load, the rate of the crack growth speed, and fracture resistance curves are presented. It is also discussed how rate of loading and crack path restrictions can affect the results.

Keywords: Cohesive zone modeling, Rate sensitivity, mismatch, Dynamic loading

1 Introduction

Aluminum weldment has a vast application in different fields of industry. The load bearing capacity and the fracture resistance of weldments are difficult to predict due to the inhomogeneous microstructures and complex geometries. They also consist of different zones with a variety of mechanical properties. These zones, in a laser weldment, are divided into three main areas, weld zone or fusion zone (FZ), heat affected zone (HAZ) which has been affected by the heat input during welding, and the zone which has not been affected by the welding process and is called base metal (BM). A welded structure happens to contain cracks either at the time of manufacturing or after it is loaded by fluctuating forces or environmental changes. The crack growth can affect the mode of failure and the amount of energy absorption under dynamic loading conditions. Although classical fracture mechanics approaches have been used for many weldment applications, they have a number of limitations that affects the reliability of their predictions. In addition to the limitations regarding to the amount of plasticity at the crack tip, geometry and dimensional requirements, etc., they need the requirement of the presence and location of a crack as a priority. There is also the difficulty in accounting for mechanical and fracture properties variation within the weldment. Local fracture mechanics approaches offer an alternative to solve welded structures and to obtain more detailed analyses compared to linear-elastic fracture mechanics and elastic-plastic fracture mechanics approaches. To use local approaches under dynamic loading conditions, it is important to have an effective numerical tool to be

able to simulate crack growth while considering the dynamic loading influences.

One of the local approaches that has been widely used in numerical fracture mechanics is the cohesive zone model which is based on the strip yield models proposed by Dugdale [1] and Barenblatt [2]. In finite element representation of cohesive zone modeling, cohesive elements are introduced as interfaces between continuum elements. The material separation and damage occur only in the interface elements which obey a constitutive equation named traction separation law (TSL). Separation is calculated from the difference of the displacements of the continuum elements adjacent to the cohesive element.

When a welded structure is under dynamic loading conditions, rate dependency of the material can affect the energy absorption and mode of failure of the structure. The rate dependency has several sources; rate dependency of the bulk plastic response, rate dependency of the weld failure processes, and the effects of temperature dependency in the responses due to the heating that results from the localized plasticity and heating. In addition to these influences, elastic waves and inertia can affect the crack path and crack growth speed.

In the present paper, a laser welded compact tension C(T) specimen, 50x60 mm^2, made of aluminum alloy 6xxx series has been analyzed under dynamic loading conditions. For simplicity, the yield strengths of HAZ and BM have been considered to be the same so that a bi-material case is analyzed. An initial crack of length 25 mm (a/w=0.5) is introduced at bi-material interface. The cohesive elements exist not only on the ligament of the interface line, but also in some extent of the FZ and BM areas. In all of the analyses, the cohesive elements and bulk material are strain-rate dependent. The effect of strength mismatch on maximum load, crack growth and fracture toughness are discussed. It is also discussed how the speed of loading and the finite element model can affect the results.

2 Method

The finite element model of the C(T) specimen and the crack area are shown in Fig. 1. The work is based on the model and simulations performed in [3]. In [3], the cohesive

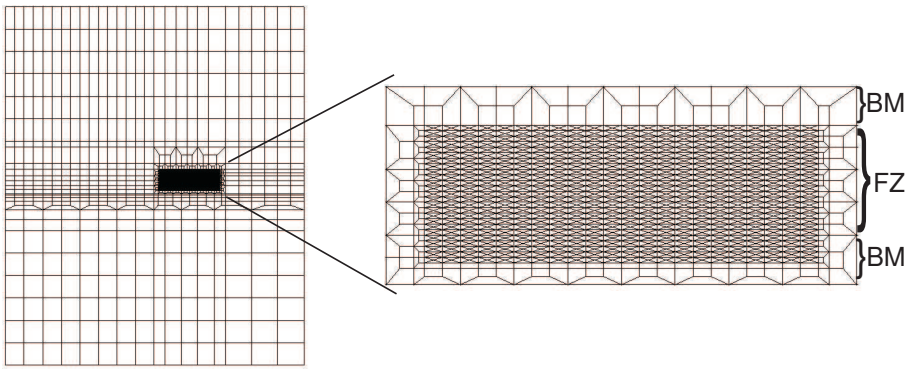

Figure 1: Finite element model of the C(T) specimen.

properties are validated by tests for three different initial crack placements, in the BM, in the middle of HAZ, and in the interface of HAZ/BM. All the experiments and analyses in that investigation are quasi-static. The cohesive and bulk material properties obtained in [3] have been used in the present article with the difference that in the current paper, all of the properties are rate dependent. The static TSL properties are different for the cohesive elements that exist on the interface, in the FZ and in the BM. Since the quasi-static experiments show crack deviation in the FZ with an average angle of 17 degrees, cohesive elements are introduced within triangular continuum elements with the same angle. In this way, the crack has the possibility to grow along the interface, normal to the interface, or with the angle of 17 degrees into the FZ or BM. It should be noted that a hybrid plane-strain/plane-stress model has been introduced. Plane strain elements have been used in the process zone in an area around the crack tip because in that area, the stresses normal to the thickness are not ignorable. Since the thickness of the specimen is only 4.2 mm, the rest of the specimen has been modeled by plane-stress elements.

The TSL used for the cohesive elements is according to Scheider and Brocks [4]. Considering only normal stresses and openings, the TSL chosen has the form of:

$$T = S\, f\left(\delta^N\right) \tag{1}$$

$$f\left(\delta^N\right) = \begin{cases} 2\left(\frac{\delta^N}{\delta_1}\right) - \left(\frac{\delta^N}{\delta_1}\right)^2 & ,0 < \delta^N < \delta_1 \\ 1 & ,\delta_1 < \delta^N < \delta_2 \\ 2\left(\frac{\delta^N - \delta_2}{\delta_0 - \delta_2}\right)^3 - 3\left(\frac{\delta^N - \delta_2}{\delta_0 - \delta_2}\right)^2 + 1 & ,\delta_2 < \delta^N < \delta_0 \end{cases} \tag{2}$$

where T is the traction, S is the cohesive strength, δ_c is the critical separation in which cohesive element fails, and δ_1 and δ_2 are the shape parameters (Fig. 2). The material rate dependency for aluminum alloy 6xxx series was obtained through experiments [5]:

$$\dot{\epsilon}^{pl} = D\left(\frac{\sigma_d}{\sigma_0} - 1\right)^p \tag{3}$$

where $\dot{\epsilon}^{pl}$ is the equivalent plastic strain rate, σ_d is the yield stress at nonzero plastic strain rate, σ_0 is the static yield stress, and D=8000 s^{-1} and p=0.8 are material constants.

Anvari et al. [6] used a Gurson type strain-rate dependent cell model to obtain the TSL for interface elements. They showed that by increasing load speed (strain rate), the stress-displacement curves (traction separation curves) are almost similar and only the maximum stresses (cohesive strengths) increase. In this way, the rate dependency of the cohesive zone is defined as:

$$S = S_0\left[\left(\frac{\dot{\epsilon}}{D}\right)^{\frac{1}{p}} + 1\right] \tag{4}$$

where S_0 is the maximum stress for rate independent material and D and p are the same constants as in Eq. 3. This formulation has been obtained and tested for normal loading (mode I) only.

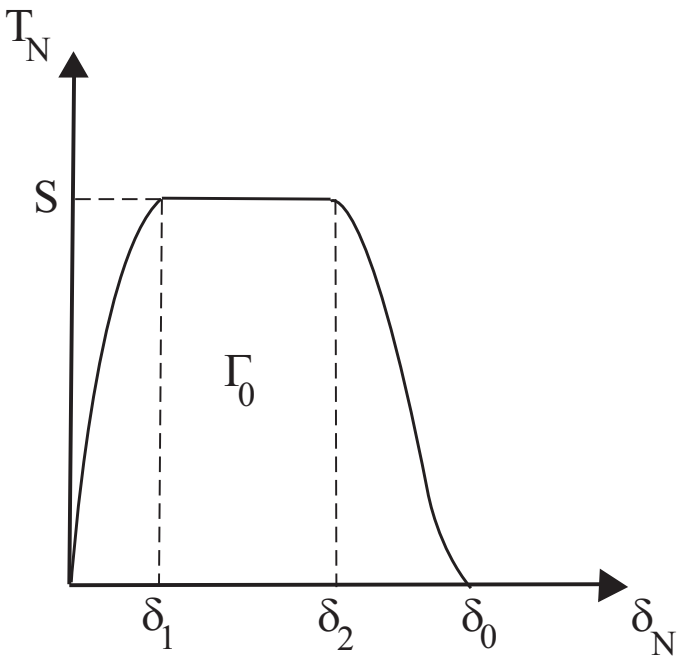

Figure 2: TSL shape proposed by Scheider and Brocks [4].

In a later investigation [5], it was shown that this assumption for rate dependency of cohesive elements produces reasonable results when compared with the experimental results. They also showed that strain rate dependency of the cohesive elements does not make the model to be highly mesh-sensitive as long as the elements are fine enough to calculate plastic strain distribution with a reasonable degree of accuracy.

Since there is not any evidence for rate sensitivity when the load is tangential, the cohesive strength on the tangential direction has been considered to be 40% of the instantaneous normal cohesive strength.

Figure 3 illustrates the strain rate transformation technique employed for the simulations using strain rate dependent cohesive elements. In this technique, the values of strain rate normal to the cohesive element are calculated in the continuum elements in the beginning of each numerical iteration. A similar technique has already been introduced by Siegmund and Brocks [7] for triaxiality dependent cohesive elements under quasi static loading conditions. The averaged values are then transformed automatically to the adjacent cohesive elements to update the cohesive strength of the elements based on Equation 4.

The implementation of the cohesive elements has been performed by user-defined element (UEL) as a FORTRAN subroutine within the non-linear finite element code ABAQUS [8]. All the analyses are transient dynamics using implicit integration.

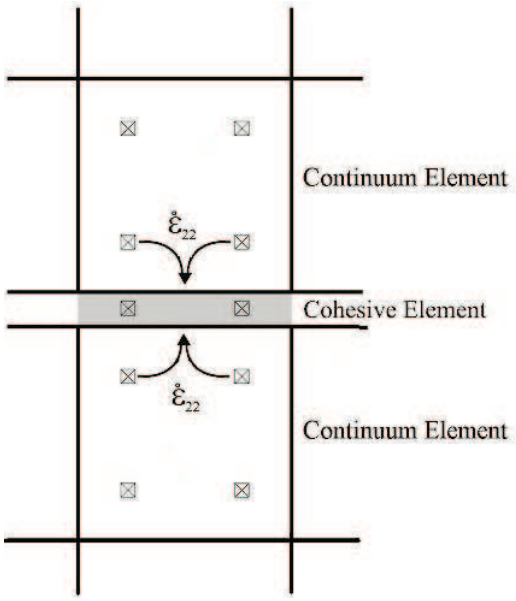

Figure 3: Schematic illustration of the strain rate transformation technique for rate-dependent cohesive elements.

3 Calculations and Results

This section is divided into three main categories and shows how maximum force, crack growth rate and fracture resistance curves are influenced by strength mismatch, rate of loading and crack path assumptions.

3.1 Effect of mismatch

The experiments performed in [3] report the yield strength values of FZ and BM to be 200 and 300 MPa, respectively which means an undermatch case with mismatch factor m=200/300=0.67. To check the effect of mismatch on the mechanical response of the specimen, the yield strength of the FZ has been increased up to 275 MPa without changing the strain hardening as shown in Fig 4. It is obvious that with changing bulk plasticity, the values of cohesive strength and cohesive energy change. As a rule of thumb, the cohesive strengths of FZ and the interface line were considered to be interpolated between the original value and the values of cohesive strength of BM with the same rate as the yield strength of the FZ changes. Loading rate of 2 m/s has been applied in all simulations.

In all simulations, the crack deviates immediately into HAZ and grows in a straight line. Figure 5 shows the force vs. load-line displacement (V_{ll}) for different mismatch cases and also the change of the maximum load vs. mismatch factor, m. The maximum load is reached when the first cohesive element fails. The fluctuations in the load is related to the elastic waves introduced into the structure due to the high rate of the change of

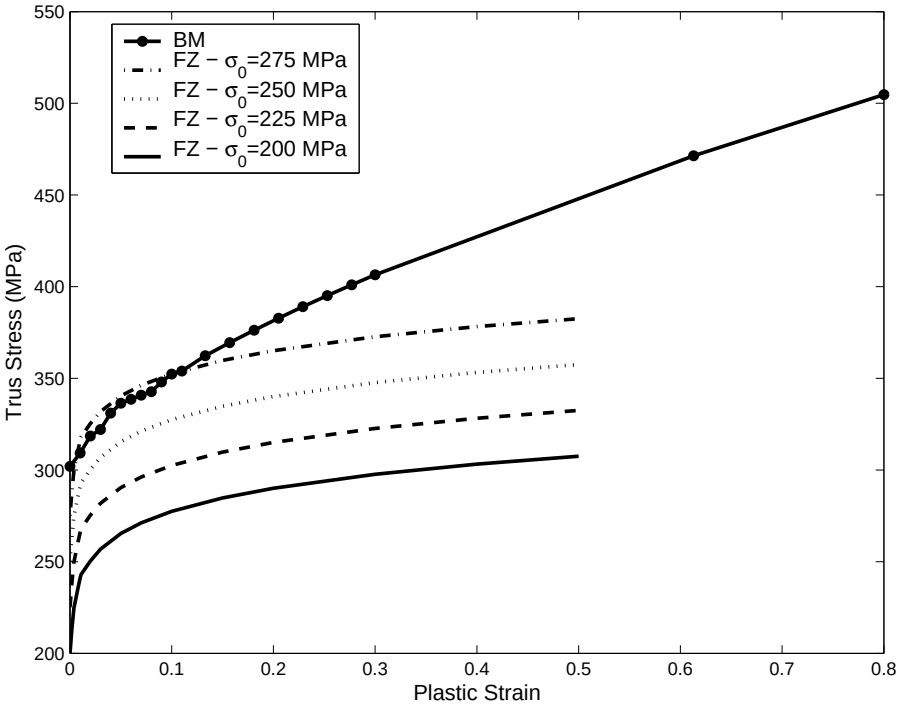

Figure 4: Stress-strain curves for BM and FZ for different values of mismatch.

the load. Figure 6 shows the crack growth vs. time for the different cases. It shows that with increasing m (decreasing mismatch), the time of crack initiation slightly increases and the speed of crack growth slightly decreases. The significant change happens when there is no mismatch and the specimen is made of only base material. In that case, the crack starts much later and it grows slowly compared to the undermatch cases. To check if this difference can be observed in the CTOD R-curves, the δ_5 values vs. crack growth are calculated as presented in Fig 7. The δ_5 measurement proposed by Schwalbe [9] is the displacement difference between two points that are 2.5 mm above and below the original crack tip. Figure 7 shows that although the existence of mismatch has a significant effect on the resistance curve, the value of mismatch has only a slight effect on this curve.

To further investigate the results presented in Fig. 7, the change of energy balance for the whole model vs. crack growth was also calculated, Fig. 8. The energy balance is the difference between the sum of kinetic and total strain energy for the bulk material and the external work and therefore can be proposed to represent the energy of separation. Figure 8 shows similar behavior to the R curves shown in Fig. 7.

3.2 Effect of the rate of loading

To check the effect of loading rate on the results and compare them with static loading, the original model (m=0.67) was simulated under dynamic load with the rate of 1 m/s

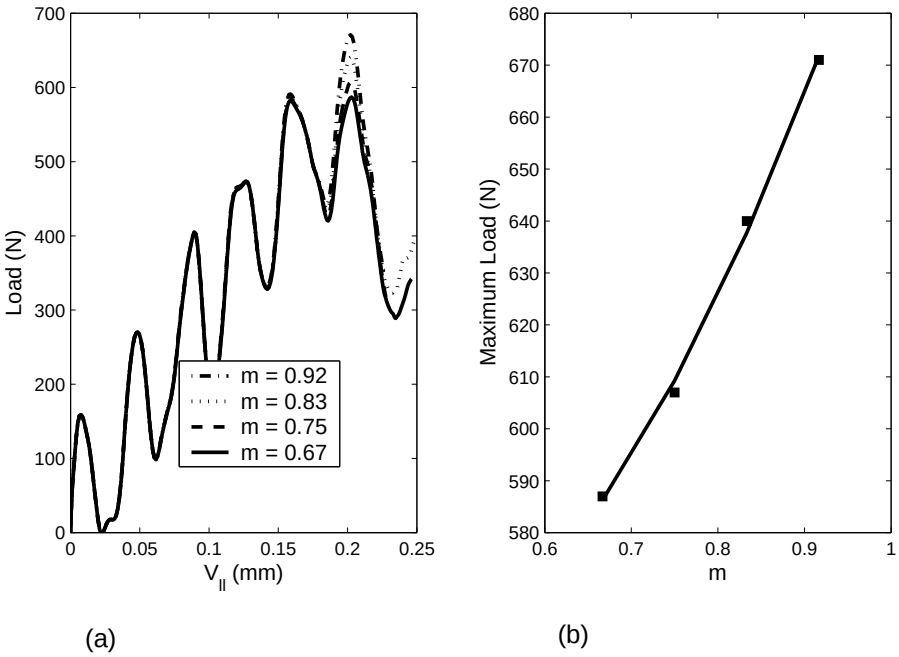

Figure 5: Effect of mismatch on load (a) Load vs. load line displacement, (b) maximum load vs. the value of mismatch

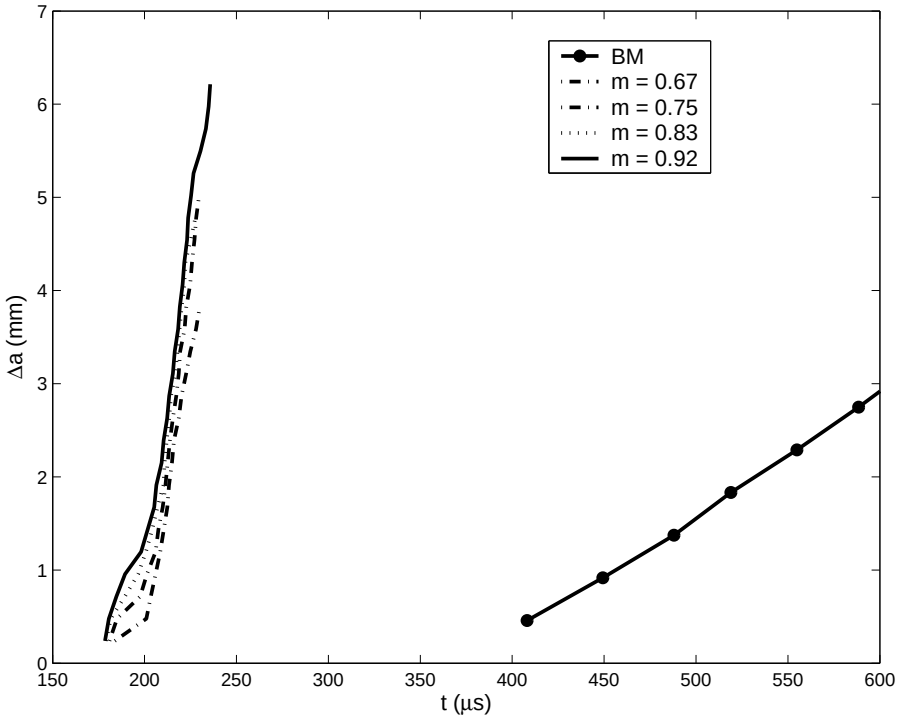

Figure 6: Effect of mismatch on crack growth rate.

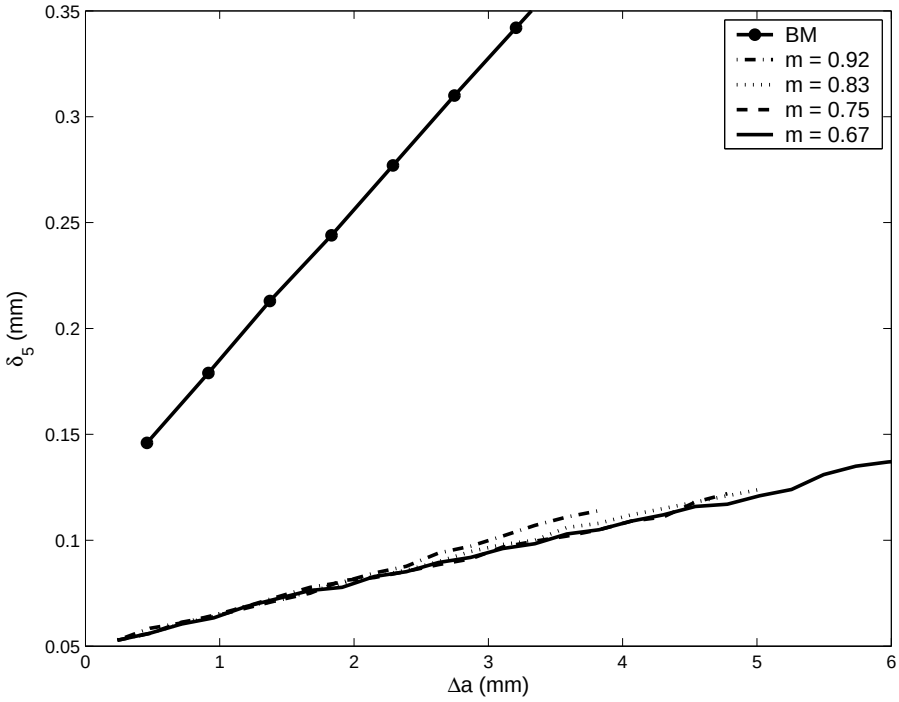

Figure 7: Effect of mismatch on resistance curve.

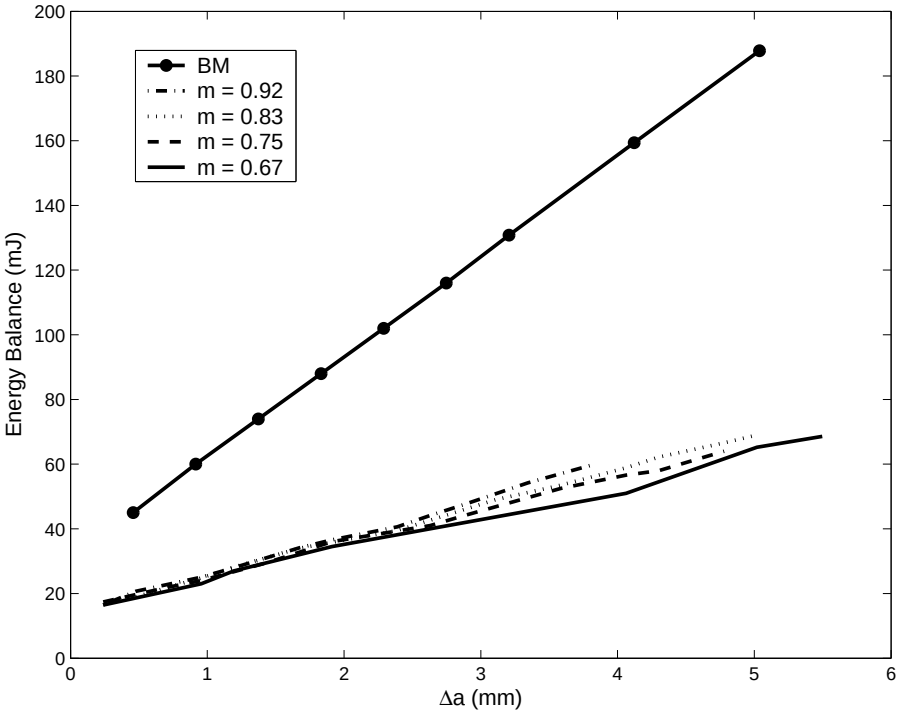

Figure 8: Effect of mismatch on the energy dissipated by separation.

in addition to 2 m/s and static analysis. The simulations show that the maximum loads, the loads when the crack starts to grow, for the two different loading rates are almost the same (587 N), while for the static analysis, this value is lower (534 N). Figure 9(a) shows the crack growth vs. time and linear curves fitted to the results. This figure shows that the rate of the crack growth is almost twice when the loading rate is doubled. Although the crack speeds are highly different, the R curves are almost coincident, Fig. 9(b).

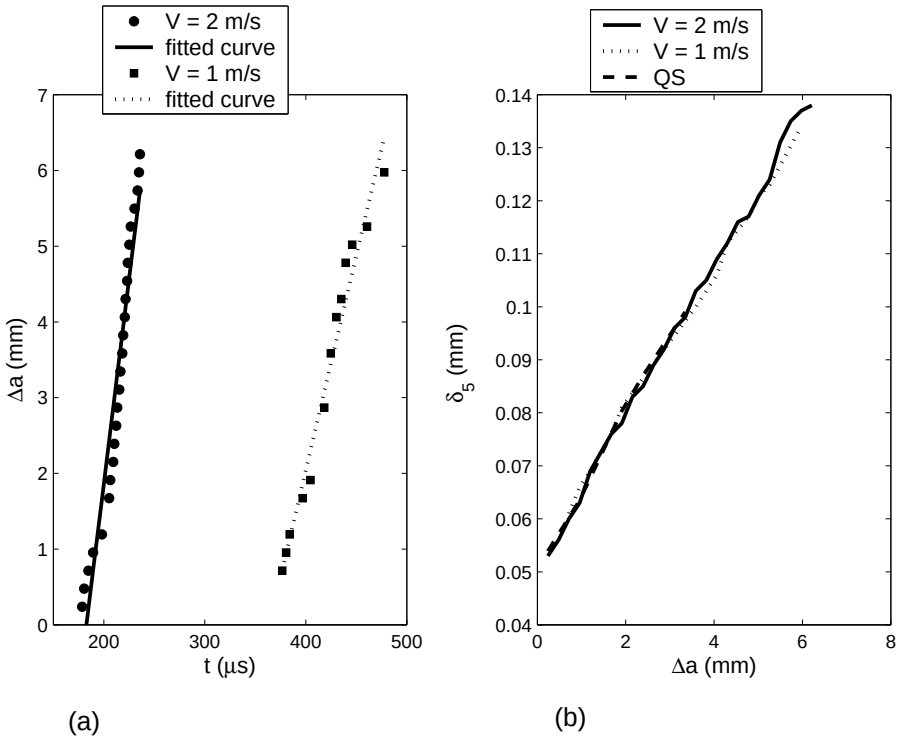

Figure 9: Effect of loading rate on (a) crack growth, and (b) resistance curve.

3.3 Effect of crack path

It is reported in [3] that the angles of crack deviations measured in the tests are not constant and vary between 10 and 25 degrees for the mismatch value m=0.67. To check how much the crack path assumption affects the results, the model was made with the cohesive elements to be in 25 degrees rather than 17 degrees simulated in the previous section. The simulation with loading rate of 2 m/s showed that the crack deviates initially into the FZ, but suddenly changes its direction and mode I becomes dominant. Figure 10 shows the crack growth paths for the two models. Figure 11 shows that the maximum load is initially higher for the 25 degree cases, which is related to the initiation of the crack growth, but it drops faster than 17 degree case when mode I becomes dominant. The fact that energy of separation decreases with the crack growth path is confirmed by Fig. 12(b)

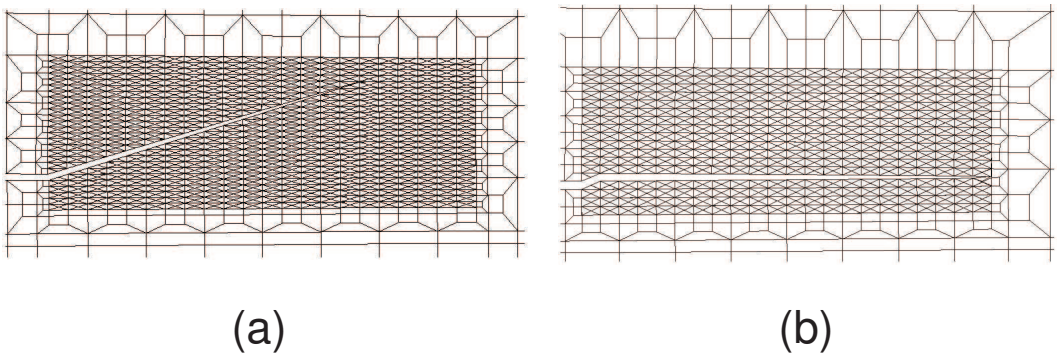

Figure 10: Effect of finite element model on crack path. (a) model with cohesive elements in 17 degree, (b) model with cohesive elements in 25 degrees.

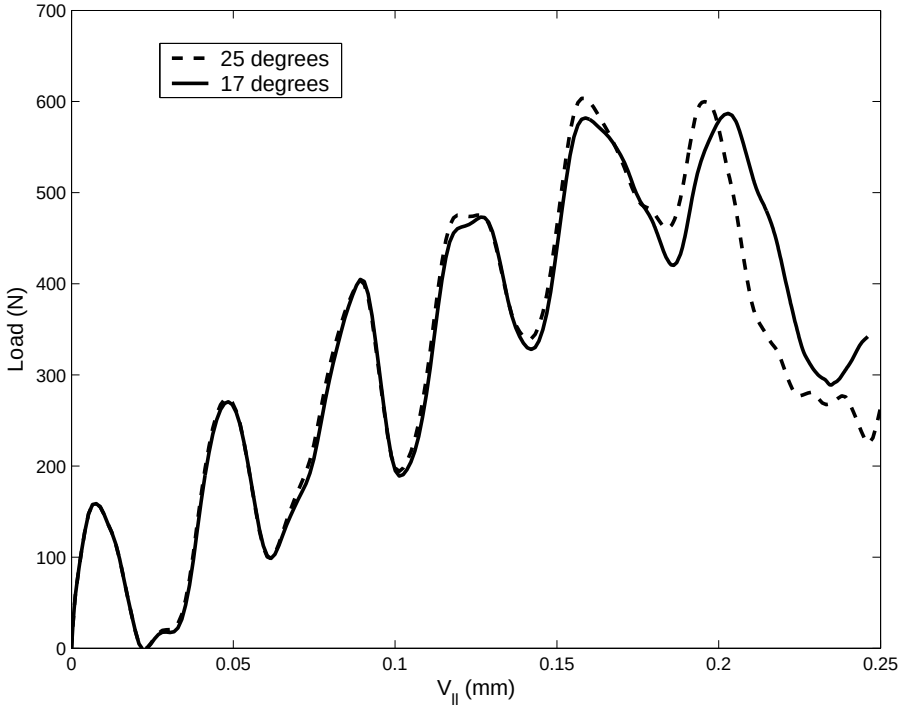

Figure 11: Effect of finite element model and crack path on load.

which shows that δ_5 is slightly higher for the 25 degree case in the beginning, but becomes less that the 17 degree case after a short crack growth. Figure 12(a) shows that the rate of the crack growth is generally slightly higher for the crack growing in mode I.

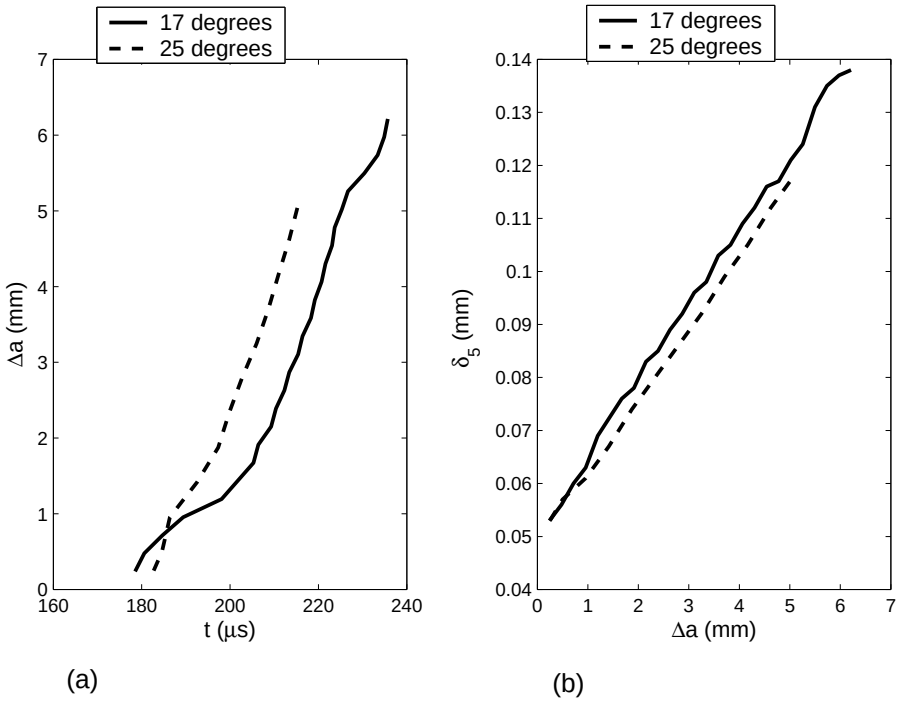

Figure 12: Effect of finite element model and crack path on (a) crack growth, and (b) resistance curve.

4 Conclusions

It has been shown how rate-sensitive cohesive elements can be used in simulating crack growth and its extension into aluminum weldment under dynamic loading conditions. The results show that although having soft zone (undermatch) in a structure made of aluminum alloy results in significant decrease of the fracture toughness, the amount of mismatch is not playing an important role for the resistance curves, crack path and the rate of crack growth. The maximum load, the load at the initiation of the crack growth, is highly affected by the amount of mismatch. The results imply that it is not the energy of separation which is influenced by the value of mismatch, but it is the energy dissipated by plastic deformation.

The simulations with different rates of loading showed that the crack growth speed is highly influenced, whereas the resistance curves are almost insensitive to the rate of loading.

The analyes performed with different mesh designs showed that the angle in which the crack grows affects the resistance curve and that the toughness is minimum for mode

I. Hence, the conventional method of modeling where cohesive elements are imposed at the boundaries of undamaged continuum elements suffers from the dependency on the orientation of the cohesive elements and it is very important to define the orientation of these elements properly. Alternatively, methods in which cohesive behavior is embedded directly into the continuum constitutive response can be applied, e.g. [10].

In all simulations, it seems that although the resistance curves represent the crack growth behavior correctly in a qualitative way, they are not reflecting the change in global behavior of the structure properly. In other words, the resistance curves (fracture toughness) are insensitive to the amount of mismatch and the rate of loading while the reaction forces show higher global differences.

Acknowledgment

The authors would like to acknowledge Hydro Aluminium and the Research Council of Norway for their support through the NorLight project.

References

[1] D.S. Dugdale. Yielding of steel sheets containing slits. *Journal of the Mechanics and Physics of Solids*, 8:100–104, 1960.

[2] G.I. Barenblatt. The mathematical theory of equilibrium cracks in brittle fracture. *Advances in Applied Mechanics*, 7:55–129, 1962.

[3] P. Négre. *Damage and fracture mechanisms investigations of an aluminium laser beam weld*. Technischen Universitåt Hamburg-Harburg, Ph.D. thesis, 2005.

[4] I. Scheider and W. Brocks. Simulation of cup-cone fracture using the cohesive model. *Engineering Fracture Mechanics*, 70:1943–1961, 2003.

[5] M. Anvari, C. Thaulow, and I. Liu. Simulation of ductile fracture in round bars using cohesive elements. In *Proceedings of the* 3^{rd} *National Conference on Computationl Mechanics, MekIT 2005*, pages 61–73. NTNU, May 11-12 2005.

[6] M. Anvari, I. Scheider, and C. Thaulow. Simulation of dynamic ductile crack growth using strain-rate and triaxiality dependent cohesive elements. *Engineering Fracture Mechanics*, 73:2210–2228, 2006.

[7] T. Siegmund and W. Brocks. A numerical study on the correlation between the work of separation and the dissipation rate in ductile fracture. *Engineering Fracture Mechanics*, 67:139–154, 2000.

[8] ABAQUS. *ABAQUS Version 6.4*. H.K.S. Inc. Pawtucket, U.S.A., 2003.

[9] K.H. Schwalbe. *The crack tip opening displacement in elastic-plastic fracture mechanics*. Springer, 1986.

[10] G. Zi and T. Belytschko. New crack-tip elements for xfem and applications to cohesive cracks. *Intenational Journal of Numerical Methods in Engineering*, 57:2221–2240, 2003.